Design and Implementation of Solar Photovoltaic Based Power Supply for Portable Mini-Refrigeration System Utilizing Peltier Effect

Dawit Dubela Someno

A Thesis Submitted to
The Department of Electrical Power and Control Engineering
School of Electrical Engineering and Computing

Presented in Partial Fulfillment of the Requirement for the Master of Science Degree in Electrical Power and Control Engineering (Specialization in Power Electronics)

Office of Graduate Studies
Adama Science and Technology University

Adama, Ethiopia
October, 2020

Design and Implementation of Solar Photovoltaic Based Power Supply for Portable Mini-Refrigeration System Utilizing Peltier Effect

Dawit Dubela Someno

Advisor: Tafesse Asrat (PhD)

A Thesis Submitted to

The Department of Electrical Power and Control Engineering

School of Electrical Engineering and Computing

Presented in Partial Fulfillment of the Requirement for the Master of Science Degree in Electrical Power and Control Engineering (Specialization in Power Electronics)

Office of Graduate Studies

Adama Science and Technology University

Adama, Ethiopia

October, 2020

APPROVAL OF BOARD OF EXAMINERS

We, the undersigned, members of the Board of Examiners of the final open defense by Dawit Dubela Someno has read and evaluated his thesis entitled "Design and Implementation of Solar Photovoltaic Based Power Supply for Portable Mini-Refrigeration System Utilizing Peltier Effect" and examined the candidate. This is, therefore, to certify that the thesis has been accepted in partial fulfillment of the requirement of the Degree of Masters of Science in Electrical Power and Control Engineering Program (Specialization in Power Electronics).

Name of Student	Signature	Date
Advisor / Supervisor /	Signature	Date
External Examiner	Signature	Date
Internal Examiner	Signature	Date
Chairperson	Signature	Date
Head of Department	Signature	Date
School Dean	Signature	Date
Postgraduate Dean	Signature	Date

DECLARATION

I hereby declare that this MSc thesis is my original work and has not been presented for a degree in any other university and all sources of material used for this thesis have been duly acknowledged.

Name: ______________________

Signature: ___________________

This MSc thesis has been submitted for examination with my approval as a thesis advisor.

Name: __________________________

Signature:_______________________

Date of submission: ______________

ADVISOR APPROVAL SHEET

To: Department of Electrical Power and Control Engineering (EPCE)

Subject: Thesis Submission

This is to certify that the thesis entitled "Design and Implementation of Solar Photovoltaic Based Power Supply for Portable Mini-Refrigeration System Utilizing Peltier Effect" submitted in partial fulfillment of the requirements of the Master of Science Degree in Electrical Power and Control Engineering, postgraduate in Power Electronics, and has been carried out by Dawit Dubela Someno Id No. PGR/18107/11 under my supervision. Therefore, I recommend that the student has fulfilled the requirements and hereby he can submit the thesis to the department.

___________________	_________________	_______________
Name of advisor	Signature	Date

ACKNOWLEDGMENT

First of all, I would like to express my deepest gratitude to my Almighty GOD.

I would like to thank my supervisor **Dr. Tafesse Asrat** for his supervision, friendly attitude, and sharing of many good ideas. Regardless of his often high workload, he always makes time to answer questions as well as giving encouraging advice. You are highly appreciated!

I am also very grateful to **Mr**. **Minyamer Gelawe Wase (MSc.)** for lots of advice and helping in preparing the thesis documentation, but also for good ideas and discussions regarding everything from implementations of the system in Simulink in general.

I would moreover like to thank **Mr. Hailu Abebe (MSc.), Mr. Yoseph Dubela,** and **Mr. Menlik Sahilu** for their patience, helpful attitude, and sharing of their knowledge regarding the implementation of the prototype.

Furthermore, I would also like to thank the EPCE department head **Mr. Hinsermu Alemayehu Garbaabaa (MSc.)** and ASTU-CTVE staff members for encouraging, for a very friendly working environment, and for making me feel very welcome during my thesis work.

Finally, I would like to thank my whole family, friends for their love, encouragement, and all of the sacrifices that they have made on my behalf.

ABSTRACT

In medical service, provisioning vaccination plays an important role in immunizing adults and children by triggering the body to produce antibodies. Most vaccines are heat and temperature-sensitive products. Therefore, effective cold storage systems are required to store and transport vaccines. Rural areas in Ethiopia do not get sufficient vaccines because most vaccines are produced and temporarily stored in cities. Nowadays, several kinds of vaccine storage systems are available commercially. Thermoelectric-refrigeration cooled storages are an innovative and alternative kind of vaccine storages. These storages are rugged, reliable, quiet, and require less maintenance. Peltier module is an excellent thermoelectric device as it is energy-efficient and has better performance features under different working conditions. But the low efficiency and large cooling time is still an issue. To overcome this issue, it has to improve the coefficient of performance (COP) of the module. With this consideration, an improved vaccine storage system consisting of Peltier modules, solar modules, DC-DC buck-boost converter, temperature regulation system, and a back-up battery is presented. To achieve this, a cooling load, a Peltier module, a solar module, and a DC-DC converter are modelled mathematically. For the implementation, the selected environment has a 58.6905W cooling load, minimum solar insolation of G_{min} *5000 Wh/m*^{2}*/day, and has a maximum ambient temperature of 40.38*^{o}*C. So, the 94.138W electric power consumed has been designed and simulated using MATLAB Simulink and HOMER software. The designed solar panel a 45W, 10AH backup battery, and DC-DC converter lead to achieving the COP is 0.692 of the developed system and drop 11*^{o}*C of temperature within 21.5 minutes. The cost to develop this system needs an overall net present cost (NPC) of $120.04 and a cost of energy (COE) of $0.073/kWh. The COE is feasible as it is comparable with the national tariff. The prototype of the proposed system excluding the solar panel and a back battery has been developed. In general, this research work's for improvement of cooling time with a better COP.*

Keyword*: Solar panel, Peltier module, Temperature regulator, Buck-boost converter, COP*

TABLE OF CONTENTS

LIST OF TABLES

LIST OF FIGURES

LIST OF ABBREVIATIONS AND ACRONYMS

AC	Alternating Current
ADC	Analog to Digital Converter
APDA	Afar Pastoralist Development Association
APR	April
ASTU	Adama Science and Technology University
CDC	Center of Disease Control and Provision
COE	Cost of Energy
COP	Coefficient of Performance
COVID-19	Corona Virus
CRF	Current Ripple Factor
DC	Direct Current
ESS	Energy Storage System
FMOH	Federal Minister of Health, Ethiopia
HOMER	Hybrid Optimization Model for Electric Renewable
IM	Induction Motor
ISCL	Immunization Supply Chain Logistic
MPPT	Maximum Power Point Tracking
NASA	National Aeronautics and Space Administration
NOC	Net Present Cost
NREL	National Renewable Energy Laboratory
N-type	Negative type
P-type	Positive type
PV	Photovoltaic
R.Q.	Research Question
TE.	Thermoelectric
TEC	Thermoelectric Cooler
TEG	Thermoelectric Generator
TEM	Thermoelectric Module
U.S.	United State of America

LIST OF SYMBOLS

$\vec{q}$	Rate of heat flows per unit area
α	Seebeck coefficient
ρ	Electrical conductivity
η	Efficiency
ΔQ	Charge carrier
°C	Degree centigrade
°F	Degree Faranite
A	Outside area of section
C	Capacitor
D	Duty ratio
D_t	Doorway time factor
FF	Fill-factor
G	Irradiation
H_i	Enthalpy
K_t	Thermal conductivity
L	Inductor
N	Number of P and N of the module
N_m	Number of solar modules
^oK	Degree kelvin
P_{PV}	Solar photovoltaic power
Q_c	Cooling power
Q_h	Heating power
Q_{inf}	Infiltration load
$Q_{product}$	Product load
Q_{remove}	Heat removed
Q_{trans}	Heat gain by transmission
R	Electrical resistivity
U	The overall coefficient of heat transfer
ZT	Figure of merit

CHAPTER 1

INTRODUCTION

1.1. Background

Basic medical programs are essential for any country, particularly for the survival of infants and the improvement of human living conditions. In this regard, one of the fundamental medical services is the provision of vaccines. Most of the vaccines belong to the so-called thermolabile products. The thermolabile medicines are those that require specific conservation conditions and usually requiring low temperatures [1] [2]. The cold chain is the framework of transporting and putting away immunizations inside the secure temperature run of 2°C to 8°C agreeing to the WHO prerequisite. The chain starts with the fridge or cooler at the immunization fabricating plant, immunization distributor, and after that to the provider's office (immunization clinic), and closes with the management of the vaccine to the beneficiaries.

The temperature requirement is not full fill the vaccine will damage and wastage. The cost of most vaccines is expensive, so wastage results in a considerable economic loss. Imperatively, when vaccines lose strength, there's a misfortune of certainty in immunization treatment [3]. Hence, diminishing immunization wastage whereas expanding power will give more compelling immunization within the country, developing world at a decreased fetched per dosage. One way to address perspectives of the wastage issue is the advancement of small coolers competent in transporting immunizations, kept up within the appropriate temperature extend, from the state health center to the far-off client. Coolers utilizing stage alter materials counting ice are able of keeping up the required temperature extend for a period, but vaccines in such coolers are in some cases subject to overheating or solidifying since to the need for temperature regulation.

Solid-state thermoelectric cooling, employing the Peltier effect, offers an important alternate solution to temperature-regulated vaccine refrigeration. For small loads, thermoelectric coolers offer critical preferences compared to the more ordinary vapor-compression refrigeration. Ordinary compression mini refrigeration causing the need for more electricity and consequently more release of CO_2 which intern exacerbating global warming. Ordinary cooling and air conditioning frameworks are devouring colossal energy. In line with this, the use of Chlorofluorocarbons in the convectional systems leads to depletion of the ozone layer. This calls for alternative environment-friendly energy sources [1]. On the other side, thermoelectric mini refrigeration (Peltier refrigeration) are distant fewer moving parts that will require upkeep, no dangers of refrigerant spillage, a lighter, and more compact size. But the efficiency and cooling time required of the system is still an issue.

The efficiency and cooling time required of a Peltier element application depends on the coefficient of performance (COP). COP is the ratio of the cooling power of the Peltier module to the input power of the supply [L1]. To obtain the cooling performance from the thermoelectric cooler (TEC) by optimizing the size, material, cooling capacity, and the temperature difference for improving the COP of TEC.

The cooling COP of TEC is depending on the current supply of the module and the temperature difference between the hot and the cold sides of TEM [4]. To attain this condition efficient power supply and converters are recommended. Besides, thermal design is needed to reduce the temperature different. This obtains by optimizing the heatsink and fan [L2]. Attaining more efficiency is parallelly achieving the small cooling time.

This research provides a concept for the solar and battery-powered thermoelectrically small cooler to transport safe vaccines. Several similar designs have been proposed in a previous study. By contrast to many previous studies that were conducted at room temperature. This cooler was tested with the express purpose of preserving vaccines at a high temperature (40.38°C), typical of temperatures that would be in the Logiya town the hottest pastoralist place located Afar region.

The results suggest that vaccines can be maintained safely for 15 hours at its ambient temperature with one battery full charge. This is enough time in a working day to deliver vaccines from a regional distribution center to clients' administration and the return trip to the center. Since many parts of the pastoralist area in Ethiopia have sunny climates, the potential for solar panels affixed to the sides of the cooler to recharge the onboard battery was explored.

1.2. Statement of the Problem

The vaccine is the major economic cost and component of the worldwide battle against infectious and transmitted diseases. WHO ISCL states that about 2.8 million vaccine doses were lost in east Africa includes Ethiopia. One reason is lacking enough vaccination coverage due to insufficient cold storage in the vaccine supply chain. In Ethiopia, 30% of cold-chain equipment being nonfunctional due to lack of maintenance [5]. Among these 7% of infant death responsible for the cold chain failure which includes vaccine distribution, storage, and transport [L3]. Most rural areas in Ethiopia such as Logiya, Afar, since a huge number of the population is living, is suffering this kind of problem.

Currently, Peltier mini refrigeration introduces in different countries to overcome the wastage of vaccines. However, this mini refrigeration system has issues of efficiency and cooling time (taking too much cooling time to come to the vaccine temperature requirement). The efficiency and cooling time of TEC is depending on COP, one way of addressing the better efficiency is improving COP. COP depends on the current supply of the Peltier module and the temperature difference between the two sides of TEM. The maximum COP can be improved by carefully designing the stability and efficiency of the current supply. The DC-DC converter is responsible for improving the efficiency of the current supply and the power converter efficiency. Alongside the DC-DC converter, regulating the temperature difference between the two sides of TEM is crucial for the thermal design of the system. In this research, different values of COP are compared and discussed with other performance conditions by considering the power supply and portability of the system.

1.3. Research Questions

This work intends to answer the following basic research questions.

RQ.1. How to determine the maximum load of a mini refrigeration system?
RQ.2. How to select the Peltier module size and specifications?
RQ.3. How to model the solar photovoltaic power supply of the system?
RQ.4. How to control the inside temperature of the refrigeration system?
RQ.5. How to model the entire system with MATLAB/Simulink?

1.4. Objectives

1.4.1. General Objective

The general objective of this thesis is to design and implementation of a solar photovoltaic power supply based portable mini-refrigeration system utilizing the Peltier effect.

1.4.2. Specific Objectives

To achieve the main goals, the study has the following specific objectives:

- To design the maximum load of the mini refrigeration system.
- To design the solar PV power supply.
- To design a temperature regulator for the developed model.
- To simulate the system by using MATLAB software.
- To implement the prototype of the proposed system.

1.5. Scope of the Study

The thesis focuses on the mathematical modeling of solar panel, Peltier module, and cooling load of the selected area. Simulation of the design of both the solar module and the Peltier module using MATLAB/Simulink and cost analysis using HOMER software are presented in this thesis. Additionally, the implementation of the system is done.

1.6. Limitation of the Study

The limitation of this study is the purchased electronic items are not industrial grade, because of the COVID-19 pandemic it was difficult to procure industrial grade items, despite their obvious expensive price. Therefore, the items acquired had a different characteristic than initially anticipated for the prototype.

1.7. Significance of the Study

The shortage of energy assets and air pollution are the major issues within the world as well as in our nation. So, the world is moving the energy source utilization from non-renewable sources that will not accessible after many decades to the renewable energy source.

Renewable energy sources are eco-friendly with the environment. Currently, these types of energy sources are accepted in many countries including Ethiopia due to this reason this research work will help the country for the development of eco-friendly products.

This research will help the APDA (Afar Pastoralist Development Association), located in Logya town, which works on a wide variety of projects to contribute to the development and wellbeing of the Afar people. This association focusing on vulnerable women and children, including mobile health and vaccination. Additionally, it uses for Ethiopia Public Health institutions sectors for an effective cold chain system for addressing the rural area. This research work will be adding value for the ASTU Health Center for the case of emergency first aid service to university workers and the student. It also uses for current world situation coronavirus (COVID-19) vaccine transport through the regional public health institution immunization purpose.

Finally, the Peltier mini refrigeration system has enormous use in the field of medical applications, it has too many advantages over the conventional fridge for small-scale applications. Based on easy manufacturers, eco-friendly, and small initial capital is required, this research work will turn to an entrepreneurship business idea for the Ethiopian market.

1.8. Thesis Organization

This thesis organizes into five chapters.

Chapter 1: Presents introduction of the research work, statement of the problems, objectives, research questions, significance, scope, and limitation of the research.

Chapter 2: Includes a literature review of the previous work and theoretical background of the thermoelectric refrigeration system and different types of the thermoelectric effect, the working principle of Peltier cooling, and an overview of the solar panel technology.

Chapter 3: The analysis of data, cooling load calculation, Peltier module modeling, solar module modeling, and the proposed system implementation are covered.

Chapter 4: The proposed system results are discussed in this chapter.

Chapter 5: Finally, this chapter made conclusions and recommendations.

CHAPTER 2

THEORETICAL BACKGROUND AND LITERATURE REVIEW

2.1. Chapter Overview

This chapter reviews vaccine cold chain properties, the interaction of vaccines with temperature, and sensitivity of the heat and light. Also, it discusses the history of thermoelectric with its material types, effects, and application for the refrigeration system; additionally, the Peltier cooling principles of N-type, P-type, and P and N-type materials semiconductors are reviewed and discussed. Also, the overview of solar panel, energy storage system, comparison of batteries, charge controller, and DC-DC converters are discussed. Finally, closely related works-are reviewed and discussed.

2.2. The Vaccine Cold Chain

The system utilized for putting away vaccines in great condition is called the cold chain. It is in some cases alluded to as the Vaccine supply chain, or the immunization supply chain. The cold chain comprises an arrangement of links that are planned to keep immunizations inside WHO-recommended temperature ranges, from the point of manufacture to the point of administration [6]. The reason for the vaccine cold chain is to preserve product quality by guaranteeing that vaccines are stored and transported within recommended temperature ranges. To preserve a reliable vaccine cold chain at the peripheral level it has to follow the following conditions

- Store immunizations and diluents inside the specified temperature range at all destinations,
- Pack and transport vaccines to and from outreach locales agreeing to prescribed procedures, and
- Keep immunizations and medicines inside the suggested cold chain conditions amid an immunization session.

The overall cold chain flowchart as shown in Figure 2-1. The best push of bolts appears the stream of vaccine down to the health facilities; the foot push of bolts appears where information is collected, recorded, checked, and analyzed, and how reporting data streams back up the chain. Taking after this grouping guarantees that cold chain performance is properly observed in which the vital data is assembled for vaccine determining.

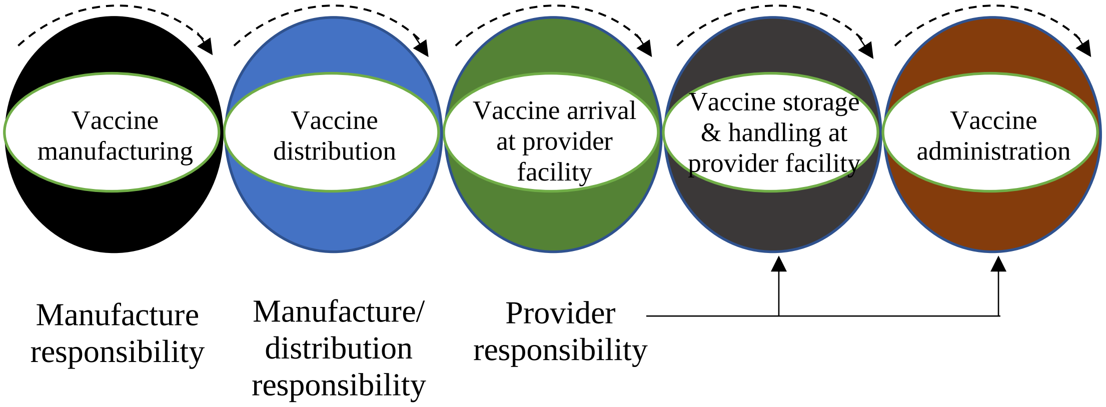

Figure 2-1 The cold chain flowchart

2.2.1. Temperature Requirements for Vaccines

Vaccines are biological product items. A few vaccines are delicate to solidifying, a few to warm, and others to light. Vaccine potency, meaning its capacity to satisfactorily ensure the inoculated understanding, can lessen when the vaccine is uncovered to unseemly temperatures. Once misplaced, vaccine strength cannot be recaptured.

To preserve quality, immunizations must be ensured from temperature extremes. Note that the heat stability data appeared for freeze-dried immunizations applies as it were to unopened vials; most freeze-dried vaccines quickly lose strength after reconstitution. Other than, it is imperative to keep opened multi-dose antibody vials that don't contain additive at temperatures between +2°C and +8°C amid the immunization session, or within six hours after opening.

Table 2 1 appears prescribed immunization capacity temperatures at each level of the cold chain. All those who handle vaccines and diluents must know the temperature sensitivities and the prescribed capacity temperatures for all the immunizations. The vaccine also sensitive to heat, freezing, and light.

Table 2-1 Recommended temperatures and storage times [6]

<table>
<tr><th rowspan="3">Vaccines</th><th rowspan="2">Primary</th><th colspan="2">Intermediate</th><th rowspan="2">Health center</th><th rowspan="2">Health post</th></tr>
<tr><th>Region</th><th>District</th></tr>
<tr><th>6 months</th><th>3 months</th><th>1 month</th><th>1 month</th><th>Daily use</th></tr>
<tr><td>OPV</td><td colspan="2">-15^{o}c to -25^{o}c</td><td colspan="3" rowspan="14">+2^{o}c to +8^{o}c</td></tr>
<tr><td>BCG</td><td colspan="2" rowspan="6">WHO no longer recommends that freeze-dried vaccine be stored at -20^{o}c. Storing them at -20^{o}c is not harmful but is unnecessary. Instead, these vaccines should be kept in refrigeration and transported at +2^{o}c to +8^{o}c</td></tr>
<tr><td>Measles</td></tr>
<tr><td>MMR</td></tr>
<tr><td>MR</td></tr>
<tr><td>YF</td></tr>
<tr><td>Hib freeze-dried</td></tr>
<tr><td>DT</td><td colspan="2" rowspan="7"></td></tr>
<tr><td>DTP</td></tr>
<tr><td>DTP-HepB</td></tr>
<tr><td>HepB</td></tr>
<tr><td>Hib liquid</td></tr>
<tr><td>TD</td></tr>
<tr><td>TT</td></tr>
</table>

2.2.2. The Cold Chain at the Health Center

At the health facility level (usually health centers and health posts), all health specialists in a facility ought to know how to screen the cold chain. They can satisfactorily secure vaccines by doing the taking after:

- Keep immunizations improper vaccine refrigeration hardware.
- Temperature observing device to guarantee temperatures stay between +2 to+8 °C.
- Checking and recording vaccine temperatures twice a day regularly.
- Properly putting away vaccines, diluents, and water packs.
- Handling preventative upkeep of the cold chain equipment.

2.3. Thermoelectric Technology

The converter of heat into electricity is called thermoelectric generator (TEG) or thermoelectric pile (within the 19th century). The working rule of the TEG is based on the

Seebeck effect found in 1821. The conspire of direct conversion of heat energy into electricity of different materials A and B sets associated in an arrangement through electrical conductor [7]. The device shown in Figure 2-2 can be utilized not as it were for the conversion of the heat into electricity but moreover for the converse process. When a current is provided to this device, it produces the contrast in temperatures between its two sides (Peltier effect, found in 1834). In this case, the device is called Thermo-Electric Cooler (TEC) [8]. The TECs were created within the form of Peltier pastilles for little capacity applications and constrained space. They are utilized broadly for controlling the temperature of electronic components and cooling it.

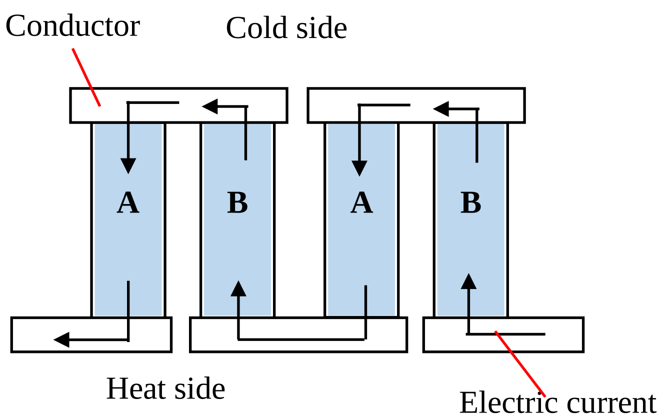

Figure 2-2 TEG / Thermoelectric pile

2.3.1. Thermoelectric Material

In order to choose the thermoelectric material, the figure of merit (ZT) will be considered. The figure of merit (ZT) characterizes as the proportion of electric potential difference to temperature difference within the absence of electric current flow [9]. ZT may be an exceptionally helpful figure for comparing the potential efficiency of devices built of distinctive materials. The values of ZT is an approach to one considered to be great material. Different types of a thermoelectric material are listed in Table 2-2. The figure of merit of those materials is listed in Figure 2-3.

In order to choose the thermoelectric material, the figure of merit (ZT) will be considered. The figure of merit (ZT) characterizes as the proportion of electric potential difference to temperature difference within the absence of electric current flow [L4]. Values of ZT = 1 are considered great material type.

Table 2-2 lists several semiconductor materials that are currently being used for TEG and cooling applications [L4].

Thermoelectric Material	Symbol
Silver(I) telluride	Ag_2Te
Bismuth (III) selenide	Bi_2Se_3
Bismuth selenide granular (melted), 99.999% trace metals basis	Bi_2Se_3
Bismuth (III) telluride powder, −325 mesh, 99.99% trace metals basis	Bi_2Te_3
Lead (II) selenide 99.99%	PbSe
Lead (II) telluride 99.998% trace metals basis	PbTe
Antimony (III) selenide 99.99% trace metals basis	Sb_2Se_3
Antimony (III) telluride powder, −325 mesh, 99.96% trace metals basis	Sb_2Te_3

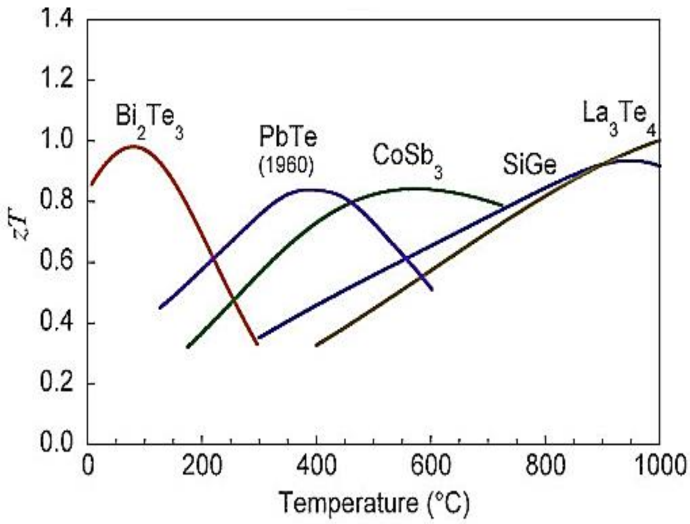

Figure 2-3 Approximate figure of merit (ZT) for various p-type and n-type thermoelectric materials [L4]

2.4. Application of Thermoelectric

2.4.1. Refrigeration

Thermoelectric materials can be utilized as refrigerators, called "thermoelectric coolers", or "Peltier coolers" after the Peltier effect that controls their operation. As a refrigeration innovation, Peltier cooling is distant less common than vapor-compression refrigeration. The most focal points of a Peltier cooler (compared to a vapor-compression fridge) are its need no moving parts or refrigerant, required low power, and it's small in size and adaptable shape. Today, Peltier coolers are widely used in small-scale applications [L5].

2.4.2. Power Generation

Thermoelectric proficiency depends on the figure of merit, ZT. There's no hypothetical upper restrain to ZT, and as ZT approaches infinity, the thermoelectric productivity approaches the Carnot limit. Thermoelectric generators serve application specialties where effectiveness and the cost are less imperative than unwavering quality, lightweight, and small in size [L5].

2.4.3. Comparison of Thermoelectric Refrigeration with a Compressor Fridge

Table 2-3 Comparison of thermoelectric based and compressor-based fridge [10]

Features	Thermoelectric Based	Compressor Based	Comment
Power usage	Best with proportional control in cooling mode and heating mode	No proportional control; affects the overall efficiency	Thermoelectric cooler assembly is more efficient over a wider range of T
Working Time	> 70,000 hours	Undetermined	Thermoelectric has little maintenance required
Power input	DC required	AC required	DC more flexible to accommodate multiple geographic regions
Reliability	Solid-state heat pumping; proportional control;	Mechanical pump, refrigerants, fans. On-off switching cycle	Fan is only moving part in a thermoelectric cooler

Refrigeration utilizing thermoelectric coolers are often considered as an alternative to conventional vapor-compression systems for enclosure cooling. Because a thermoelectric cooler is compact, robust, and completely solid-state, the inherent reliability of such a system is attractive to engineers and end-users alike. However, there is an inherent reluctance to choose a thermoelectric-based system due to preconceptions about energy efficiency or lack of experience with thermoelectric [10]. The comparison has been made by contrast two cooling technologies. Comparisons of efficiency, reliability, control, as well as installation and maintenance, demonstrate that a thermoelectric based solution can have significant advantages over conventional compressor-based systems. The comparison are shown in Table 2-3

2.5. Thermoelectric Effect

The thermoelectric effect is the change of a temperature gradient into a voltage difference or the process of using electricity to gain a temperature gradient between two different materials that conduct electricity [11]. By the advancement of current semiconductor materials, the thermoelectric effect can be utilized for thermoelectric power generation or thermoelectric cooling. The term "thermoelectric effect" encompasses three separately known effects those are the Seebeck effect, Peltier effect, and Thomson effect.

2.5.1. Seebeck Effect

The Seebeck effect named after Thomas Johann Seebeck is the phenomenon in which a temperature gradient between two different electricals (semi)conductors produces a voltage difference [11]. Once the semiconductors are connected to an electric circuit in series, heat can be converted into electricity. The Seebeck effect results from the diffusion of charge carriers from the hot side to the cold side in the thermoelectric material due to the charge carriers having higher thermal energy on the hot side compared to the cold side as illustrated in Figure 2-4.

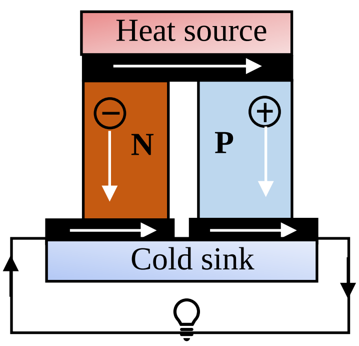

Figure 2-4 Seebeck effect

2.5.2. Peltier Effect

The Peltier effect is the reverse process of the Seebeck effect. When an electrical current is passed through two different electricals (semi) conductors, heating occurs at one end of the junction and cooling at the other end [11] as shown in Figure 2-5.

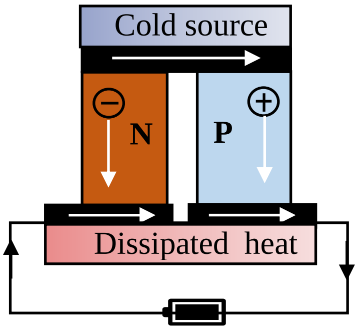

Figure 2-5 Peltier effect

2.5.3. Thomson Effect

The Thomson effect characterizes as an electric current is passed through a conductor having a temperature gradient over its length, heat will be either retained by or removed from the conductor [11]. Whether heat is retained or ousted depends on the direction of both the electric current and temperature slope shown in Figure 2-6. This phenomenon is known as the Thomson effect.

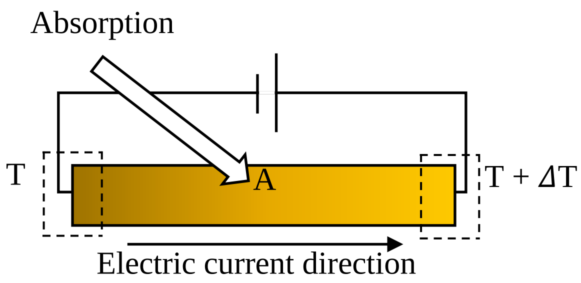

Figure 2-6 Thomson effect

2.6. Peltier Cooling

The Peltier effect happens at whatever point electrical current flows through two different conductors; depending on the heading of the current stream, the intersection of the two conductors will either retain or release heat. The heat will be moved within the course of charge carrier movement throughout the circuit [12]. In the world of thermoelectric technology, semiconductors (ordinarily Bismuth Telluride) are the material of choice for creating the Peltier effect since they can be more effectively optimized for pumping heat.

2.6.1. Peltier Cooling with N-type Semiconductor

The N-type semiconductor material is utilized to manufacture the pellet so that electrons will be the charge carrier utilized to make the bulk of the Peltier effect [16]. As shown in Figure 2-7 N-type semi-conductor has an electron in its Fermi level. When the DC voltage source connected as shown in figure 2-8, electrons will be repulsed by the negative pole and pulled in by the positive pole of the supply; due to this fascination, electrons at the Fermi level move towards the positive terminal by discharging heat and making the holes within the Fermi level.Due to the continuous supply of current, electrons move from the valance band (lower energy band) to the Fermi level by absorbing energy from the intersection [12]. so, it can say that, in Peltier cooler utilizing N-type of semiconductor, heat is ingested within the junction close to the negative terminal, and heat is rejected at the junction close to the positive terminal.

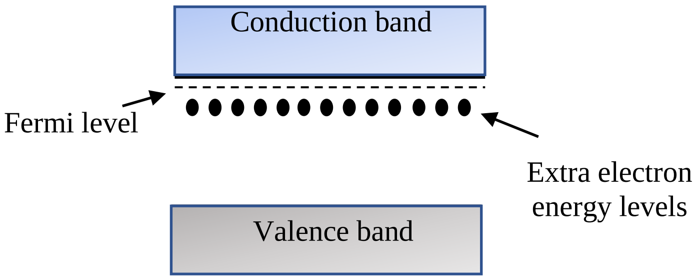

Figure 2-7 N-type semiconductor energy band diagram

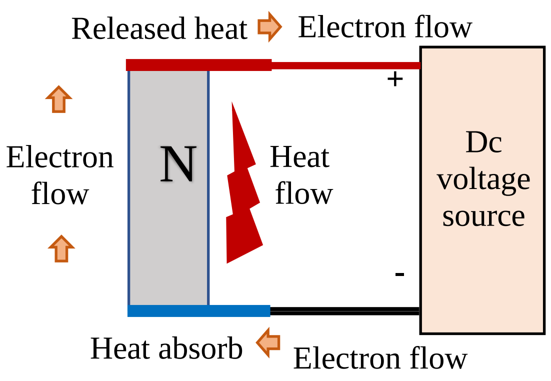

Figure 2-8 Peltier cooling with N-type semiconductor

2.6.2. Peltier Cooling with P-type Semiconductor

In the thermoelectric industry, P-type semiconductor pellets are also employed. Figure 2-9 shows the energy band diagram of the P-type semiconductor. In this, holes are at the Fermi level (higher energy level). When DC voltage source is applied through the circuit as shown in Figure 2-10; holes get attracted to the negative terminal of the source. By this attraction, holes move to the negative terminal by releasing heat. Due to the continuous supply of current, holes from the conduction band moves to Fermi level by absorbing heat from the junction So, we can say that in Peltier cooler using a P-type of semiconductor, heat is absorbed in the junction near the positive terminal, and heat is rejected at the junction near the negative terminal. [12].

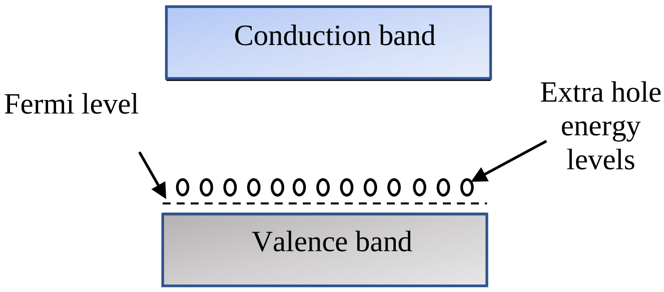

Figure 2-9 P-type semiconductor energy band diagram

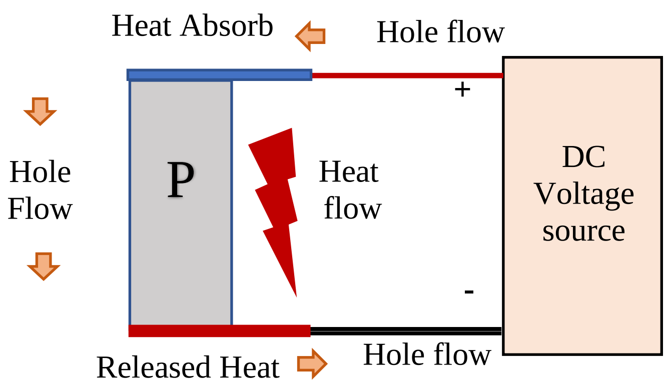

Figure 2-10 Peltier cooling with P-type semiconductor

2.6.3. Peltier Cooling with P & N-type of Semiconductors

By arranging N and P-type pellets in a couple and forming a junction between them with a plated copper tab, it is conceivable to design an arrangement circuit that can keep all of the heat moving in the same direction. Figure 2-11 outlined that the free (foot) conclusion of the

P-type pellet is associated with the positive voltage potential and the free (foot) end of the N-type pellet additionally associated with the negative side of the voltage.

By arranging the circuit as like in Figure 2-11, it is conceivable to discharge heat to one side and retain it from another side. Utilizing these special properties of the TE “couple”, it is conceivable to group numerous pellets in rectangular clusters to make practical thermoelectric modules as in Figure 2-12.

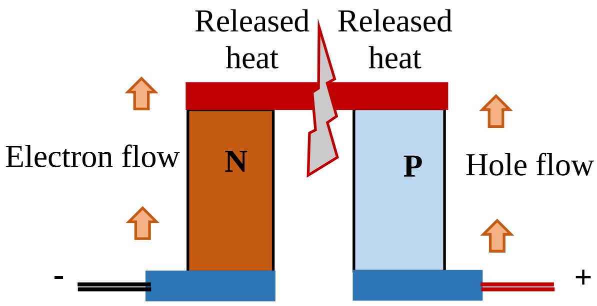

Figure 2-11 Peltier cooling by a couple of N&P

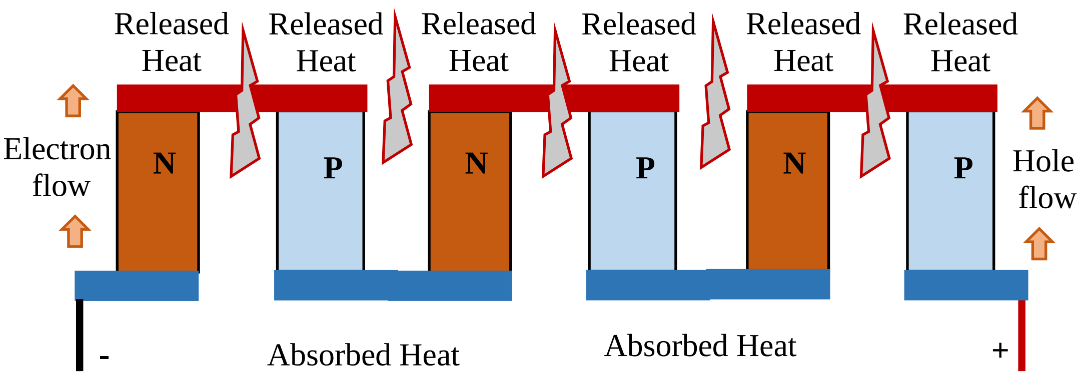

Figure 2-12 Peltier cooling by multiple pallets

2.6.4. Fabrication of Peltier Cooler

Based on the previous section, for creating thermoelectric effect couples of P-type and N-type semiconductors are associated in series by metal plates. By doing this it retains the heat from one side and releases the heat to another side. So, the solid-state P-N materials are associated electrically in series and thermally in parallel, it makes one thermoelectric unit as shown in Figure 2-13. Considering an ordinary thermoelectric system planned to cool air in a walled-in area is shown in Figure 2-14. This is often likely the foremost common sort of

TE application. Here the challenge is to accumulate heat from the inside of the box, pump it to a heat exchanger on the outside of the box, and release the collected heat into the surrounding air. Ordinarily, typically done by utilizing two heat sink/fan combinations in conjunction with one or more Peltier devices. One of the heat sinks is utilized on the inside of the walled-in area; cooled to a temperature underneath that of the air within the box, the sink picks up heat as the air circulates between the fins.

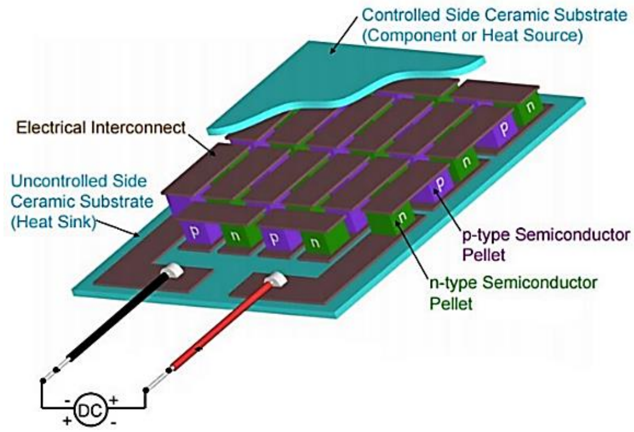

Figure 2-13 Fabrication of Peltier module [12]

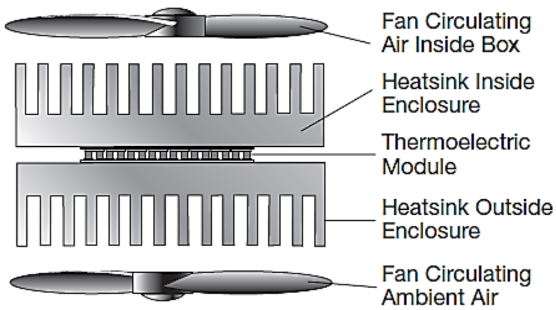

Figure 2-14 Configuration of air-to-air thermoelectric cooler [12]

2.7. Overview of Solar Panel

Increasing the demand for eco-friendly energy sources and the steady decay of solar photovoltaic (PV) costs have been the driving drive behind the development in solar capacity [13]. Figure 2-15 shown that solar clusters that deliver electricity through individual PV boards connected in series or parallel. This form of energy collection is practical in districts of the world where the sun is abundant and can be utilized in isolated locales or on houses to supplement the rising cost of power from a power grid. The efficiency of the panel is determined by the semiconductor material that the cells are made from as well as the process used to construct the cells [14]. Figure 2-16 shows the photovoltaic system typically includes an array of solar panels, MPPT, an inverter, and sometimes a battery and interconnection wiring [15]. Considering ample resource availability, significant market potential, and cost competitiveness, solar PV is expected to continue driving overall renewables growth in several regions over the next decade.

Figure 2-15 Solar panel [13]

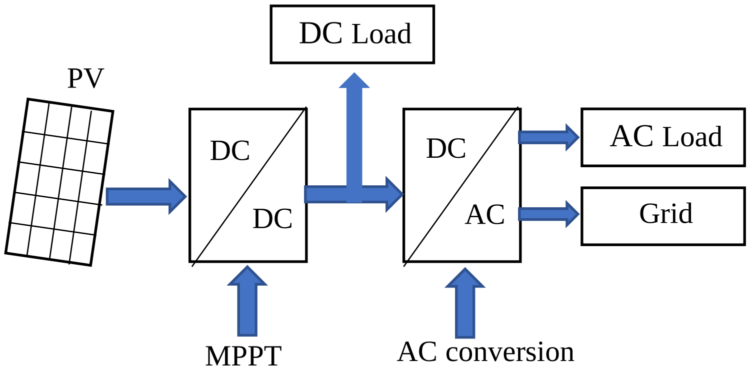

Figure 2-16 Solar installation block diagram

2.7.1. Working Principle of Solar PV

Solar cells change over the energy in daylight to electrical energy. Solar cells contain a material such as silicon that retains light energy. The energy thumps electrons free so they can flow openly and deliver a distinction in electric potential vitality, or voltage. The flow of electrons or negative charge makes an electric current. Solar cells have positive and negative contacts. If the contacts are connected with a conductive wire, current flows from the negative to positive contact which illustrated in Figure 2-17. A single photovoltaic cell can deliver approximately 1 to 2 watts of electricity. To extend the yield of power, several photovoltaic cells are electrically connected to create a photovoltaic module and these modules are further electrically connected to make a photovoltaic board photovoltaic array shown in Figure 2-18. The number of modules associated to make a cluster depends on the sum of solar electrical energy required [L6].

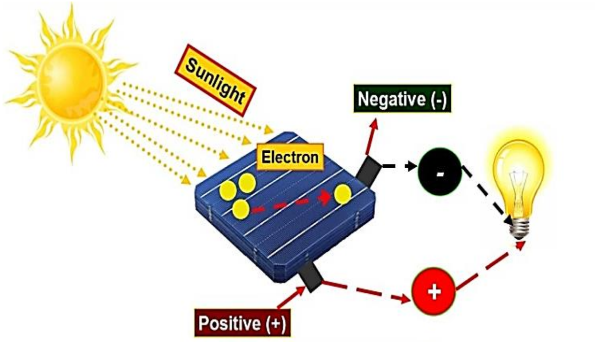

Figure 2-17 PV cell working principle [L6]

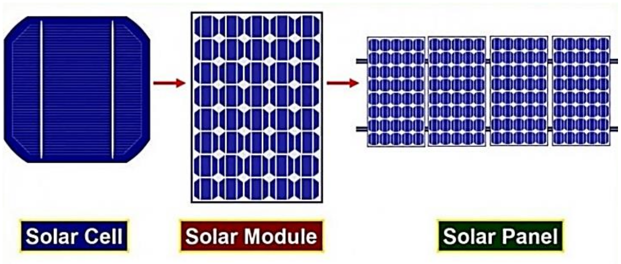

Figure 2-18 Solar cells, solar module and solar panel [L6]

2.7.2. Comparison of different types of solar panel

Most of the solar panel options currently available fit in one of three types: monocrystalline**,** polycrystalline (also known as multi-crystalline), and thin-film**.** These solar panels vary in how they're made, appearance, performance, costs, and the installations each are best suited for. Depending on the types of installation will considering, one option may be more suitable than the others. There are three major types of solar panels: monocrystalline, polycrystalline, and thin-film. Each type has its unique advantages and disadvantages, and the solar panel type best suited for your installation will depend on factors specific to the property and desired system characteristics [16].

Table 2-4 Comparison of different types of solar panel [16]

Types of panel	Advantage	Disadvantage
Monocrystalline	• High efficiency • High performance • Aesthetics	• Higher costs
Polycrystalline	• Low cost	• Lower efficiency • Lower performance
Thin-film	• Portable and flexible • Lightweight • Aesthetics	• Lowest efficiency • Lowest performance

2.7.3. Energy Storage System

The sun-based energy is fluctuating in nature and to preserve the steadiness of the power network supporting energy sources is required. It is ordinarily an energy storage framework and it gives supplementary or reinforcement power when it is required. The energy storage system (ESS) can provide a wealthy extend of points of interest to the electric system, to power end-clients, and society in general. The assortment of ESS can be assembled with diverse application/use classifications [17]:

- Charging and discharging cycle based on time,
- Reduction of network infrastructure,
- Benefits to clients,
- Integration with the renewable energy era, and others.

2.7.4. Battery

Solar energy has to be stored for use of the sun is not shining. To store this energy battery is used. There are two types of battery those are primary battery and secondary battery. The basic difference of this battery is; the primary battery is not rechargeable its one-time use and has a short life but the secondary battery is rechargeable and has long time usage. Most solar technologies are used secondary battery to store the energy.

2.7.5. Comparison of Battery

Rechargeable batteries play a critical part in our lives and numerous day by day chores would be incomprehensible without the ability to energize. The foremost common rechargeable batteries are lead-acid, NiCd, NiMH, and Li-ion. Here could be a rundown of their characteristics in Table 2-5. The foremost commonly used battery for residential PV applications is the lead-acid battery [L8].

Table 2-5 Summary of the characteristics of different type of battery [L8].

<table>
<tr><th rowspan="2">Specification</th><th rowspan="2">Lead Acid</th><th rowspan="2">NiCd</th><th rowspan="2">NiMH</th><th colspan="3">Li-ion</th></tr>
<tr><th>Cobalt</th><th>Manganese</th><th>Phosphate</th></tr>
<tr><td>Specific Energy (wh/kg)</td><td>30-50</td><td>45-80</td><td>60-120</td><td>150-250</td><td>100-150</td><td>90-120</td></tr>
<tr><td>Charge Time</td><td>8-16h</td><td>1-2h</td><td>2-4h</td><td>2-4h</td><td>1-2h</td><td>1-2h</td></tr>
<tr><td>Cell Voltage</td><td>2v</td><td>1.2v</td><td>1.2v</td><td>3.6v</td><td>3.7v</td><td>3.2-3.3v</td></tr>
<tr><td>Coulombic Efficiency</td><td>90%</td><td colspan="2">70% slow charge
90% fast charge</td><td colspan="3">99%</td></tr>
</table>

2.7.6. Charge Controller

A charge controller sometimes alluded to as a photovoltaic controller or battery charger, is as it were necessary for frameworks with battery back-up. The essential work of a charge controller is to avoid overcharging of the batteries. Most have a low voltage disengage that avoids over-discharging batteries. Other than, charge controllers avoid a charge from depleting back to solar modules at night. A few modern charge controllers join the most extreme power point following, which optimizes the PV array's yield, expanding the energy it produces [18].

2.7.7. DC-DC Converter

For the control of electric power or power conditioning, the conversion of electric power from one form to another is necessary and the switching characteristics of the power devices permit these conversions. The static power converters perform these functions of power conversions. A continually increasing demand for power systems has placed power consumption at a premium.

2.7.7.1. Working Principle of DC-DC Converters

The general principle of DC-DC convertors involves the storage of electrical energy into components, such as capacitors and inductors, and the release of energy to loads. By controlling the time for energy storage and release, the average voltage level that appeared at the converter load can be controlled. The average load voltage level can thus be either higher or lower than the voltage level of the power source. DC-DC converters utilize duty ratio as the switching control signal for its advantage of linear control over the load power.

2.7.7.2. The Topology of a DC-DC Converter

The dc converters can be used as switching mode regulators to convert a dc voltage, usually unregulated to a regulated dc output voltage. The regulation is normally achieved by duty ratio at a fixed frequency and the switching driver is normally BJT, MOSFET, or IGBT [19]. There are different topologies of switching-mode regulators that are shown in Figure 2-19, this research work uses non-isolated converters especially buck-boost converter.

A buck-boost converter gives a yield voltage that will be less than or more prominent than the input voltage thus the title “buck-boost”; the yield voltage polarity is opposite to that of the input voltage. This converter is additionally known as an altering controller. The circuit course of action of a buck-boost converter is shown in Figure 2-20.

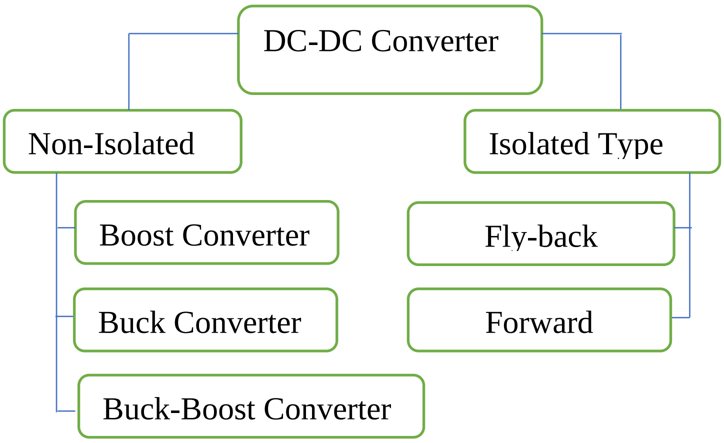

Figure 2-19 Different topologies of a DC-DC converter

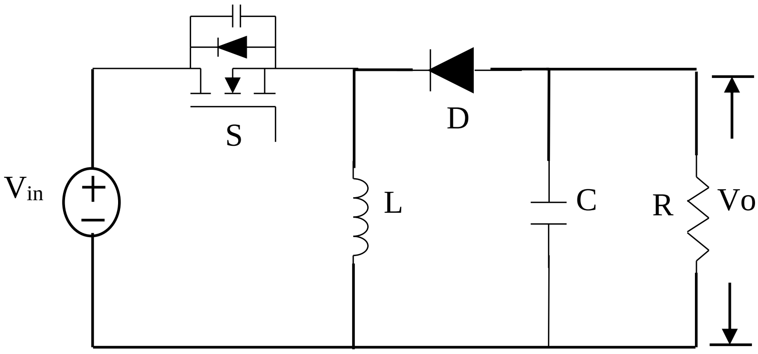

Figure 2-20 Circuit diagram of the buck-boost converter

2.8. Related Works on the Thermoelectric Refrigeration System

This portion reviews some researches that have been done before based on a thermoelectric refrigeration system by the criterion of time taking for cooling the environment, power consumption, designed temperature, and desired temperature.

The improvement of the COP of a thermoelectric cooler is presented in [20]. The author of this paper uses the multistage of thermoelectric modules to improve the COP. It obtains 1.2 COP using those overlap of the modules. It is good achieving but the multistage of the module is increases the size of the heat sink and the box. So, it difficult to transport from place to place.

The author in [21] , studied smart refrigeration systems based on an embedded system. This paper emphasizes is to achieve long-term cooling in case of power failure for the refrigerator by using a 12V battery. Also, it uses the AC power supply. The system developed to provide active cooling with the help of a 12V thermoelectric module is used to provide adequate cooling. The merit of this paper is to achieve long-term cooling in case of power failure for refrigerators and use an embedded system to control the temperature. On the other side, the demerit of this paper is, it takes more than three hours to drop the inside temperature to 5^{o}C from ambient temperature. This is not suitable for the storage of vaccines because vaccines need a fast recovery of temperature.

The paper in [22], studies the solar-powered eco-friendly mini-fridge. This paper establishes a solar fridge with temperature monitoring as well as controlling. And also implemented using solar panels for charging a Lead Acid Battery (12V, 1.2 Amp hrs.) and Peltier thermoelectric device. It uses a limited number of Peltier modules. So, it doesn't give sufficient performance of the cooling environment for the box. The design temperature is not suitable for vaccine storage as well.

Peltier based eco-friendly smart refrigerator for rural areas is studied in the paper [23]. It demonstrated that an eco-friendly methodology for the implementation of the solar-powered thermoelectric refrigeration system. The merit of this study was achieving of cooling effect for the ambient temperature of 32^{o}C. This paper has experimental results based on its result and it takes more power to cool down 12.5 liters of the box from ambient temperature to 14.28^{o}C.

The author in [24], a solar energy-based temperature-controlled chamber is presented in this paper. In this paper, the Peltier module is used for heating and cooling. Both heating and cooling are done in the same chamber. The minimum temperature achieved was found to be 20^{o}C for cooling and the maximum temperature was 60^{o}C for heating in this experiment. The achieving temperature is not sufficient for vaccine storage. Technically vaccine storage needs a specific range of temperature.

In paper [25] is developed the portable solar thermoelectric refrigerator. This paper uses a solar panel, Peltier module, and battery. And shows that the temperature of the refrigeration was reduced 500ml of water from 27^{o}C to 12^{o}C in approximately 50 min. The coefficient of performance of the refrigerator was calculated and found to be about 0.17 by using 10 modules. As an advantage, it reduces 15^{o}C within an hour but the number of Peltier modules will consume too much power. This may lead to the net weight of the mini-fridge will large, the size of the solar panel will large.

Paper [26] investigated the solar energy-based refrigeration system using the Peltier device. This paper aims that providing a refrigeration system to the remote area where power supply is not accessible by using a thermoelectric module, battery, and solar panel like other but the capacity of the cooling chamber is 7.8L. this paper puts one of the application areas of this system is medical and pharmaceutical equipment. This application is focusing on this research work.

As a summary of the reviewed literature in this section, the thermoelectric refrigeration system takes too much time to meet the desired temperature, designed ambient temperature is low and some of them have taken high power. Based on that, this research can take the merit of each research and overcome the demerit of those reviewed. Tha Table 2-6 show some of the literature comparison based on the performance of the refrigeration system.

Table 2-6 Some literature review comparison

Paper	Temperature range (^oC)	Number of modules	COP	Time required (min)	Advantage	Disadvantage
M. Barawkar et.al	35-5	Multi-stage	-	150min	Reached the lowest temp	Uses large cooling time
K. Rokde et.al	35-15	3	-	570min	Small No. module	Uses large cooling time
Abhijit Raju et.al	27-12	10	0.17	50min	-	Uses large No. of module and cooling time
Jatin Patel et.al	Up to 10	3 Multi-stage	1.21	-	High COP	Needs large size of box

CHAPTER 3

METHODOLOGY

3.1. Introduction

This chapter deals with data collection and analysis; mathematical modeling and selection of the thermoelectric module (Peltier module); cooling load calculation of designed temperature; solar panel selection, sizing, MPPT design using Perturb and observation method, and battery sizing and selection; and temperature controller using Arduino microcontroller. Finally, the system is simulated by using MATLAB software both in Simulink and script.

3.2. Methods

The method used in this thesis to accomplish the required task is shown in Figure 3-1. The closely related papers and literature are reviewed. Then the necessary data used throughout this research are collected and analyzed. This research could follow this method to solve the problem state in chapter one.

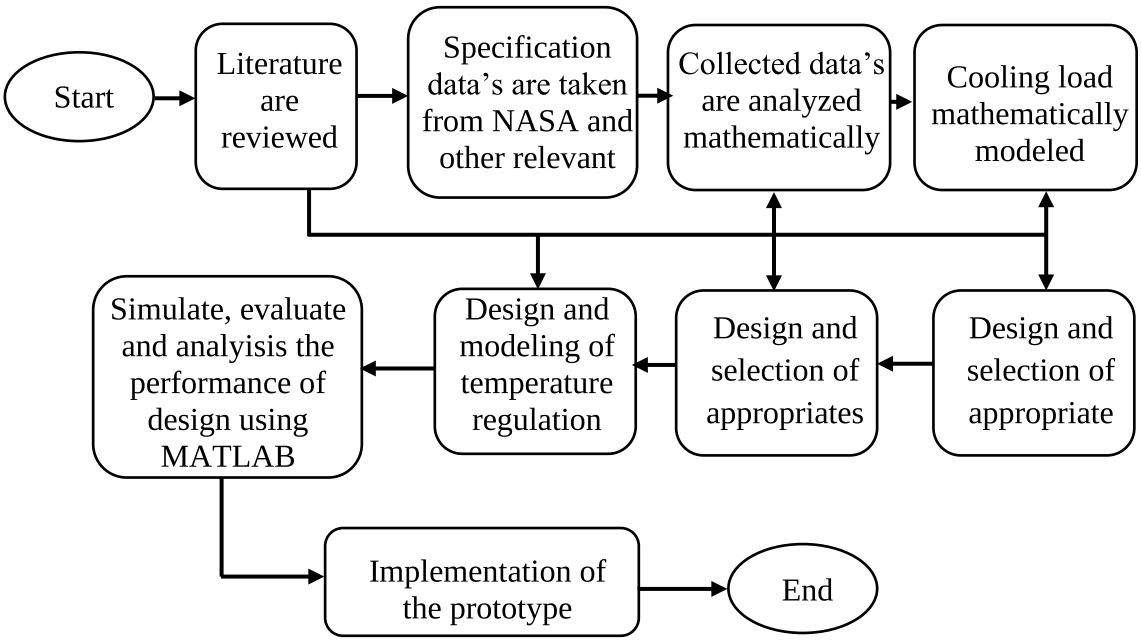

Figure 3-1 Methodology

The block diagram of the developed system shown in Figure 3-2 The purpose of a solar panel of this system is to deliver electrical power to the system. The solar panel power is depending on the irradiation of the environment. So, it will fluctuation according to the variation of the irradiance. The Peltier module needs a regulated DC power supply. To regulate the power solar panel perturbs and observer MPPT technique is used. The heat sink and the fan is integrated into the Peltier module to reduce the difference temperature of each side of the module. Together the MPPT, heat sink, and fan are helping the system achieve maximum COP.

Giving a cooling effect is not enough for this system, the temperature inside the mini-refrigeration system must be regulated. The is a close loop operation is available in the temperature controlling process. The microcontroller takes the action of the temperature regulation process in this system. A temperature sensor called DHT22 play a vital role in the regulation process, it senses the environment and gives the feedback signal to the microcontroller. This microcontroller operates the refrigeration temperature according to the required range. The control action is including the on/ off control of the Peltier module and fan, the LCD temperature display for human interaction, and the indicator of multi-LED to show the status of the temperature.

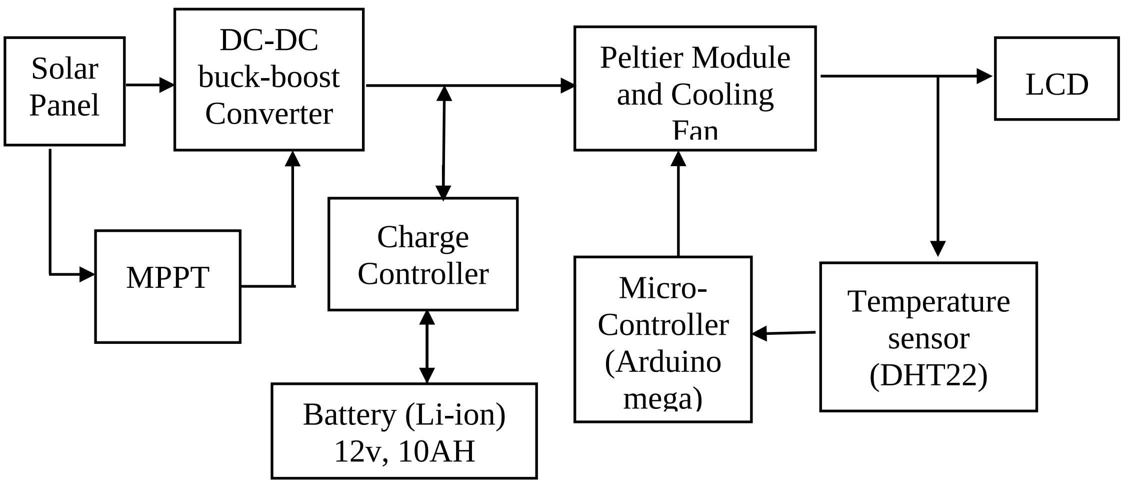

Figure 3-2 System block diagram

3.3. Description of the Case Study Area

Afar is one of the hottest regions in Ethiopia located in northeast Ethiopia have it covers a vast area of 270,000 square km running up the border with Djibouti and Eritrea [L9]. Logiya is one of the towns in the Afar region with a latitude of 11.7559, longitude of 40.95876. Logiya has a low altitude in Afar and hot dry climatic conditions. a total population of 23,300.

3.3.1. Data Gathering

The secondary data used in the design of the solar module and cooling load estimation collected from the National Meteorological Agency Research and Training Center (NMARTC) and the Federal Minister of Health-Ethiopia (FMOH), World Health Organization (WHO), Center for Disease Control and Provision (CDC) and from NASA using the latitude and longitude of the address of the site.

3.3.2. Solar Insolation and Temperature Data

The solar insolation data of Logiya town at Latitude: 11.7559 or (11^{o}48'21''), Longitude: 40.95876, or (40^{o}57'31'') is given in Table 3-1. It is a 30-years meteorological and solar monthly & annual climatologies from January 1984 to December 2013 at two meters [L10].

Table 3-1 Solar insolation and temperature data of Logiya [L10].

Month	Solar Insolation (kW/m^2/day)	Temperature (^{o}C)
JAN	6.46	32.43
FEB	6.33	34.04
MAR	6.25	35.56
APR	6.25	36.59
MAY	6.66	38.87
JUN	6.07	40.38
JUL	5.23	36.69
AUG	5	35.12
SEP	5.65	36.16
OCT	6.7	35.81
NOV	7.75	34.06
DEC	7.23	32.4
ANN	6.3	35.67

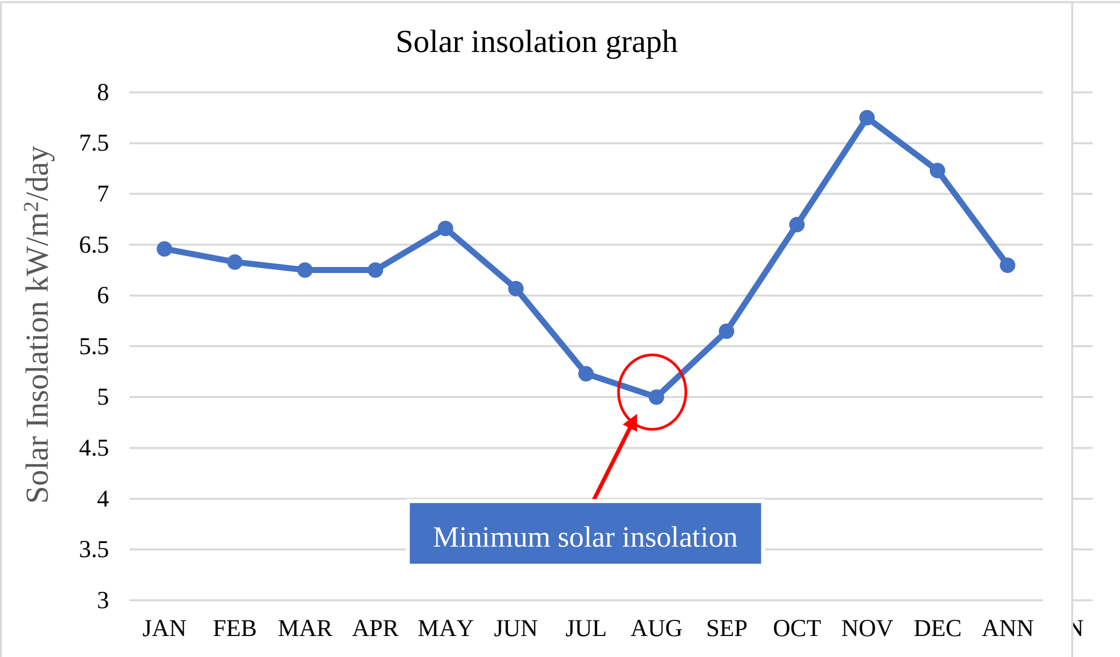

Figure 3-3 Annual solar insolation graph

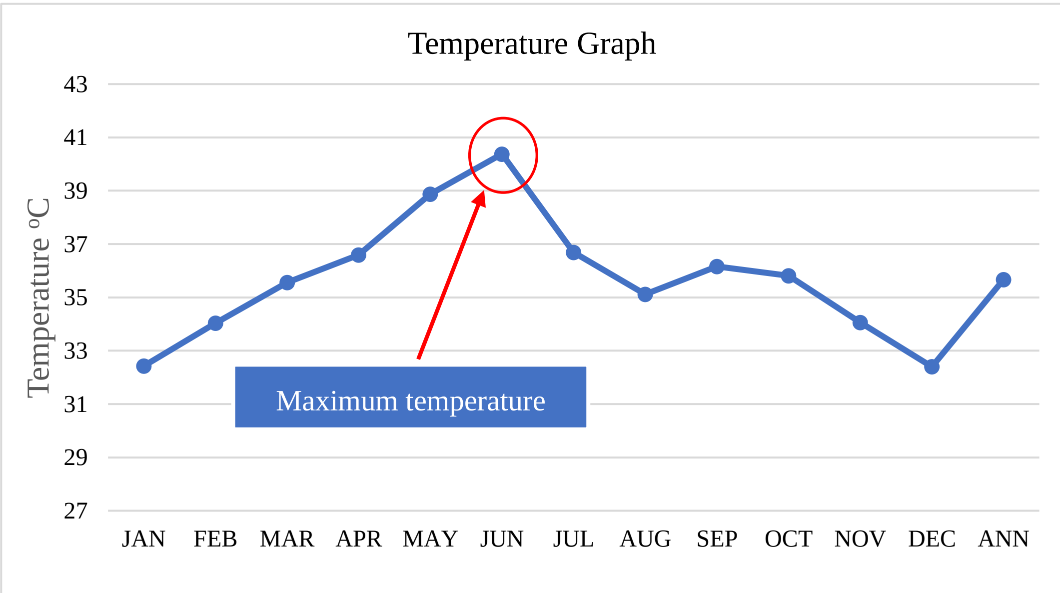

Figure 3-4 Annual temperature graph

3.4. Vaccine Cold Chain System Specifications

The recommended vaccine storage temperatures at each level of the cold chain shown in Figure 3-5. All those who handle vaccines and diluents must know the temperature sensitivities and the recommended storage temperatures for all the vaccines in the national schedule [6]. According to the CDC U.S department of service [27], The refrigerators should maintain temperatures between 2°C and 8°C (36° F and 46° F) and freezers should maintain temperatures between -50° C and -15° C (-58° F and +5° F).

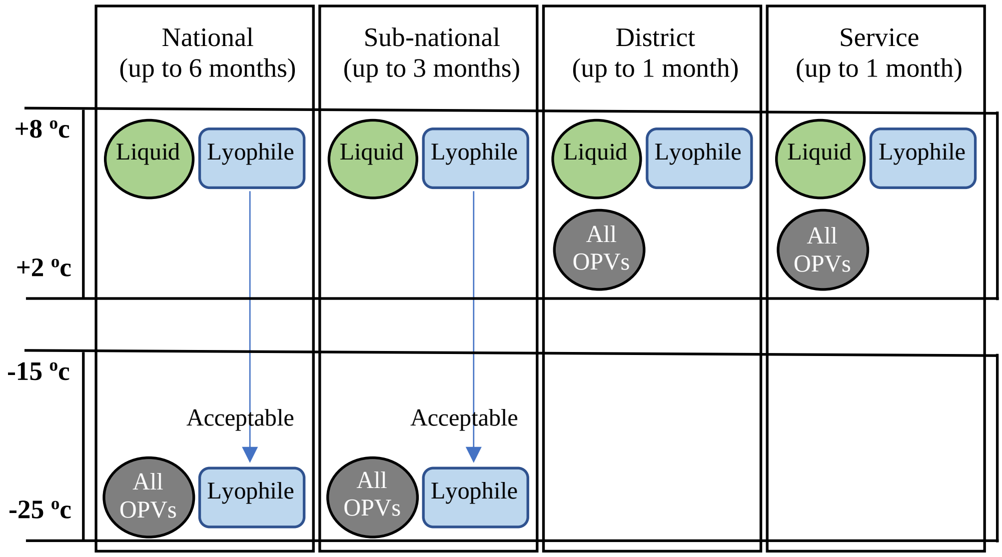

Figure 3-5 Recommended vaccine storage temperatures

3.4.1. Vaccine Storage Temperature

Vaccines can be stored in cold rooms, freezer rooms, refrigerators, or freezers. They are transported in insulated vaccine carriers or refrigerated transport vehicles. Vaccine carriers require a supply of ice packs and sufficient refrigeration capacity to freeze them. Refrigeration and transport equipment should be chosen after considering [28]:

- Space requirements;
- Infrastructure costs;
- Equipment purchases costs;
- Equipment installation costs;
- Running costs;
- Replacement costs.

3.5. Cooling Load Calculation for Vaccine Storage

The total refrigeration load in vaccine transport refrigeration systems have transmission load, product load, internal load, infiltration air load. These loads constitute the net heat load for which a refrigeration framework is to be given. Hence, the net heat load furthermore equipment heat load is the whole refrigeration load for which a Peltier module must be chosen [29].

3.5.1. Transmission Load

Transmission load is heat exchanged into the refrigerated space through its surface. This transmission load can depend on cold box shape, material type, thermal conductivity, insulation thickness and sun effects on each surfaces this can be illustrated in Table 3-2, Table 3-3, and Table 3-4. The sun effect can calculate with the ambient temperature of the selected place which has 40.5^{o}c. The designed temperature is 5°C. The circular shape icebox can capable of holding 7 liters of vaccine and have only one door at the top side. Figure 3-6 shows the selected cold box shape and structure for vaccine storage. This cooler choice is by considering the worst-case design and accessibility in the Ethiopian market.

Table 3-2 Refrigeration icebox specification

Dimension		Internal Material	External Material	Thermal Conductivity
Diameter	Height			
23cm	25.2cm	Polyethylene	Polyethylene	0.033 W/mK

Figure 3-6 Selected cold box

Sensible heat gain through walls, floor, and the ceiling is calculated at a steady state in Equation (3.1)and the overall coefficient of heat transfer U of the sides, floor, and roof can be stated in Equation (3.2) [29]:

$$Q_{trans} = UA\left(T_o - T_i\right) \quad (3.1)$$

$$U = \frac{1}{\frac{x_1}{k_1} + \frac{x_2}{k_2} + \frac{x_3}{k_3}} \text{ for a single material, } U = \frac{1}{\frac{x}{k}} = \frac{k}{x} \quad (3.2)$$

Where Q_{trans} is heat gain (w) by transmission due to temperature difference, A is outside area of section (m^2), T_o is the outdoor temperature (K), T_i is Indoor temperature (K), U is overall coefficient of heat transfer (W/m^2K).

Table 3-3 Allowance for sun effect on light-colored surfaces and Insulation thickness

		Sun effect		Insulation thickness	
		Sun effect (°C)	Surface temperature (°C)	Thickness, x (m)	Thermal conductivity(w/mK)
Roof		5	45.5	0.035	0.033
Floor		0	40.5	0.035	0.033
Sides	East	3	43.5	0.013	0.033
	North	2	42.5	0.013	0.033
	West	3	43.5	0.013	0.033
	South	2	42.5	0.013	0.033

Table 3-4 Transmission load

		Diameter (m)	Height (m)	Area (m^2)	U (w/m^2k)	Adjacent Temp, (K)	ΔT (K)	Transmission load (W)
Roof		0.23	0	0.01323	0.94285	298.15	40.5	0.24938
Floor		0.23	0	0.01323	0.94285	293.15	35.5	0.18704
Sides	East	0.23	0.225	0.05175	2.53846	296.15	38.5	2.36458
	North	0.23	0.225	0.05175	2.53846	295.15	37.5	2.23321
	West	0.23	0.225	0.05175	2.53846	296.15	38.5	2.36458
	South	0.23	0.225	0.05175	2.53846	295.15	37.5	2.23321
Total								7.26743

3.5.2. Product Load

Product load is heat removed from the products brought into the refrigerated space [29]. The heat that must be removed from the product to reduce the product temperature to storage temperature and the heat generated by the products in storage, mainly vaccines. Table 3-5 shows the product load mathematical calculation by using Equation (3.3) and Equation (3.4).

$$Q_{product} = \frac{Q_{remove}}{3600 \times n} \tag{3.3}$$

Where n is allotted time in hrs.

$$Q_{remove} = mc_{p(vaccine)}\left(T_1 - T_2\right) \tag{3.4}$$

Table 3-5 Product load

Mass (m)	Specific heat capacity of vaccine ($c_{p(vaccine)}$)	Actual Temperature	Desired Temperature	Heat Removed	Product Load
7kg	4.17588kJ/kg	T_1=8 °C	T_2=5 °C	175.387kJ	12.181W

The refrigeration capacity required for products brought into storage is determined from the time allotted is 24 hours for heat removal and assumes that the product is properly exposed to remove the heat at that time.

3.5.3. Infiltration Load

Infiltration load is heat gain associated with air entering the refrigerated space. The contribution of the air exchange to the refrigeration load is more complex to assess. Penetration by direct flow through entryways, whereas opening, in refrigerated spaces prepared with always or regularly open entryways, these air flows specifically through the entryway.

The impact is indistinguishable from that of open entryways uncovered to the wind and the heat pick up may be exceptionally huge. The typical air velocity through a door is 0.3 to 1.5 m/s. this infiltration load is calculated in Table 3-6 using Equation(3.5) [29].

$$Q_{inf} = vA\rho_r D_t\left(h_i - h_r\right) \tag{3.5}$$

Table 3-6 Infiltration load

Door dimension (m)	Door area (m^2)	Enthalpy (kJ/kg)		Density (kg/m^3)		Doorway time factor	Velocity m/s	Infiltration load (W)
Diameter	A	h_i	h_r	ρ_r	ρ_i	D_t	v	Q_{inf}
0.23	0.166106	22.1	-4.7	1.41	1.3	0.0043	1.5	5.889

3.5.4. Internal Load

The internal load is warm created by inner sources [29]. All electrical hardware is dissipated warm energy within the refrigerated space. So, this warm must be evacuated from the refrigerated space. For this reason, this refrigeration system uses a BLDC motor that has 1.24W power.

3.5.5. Total Cooling Load

The total cooling load (refrigeration load) of the vaccine transport refrigeration system which has been removed from refrigerated space. Table 3-7 shows the total cooling load of refrigerated space which includes 10% safety protection of the vaccine and answered RQ.1.

Total cooling load = Transmission load + Product load + Infiltration load + Internal load

Table 3-7 Total cooling load

Load Summary	Load (W)
Transmission load	12.466
Product load	12.181
Infiltration load	27.468
Internal load	1.24
Sub-total	53.355
Safety 10%	5.3355
Total Load	58.6905

3.6. Thermoelectric Coolers

This area defines a set of rearranged ideal equations for a thermoelectric cooler, with a few suspicions, to display the common characteristics of thermoelectric coolers. The maximum parameters are characterized, which are the most extreme current, greatest temperature distinction, greatest cooling power, and greatest voltage. At that point, the normalized parameters are plotted as common characteristics for the coolers. The ideal equation is based on three fabric properties: the Seebeck coefficient, electrical resistivity, and thermal conductivity. The basic equation for the rate of heat flows per unit area q was defined as shown in Equation (3.6) [30],

$$\vec{q} = \alpha T \vec{J} - k \vec{\nabla} T \tag{3.6}$$

where α is the Seebeck coefficient, j is the current density, k is the thermal conductivity, and $\vec{\nabla}$ is the gradient. This equation relates the heat flow, the electric current, and the thermal conduction, leading to the steady-state heat diffusion equation [30], which is rewritten as:

$$\vec{\nabla} . \left(k \vec{\nabla} T \right) + j^2 \rho - T \frac{d\alpha}{dT} \vec{J} . \vec{\nabla} T = 0 \tag{3.7}$$

Where ρ is the electrical resistivity. The primary term gives the thermal conduction, the moment term gives the Joule heating, and the third term gives the Thomson effect, which comes about from the temperature-dependent Seebeck coefficient. Equation (3.6) and (3.7) govern thermoelectric phenomena.

Consider a steady-state thermoelectric cooler module as appeared in Figure 3-7. The module comprises of numerous p-type and n-type thermocouples, where one thermocouple (uni-couple) with length L and cross-sectional area A appears in Figure 3-8.

An electrical current is connected and actuates a warm flow at the cold and hot intersection temperatures as appeared. With the suspicions that the Seebeck coefficient is free of temperature, no thermal or electrical contact resistances, and no heat losses [30], Equation (3.7) rearranged to:

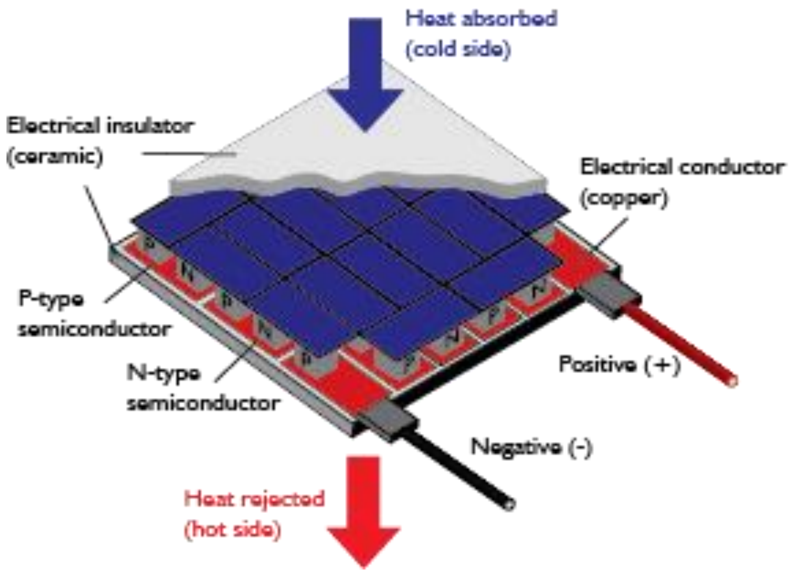

Figure 3-7 Cutaway of a typical thermoelectric module [L11]

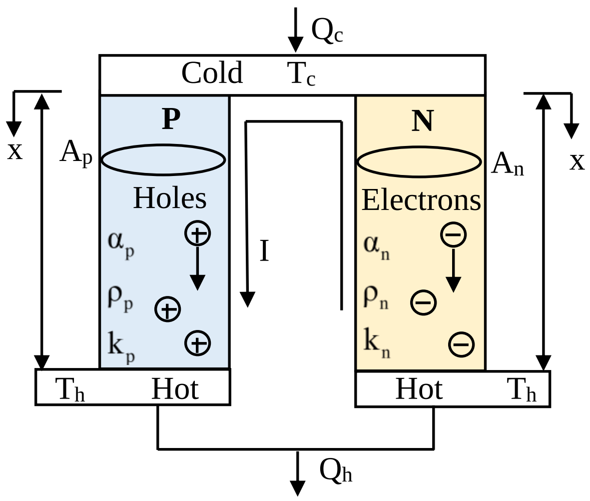

Figure 3-8 Thermoelectric cooler with p-type and n-type thermoelements [L12]

$$\frac{d}{dT}\left(kA\frac{dT}{dx}\right)+\frac{I^2\rho}{A}=0 \tag{3.8}$$

The solution for the temperature gradient with two boundaries ($T_{x=0}=T_c$ and $T_{x=L}=T_h$) is

$$\left.\frac{dT}{dx}\right|_{x=0}=\frac{I^2\rho L}{2A^2k}+\frac{T_h-T_c}{L} \tag{3.9}$$

Equation (3.6) is expressed in terms of p-type and n-type thermocouples [30],

$$Q_c = n^*\left[\left(\alpha_p - \alpha_n\right)T_c I + \left(-kA\left.\frac{dT}{dx}\right|_{x=0}\right)p + \left(-kA\left.\frac{dT}{dx}\right|_{x=0}\right)n\right] \tag{3.10}$$

Where n* is the number of thermocouples.

where n is the number of thermocouples and Q_c is the rate of heat absorbed at the cold junction. Substituting in Equation (3.9) in Equation (3.10) gives

$$Q_c = n\left[\left(\alpha_p - \alpha_n\right)T_c I - \frac{1}{2}I^2\left(\frac{\rho_p L_p}{A_p} + \frac{\rho_n L_n}{A_n}\right) - \left(\frac{k_p A_p}{L_p} + \frac{k_n A_n}{L_n}\right)\left(T_h - T_c\right)\right] \tag{3.11}$$

Finally, the cooling power at the junction of temperature T_c is expressed as

$$Q_c = n\left[\alpha T_c I - \frac{1}{2}I^2 R - K\left(T_h - T_c\right)\right] \tag{3.12}$$

Where,

$$\alpha = \alpha_p - \alpha_n \tag{3.13}$$

$$R = \frac{\rho_p L_p}{A_p} + \frac{\rho_n L_n}{A_n} \tag{3.14}$$

$$K = \frac{k_p A_p}{L_p} + \frac{k_n A_n}{L_n} \tag{3.15}$$

If it assumed that the p-type and n-type thermocouples are similar, we have $R = \rho L/A$ and $K = kA/L$, where $\rho = \rho_p + \rho_n$ and $k = k_p + k_n$. Equation (3.12) is called the ideal equation, which has been widely used in science and industry.

The rate of heat liberated at the hot junction is calculated as:

$$Q_c = n\left[\alpha T_c I - \frac{1}{2}I^2 R - K\left(T_h - T_c\right)\right] \tag{3.16}$$

Considering the first law of thermodynamics over the thermoelectric device,

$$W = Q_h - Q_c \tag{3.17}$$

The amount of work per unit time over the module (rate of work) is gotten substituting Equations (3.12) and (3.16) in Equation (3.17).

$$W = n\left[\alpha I\left(T_h - T_c\right) - I^2 R\right] \tag{3.18}$$

The primary term is the rate of work to overcome the thermoelectric voltage, and the moment term is the resistive loss. Because the power is W= IV, the voltage across the couple will be

$$v = n\left[\alpha\left(T_h - T_c\right) - IR\right] \tag{3.19}$$

The COP is defined as the ratio of the cooling power to the input electrical power.

$$COP = \frac{Q_c}{W} = \frac{n\left[\alpha T_c I - \frac{1}{2} I^2 R - K\left(T_h - T_c\right)\right]}{n\left[\alpha I\left(T_h - T_c\right) - I^2 R\right]} \tag{3.20}$$

For the solar-driven thermoelectric systems, the performance of the whole system ($\eta_{Peltier}$) can be written as the product of the thermoelectric refrigeration system performance (COP) and the PV efficiency (η_{PV}), that is,

$$\eta_{peltier} = COP \times \eta_{PV} \tag{3.21}$$

Two values of the current are of special intrigued: the current I_{mp} that yields the maximum cooling control and the current I_{COP} that yields the maximum COP.

The maximum cooling power can be gotten by differentiating Equation (3.12) with respect to I and setting it to zero. The current for the maximum cooling power is found to be

$$I_{mp} = \frac{\alpha T_c}{R} \tag{3.22}$$

The optimum COP can be obtained by differentiating Equation (3.20) and setting it to 0.

$$\frac{d\left(COP\right)}{dI} = 0$$

Therefore, the COP current can be written as:

$$I_{COP} = \frac{\alpha \Delta T}{R\left(\sqrt{1+Z\overline{T}} - 1\right)} \tag{3.23}$$

Where $\Delta T = T_h - T_c, Z = \frac{\alpha^2}{\rho K}$ and $\overline{T}$ is the average temperature of T_c and T_h. In terms of T_h, ZT is expressed by:

$$Z\overline{T} = ZT_h\left(1 - \frac{\Delta T}{2T_h}\right) \tag{3.24}$$

3.6.1. Maximum Parameters

Let us consider a thermoelectric module shown in Figure 3-7 with the theoretical maximum parameters in the ideal equation. The module comprises of a few thermocouples as appeared. The ideal equation accepts that there are no electrical or thermal contact resistances, no Thomson effect, and no radiation or convection. It is noted that the theoretical maximum parameters might vary from the manufacturers' maximum parameters that are as a rule gotten through estimations.

The maximum current I_{max} is the current that produces the maximum possible temperature difference ΔT_{max}, which always occurs when the cooling power is at 0. This is obtained by setting Q_c is 0 in Equation (3.12), replacing T_c with (T_h ΔT), taking the derivative of ΔT concerning I, and setting it to 0. The maximum current is finally expressed by

$$I_{max} = \frac{\alpha}{R}\left(\sqrt{\left(T_h + \frac{1}{Z}\right)^2 - T_h^{\,2}} - \frac{1}{Z}\right) \tag{3.25}$$

ΔT_{max} is the maximum possible temperature difference ΔT_{max}, which always occurs when the cooling power is 0 and the current is maximum. This is obtained by setting Q_c 0 in Equation (3.12), substituting both I and T_c by I_{max} and T_h ΔT_{max}, respectively, and solving for ΔT_{max}. The maximum temperature difference is obtained as

$$\Delta T_{max} = \left(T_h + \frac{1}{Z}\right) - \sqrt{\left(T_h + \frac{1}{Z}\right)^2 - T_h^2} \tag{3.26}$$

where the figure of merit Z (unit: K^{-1}) is given by:

$$Z = \frac{\alpha^2}{\rho k} = \frac{\alpha^2}{RK} \qquad (3.27)$$

Using Equation (3.26), I_{max} may be written as:

$$I_{max} = \frac{\alpha\left(T_h - \Delta T_{max}\right)}{R} \qquad (3,28)$$

The maximum cooling power $Q_{c\,max}$ is the maximum thermal load that occurs at $\Delta T = 0$ and $I = I_{max}$. This can be obtained by substituting both I and Tc in Equation (3.12) by I_{max} and Th, respectively, and solving for $Q_{c\,max}$. The maximum cooling power for a thermoelectric module with n thermocouples is

$$Q_{cmax} = \frac{n\alpha^2\left(T_h^2 - \Delta T_{max}^2\right)}{2R} \qquad (3.29)$$

The maximum voltage is the DC voltage that delivers the maximum possible temperature difference ΔT_{max} at $I = I_{max}$. The maximum voltage is obtained from Equation (3.19), which is shown in Equation (3.30).

$$V_{max} = n\alpha T_h \qquad (3.30)$$

3.6.2. Design for Specification Cooling

A Peltier cooler is designed as a green energy replacement for the conventional cold box type storage. A thermoelectric module with heat sinks consists of n = 127 p-type and n-type thermocouples, one of which is shown in Figure 3-8. An electric current is applied in a way that a heat flow (cooling power) should be absorbed at the cold junction temperature of 5°C and liberated at the hot junction temperature of 40.5°C.

The TEC material of bismuth telluride (Bi_2Te_3) is used having the properties as $\alpha_p = \alpha_n = 200$ μV/K, $\rho_p = \rho_n = 1.0 \times 10^{-3}$Ωcm, and $k_p = k_n = 1.52 \times 10^{-3}$/ cmK. The cross-sectional area and leg length of the thermoelement are $A_n = A_p = 2mm^2$ and $L_n = L_p = 1$ mm, respectively. Assuming that the cold and high junction temperatures are steadily maintained.

$$\alpha = \alpha_p - \alpha_n = 400\times10^{-6}\,V/K$$

Material properties: $$\rho = \rho_p + \rho_n = 2.0\times10^{-5}\,\Omega m$$

$$k = k_p + k_n = 3.04 w/mK$$

The number of thermocouples is n = 127. The hot and cold junction temperatures are:

$$T_h = (40.5 + 273.15)K = 313.65K$$

$$T_c = (5 + 273.15)K = 278.15K$$

$$\Delta T = T_h - T_c = 313.65K - 278.15K = 35.5K$$

Using Equation (3.27) the figure of merit is:

$$Z = \frac{\alpha^2}{\rho k} = \frac{\left(400x10^{-6}\,v/K\right)^2}{\left(2.0x10^{-5}\,\Omega m\right)\times\left(3.04w/mK\right)} = 2.632\times10^{-3}\,K^{-1}$$

Also, the dimensionless figure of merit is:

$$ZT_c = \left(2.632x10^{-3}\,K^{-1}\times278.15K\right) = 0.732$$

The resistance R and the thermal conductance K are calculated by using Equation (3.14) and Equation (3.15)

$$R = \frac{\rho L}{A} = \frac{\left(2.0\times10^{-5}\,\Omega m\right)\times\left(1\times10^{-3}\,m\right)}{2.0\times10^{-6}\,m^2} = 0.01\Omega$$

$$K = \frac{kA}{L} = \frac{\left(3.04w/mK\right)\times\left(2.0\times10^{-6}\,m^2\right)}{1\times10^{-3}\,m} = 6.08x10^{-3}\,w/K$$

3.6.2.1. Maximum Cooling Power

Using Equation (3.21), the current for the maximum cooling power is

$$I_{mp} = \frac{\alpha T_c}{R} = \frac{\left(400\times10^{-6}\,v/K\right)\times\left(278.15K\right)}{0.01\Omega} = 11.126A$$

Using Equation (3.12), the maximum cooling power can be written as:

$$Q_{c\,mp} = n\left(\alpha T_c I_{mp} - \frac{1}{2} I_{mp}^2 R - K\Delta T\right)$$

$$Q_{c\,mp} = (127)\left[\begin{array}{c}\left(400\times10^{-6}\,v/K\right)(278.15K)(11.126A)) - \frac{1}{2}(11.126A)^2 \times (0.01\Omega) \\ -\left(6.08x10^{-3}\,w/K\right)\times(35.5K)\end{array}\right]$$

$$Q_{cmp} = 51.596W$$

Using Equation (3.18), the power input can be written as:

$$W_{i\,mp} = n\left(\alpha I_{mp}\left(T_h - T_c\right) + I_{mp}^2 R\right)$$

$$W_{i\,mp} = (127)\left[\left(400\times10^{-6}\,v/K\right)(11.126A)(35.5K) + (11.126A)^2 \times (0.01\Omega)\right]$$

$$W_{i\,mp} = 178.671W$$

Using Equation (3.20), the COP at the maximum cooling power is

$$COP = \frac{Q_{c\,mp}}{W_{i\,mp}} = \frac{51.596W}{178.671W} = 0.289$$

Using Equation (3.21) the total energy efficiency of the system is

$$\eta_{Peltier} = COP \times \eta_{PV} = 0.289 \times 0.19 = 0.055 = 5.5\%$$

3.6.2.2. Maximum COP

$$Z\overline{T} = Z\frac{T_h + T_c}{2} = \left(2.632\times10^{-3}K^{-1}\right)\times\frac{596.8K}{2} = 0.785$$

Using Equation (3.22), the current for the maximum COP can be obtained as:

$$I_{cop} = \frac{\alpha\Delta T}{R\left(\sqrt{1+Z\overline{T}} - 1\right)} = \frac{\left(400\times10^{-6}\,v/K\right)\times(35.5K)}{(0.01\Omega)\left(\sqrt{1+0.786} - 1\right)} = 4.224A$$

Using Equation (3.12), the maximum cooling power can be obtained as:

$$Q_{c\,cop} = n\left(\alpha T_c I_{cop} - \frac{1}{2} I_{cop}^2 R - K\Delta T\right)$$

$$Q_{c\,cop} = (127)\begin{bmatrix} \left(400\times10^{-6}\,v/K\right)\left(278.15K\right)\left(4.224A\right)) - \frac{1}{2}\left(4.224A\right)^2\times\left(0.01\Omega\right) \\ -\left(6.08x10^{-3}\,w/K\right)\times\left(35.5K\right) \end{bmatrix}$$

$$Q_{c\,cop} = 21.107W$$

Using Equation (3.18), the maximum input power can be obtained as:

$$W_{i\,cop} = n\left(\alpha I_{cop}\left(T_h - T_c\right) + I_{cop}^2 R\right)$$

$$W_{i\,cop} = (127)\left[\left(400\times10^{-6}\,v/K\right)\left(4.224A\right)\left(35.5K\right) + \left(4.224A\right)^2\times\left(0.01\Omega\right)\right]$$

$$W_{i\,cop} = 30.516W$$

Using Equation (3.20), the COP at the maximum cooling power can be determined as:

$$COP = \frac{Q_{c\,cop}}{W_{i\,cop}} = \frac{21.107W}{30.516W} = 0.692$$

Using Equation (3.21) the total energy efficiency of the system can be obtained as:

$$\eta_{Peltier} = COP\times\eta_{PV} = 0.692\times0.19 = 0.132 = 13.2\%$$

3.6.2.3. Optima (mid-point) Design

$$I_{mid} = \frac{I_{mp} + I_{cop}}{2} = \frac{11.126A + 4.224A}{2} = 7.675A$$

Using Equation (3.12), the maximum cooling power can be determined as:

$$Q_{c\,mid} = n\left(\alpha T_c I_{mid} - \frac{1}{2} I_{mid}^2 R - K\Delta T\right)$$

$$Q_{c\,mid} = (127)\begin{bmatrix} \left(400\times10^{-6}\,v/K\right)\left(278.15K\right)\left(7.675A\right)) - \frac{1}{2}\left(7.675A\right)^2\times\left(0.01\Omega\right) \\ -\left(6.08x10^{-3}\,w/K\right)\times\left(35.5K\right) \end{bmatrix}$$

$$Q_{c\,mid} = 43.975W$$

Using Equation (3.18), the maximum input power can be obtained as:

$$W_{i\,mid} = n\left(\alpha I_{mid}\left(T_h - T_c\right) + I_{mid}^2 R\right)$$

$$W_{i\,mid} = (127)\left[\left(400\times10^{-6} v/K\right)\left(47.675A\right)\left(35.5K\right) + \left(7.675A\right)^2 \times\left(0.01\Omega\right)\right]$$

$$W_{i\,mid} = 89.349W$$

Using Equation (3.20) the COP at the maximum cooling power can be determined as:

$$COP = \frac{Q_{c\,mid}}{W_{i\,mid}} = \frac{43.975W}{89.349W} = 0.482$$

Using Equation (3.21) the total energy efficiency of the system can be obtained as:

$$\eta_{Peltier} = COP\times\eta_{PV} = 0.482\times0.19 = 0.092 = 9.2\%$$

In the result that gets using Equations (3.12), (3.18), and (3.20) the maximum cooling power accompanies the very low COP, while the maximum COP accompanies very low cooling power. These lead to uneconomical results. The midpoint of current between the maximum COP and maximum cooling power gives reasonable values for both. The cooling design intrinsically demands both a high COP and a high cooling power. The summary of results shown in Table 3-8

Table 3-8 Summary of the results

Parameters	Maximum Cooling Power (mp)	Maximum COP (cop)	Midpoint (mid)
Current, I_i (A)	11.126	4.224	7.675
Cooling power, Q_c (W)	51.586	21.107	43.975
Power input, W_i (W)	178.671	30.516	89.349
COP	0.289	0.692	0.482
Efficiency $\eta_{Peltier}$ (%)	5.5	13.2	9.2
Voltage, V_i (V)	16.059	7.224	11.642
Number of modules (N)	1.13 = 2	2.78 = 3	1.33 = 2

3.6.3. Electric Motor

The purpose of electric motors in this thesis work is to distribute the cooling air inside the icebox and diffused out the hot air to achieve minimum temperature difference and the safety of the Peltier module. The working principle of the motor is converting electrical power to mechanical power in the form of rotary motion. This electromechanical system is characterized by a few specific parameters. These parameters incorporate the no-load and stall speed, torque, current, and voltages, as well as the power factor, and can be gotten employing a power analyzer.

Each of the three parameters, RPM, voltage, and current, have a direct relationship with torque, and so, three important connections can be derived; the motor's torque-RPM slope, the torque-current slope, as shown in Figure 3-9. Varieties of electric motors are classified and differentiated by power sources. Among them a few of the points of interest being to select the fan motor:

- Easy installation
- Speed control over a wide range
- Quick starting, stopping, reversing, and acceleration
- High starting torque and Linear speed-torque curve

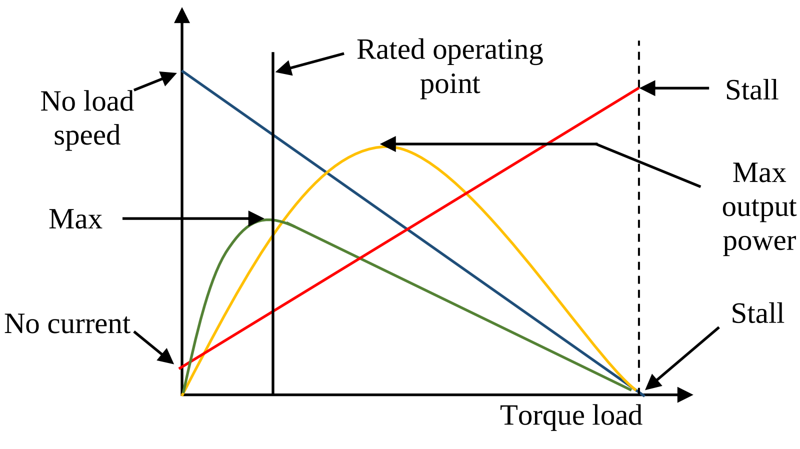

Figure 3-9 BLDC motor torque-RPM slope, the torque-current slope, torque-power, and torque efficiency graph [L13]

A basic comparison of various machine parameters of a BLDC motor with DC and IM motors and have highlighted the advantages of the BLDC motor over the other types. The comparison describes widely accepted compared to the other types for the most use of the applications. The comparison shows BLDC motor can replace all the other types owing to its wide range of merits and its capability to be applied to almost all small application system where a motor is required. This comparison is shown in Table 3-9.

Table 3-9 Comparison of BLDC moto with IM motor [31] [32] [33]

Feature	BLDC motor	Brushed DC motor	Induction motor (IM)
Power supply	Dc power	Dc power	Ac power
Output power	High	Moderate	Relatively low
Efficiency	High	Moderate	Low
Speed range	Hight	Moderate	Low
Dynamic response	Fast	Slow	Low
System cost	Moderate	Low	Low

Depending on the power supply and the performance comparison shown in Table 3-9, this research work selects a BLDC motor for the proposed system. BLDC has high efficiency, high-speed range, high dynamic response, and little maintenance. Not only the performance comparison but also the availability in the market and BLCD can available in small sizes, the foremost well-known sort is 12 and 24V. This research paper selected a small BLDC fan with the power of 1.24W [L14].

3.7. Solar Panel Selection and Sizing

The sizing of the photovoltaic framework has the coherent, to begin with, step is to consider the energy request. Hence, a standalone PV framework sizing starts at the stack side and continues back to the PV clusters. The reason is, to begin with, to choose the framework loads required and after that to choose the measure of the PV module, converter, and battery that are required to meet the energy request from the load side. The sizing technique of the PV framework is shown in Figure 3-10. The sizing of the photovoltaic system has the logical first step is to consider the energy demand. Thus, a primarily standalone PV system sizing begins at the load side and proceeds back to the PV arrays.

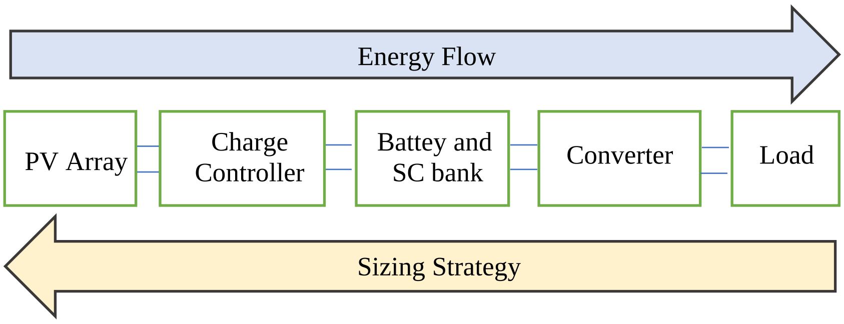

Figure 3-10 Sizing strategy for a standalone system

3.7.1. Solar Panel Sizing

Before going to the solar panel sizing it has to decide the load of the refrigeration system. Based on Table 3-7 the total cooling load required for vaccine storage is 58.6905W and based on Table 3-8 the individual Peltier module gives 21.107W cooling power, 3 Peltier modules, and 30.516W input power is required. Additionally, the load of electronics that use in the developed model has a BLDC fan that has 1.24W and Arduino microcontroller has 0.29W. The total power use for this refrigeration system is 94.318W. The summary total load of the refrigeration system has shown in Table 3-10.

Table 3-10 Total input power estimation

Equipment	Power (W)
Peltier modules	3 x 30.516
BLDC motor	2 x 1.24
Arduino microcontroller	0.29
Total input power	94.318

Before calculating the energy, based on the size, the brand, and the weight of the thermoelectric fridges usually take up to 1 hour to get cold. Not only short cooling time but also its store and hold the inside temperature (which is 5°C) about 4 hours. This condition is allowed to use a thermoelectric fridge at home or outside the home [L15]. By considering this situation the total energy is calculating as follows

$$\text{Total Energy} = \text{Total Power} \times \text{Total Working Time} \quad (3,31)$$

$$\text{Total Energy} = 94.318\ \text{W} \times 2\ \text{hr} = 0.1887\ \text{kWh / day}$$

G_{min} = 5000Wh /m^2 = day, considering summer season

$$P_{pv} = \frac{E_{pv}}{G_{min}} \times 1000 W / m^2 \quad (3.32)$$

$$P_{pv} = 35.044 W_P$$

The selected solar module is a 12V 45W Polycrystalline Silicon solar panel that has 21.24V open-circuit voltage (V_{oc}) 2.75A Short circuit current (I_{sh}), and 36 Polycrystalline cells.

$$FF = \frac{\text{Max.power\_from\_solar\_module}}{I_{sc} \times V_{oc}} \quad (3.33)$$

$$FF = \frac{45}{2.75A \times 21.24V}$$

$$FF = 0.72$$

$$PV_{array}(w) = \text{fill\_factor}(FF) \times PV_{array(wp)}$$

$$PV_{array}(w) = 0.72 \text{ x } 35.044W$$

$$PV_{array}(w) = 25.219W$$

The total number of modules is, $N_m = \frac{PV_{array\_size}(W)}{\text{Rating\_per\_module}}$ (3.34)

$$N_m = \frac{25.219W}{45W} = 0.563 \approx 1$$

The total number of modules is required for this system is 1.

3.7.2. Battery Sizing and Selection

The vaccine needs an effective storage system throughout vaccination time. The storage refrigeration system always has a back-up plan and alternative storage if the fridge needs to work in the night time and a supply power failure occurs. Battery storage has taken the responsibility of the back-up plan to store the vaccine. A battery is a storage device which used to store a DC source. By considering the specific energy, the efficiency, the charging time, and the temperature variation of the are lithium-ion (Li-ion) battery is selected shown in Table 2-5. This research work is selected a 12V 10AH lithium-ion battery based on Equation (3.35). The total capacity of the battery is calculated as follows,

$$C_{AH} = \frac{EL \times AD}{\eta_{bat} \times \eta_{conv} \times V_n \times DOD} \tag{3.35}$$

$$C_{AH} = \frac{0.0943kWh/day \times 1day \times 1000}{0.99 \times 0.96 \times 12v \times 0.8} = 9.7AH \approx 10Ah$$

Where EL = 0.0943 kWh/day, AD = 1 day, V_n = 12v, $\eta_{bat} = 0.99$ v, $\eta_{conv} = 0.96$, and $DOD = 80\% = 0.8$.

- The charging time required for the battery calculated as follows,

$$\text{Charging Time} = \frac{\text{AH(Amper\_Hour)}}{\text{I(current)}} = \frac{10AH}{10A} = 1 \text{ hour is required} \tag{3.36}$$

- The selected solar charge controller is 12V/ 17A. The System charge controller os the battery calculated as follows,

$$\text{Charge controller}, (I_{tot}) = I_{sc} \times V_{oc} \times \text{oversize factor} \tag{3.37}$$

$$\text{Charge controller}, (I_{tot}) = 14A \times 1 \times 1.2 = 16.92A \approx 17A$$

$$\text{Number of charge controller} = \frac{\text{Total current}}{\text{Selected charge controller}}$$

$$\text{Number of charge controller} = \frac{16.92A}{17A} = 0.995 \approx 1$$

3.7.3. Modeling of PV Cells

Two diode model comprising series resistance (R_s) and shunt resistance (R_{sh}) is shown in Figure 3-11. Two diodes D_1 and D_2 are connected in parallel, having saturation current I_{s1} and

I_{s2}, the diode factor A_1 and A_2 respectively. Photocurrent (I_{ph}) is generated by the current source which is dependent on radiation. Resistance R_s is connected in series and R_{sh} is connected in parallel.

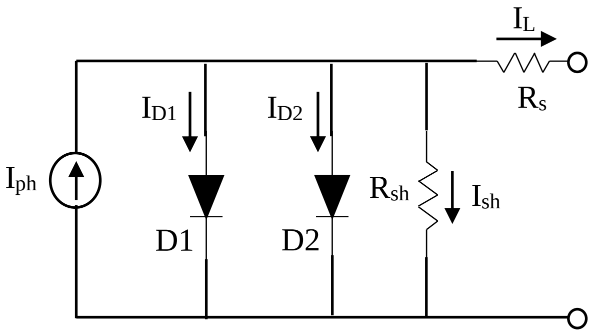

Figure 3-11 Circuit Diagram for two diode model with series and shunt resistance [L16]

The output current I_{pv}/I_L is given by the following equation,

$$I_{pv} = I_{ph} - I_{d1} - I_{d2} - I_{sh} \tag{3.38}$$

Current from second diode D_1,

$$I_{d1} = I_{s1}[\exp(\frac{q(V_{pv} + R_s \times I_{pv})}{A_1 \times K \times T}) - 1] \tag{3.39}$$

Current from second diode D_2,

$$I_{d2} = I_{s2}[\exp(\frac{q(V_{pv} + R_s \times I_{pv})}{A_2 \times K \times T}) - 1] \tag{3.40}$$

The shunt current I_{sh} is given by,

$$I_{sh} = \frac{V_{pv} + R_s \times I_{pv}}{R_{sh}} \tag{3.41}$$

So, the characteristics of the solar cell with double diode D_1 and D_2 with series R_s and shunt R_{sh} resistance is given as:

$$I_{pv} = I_{ph} - I_{s1}\left[\exp\left(\frac{q\left(V_{pv} + R_s \times I_{pv}\right)}{A_1 \times K \times T}\right) - 1\right] - I_{s2}\left[\exp\left(\frac{q\left(V_{pv} + R_s \times I_{pv}\right)}{A_2 \times K \times T}\right) - 1\right] - \frac{V_{pv} + R_s \times I_{pv}}{R_{sh}} \tag{3.42}$$

The output power P is given by:

$$P = V_{pv}\left(\begin{array}{l} I_{ph} - I_{s1}\left[\exp\left(\dfrac{q\left(V_{pv}+R_s\times I_{pv}\right)}{A_1\times K\times T}\right)-1\right]-I_{s2} \\ \left[\exp\left(\dfrac{q\left(V_{pv}+R_s\times I_{pv}\right)}{A_2\times K\times T}\right)-1\right]-\dfrac{V_{pv}+R_s\times I_{pv}}{R_{sh}} \end{array}\right) \tag{3.43}$$

The photovoltaic system displays a nonlinear current-voltage (I-V) and power-voltage (P-V) characteristics. These characteristics vary with the radiation intensity (G) and cell temperature (T). The dependence of photovoltaic power generated by a PV module is shown in the current-voltage (I-V) and power-voltage (P-V) characteristics as shown in Figure 3-12.

3.7.3.1. MPPT Techniques used in Solar PV System

The yield characteristics of a PV array are impacted by the natural components and the transformation efficiency is low. There are a few strategies accessible, which can move forward efficiency by adjusting the source and load properly. The Maximum Power Point Tracking (MPPT) is one such method, which has huge significance within the time of Photovoltaic Technology. These days this technique is unfathomably utilized to create the greatest conceivable power from a changing source beneath variable temperature and irradiance conditions.

As per the maximum power transfer theorem, the maximum power is conveyed to load when source inner impedance matches load impedance. For deciding MPPT suitable tracker is presented between the PV framework and load. It is to be designed that gives a great execution, quick response, and fewer variances. Since the efficiency of the PV is influenced by the panel’s irradiance and temperature which are stochastic and unpredictable.

A DC-DC converter serves the reason for exchanging maximum power from the solar PV module to the load. A DC-DC converter acts as an interface between the load and the module. The basic block diagram of the MPPT system is shown in Figure 3-13 and Figure 3-14.

.

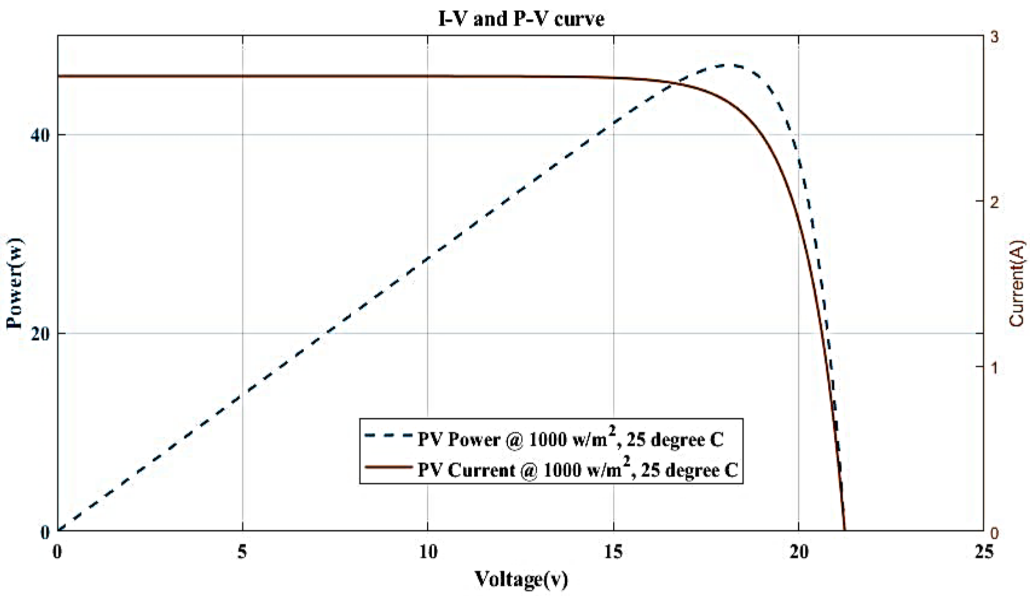

Figure 3-12 Characteristics of PV Module 45 Wp/12Volt

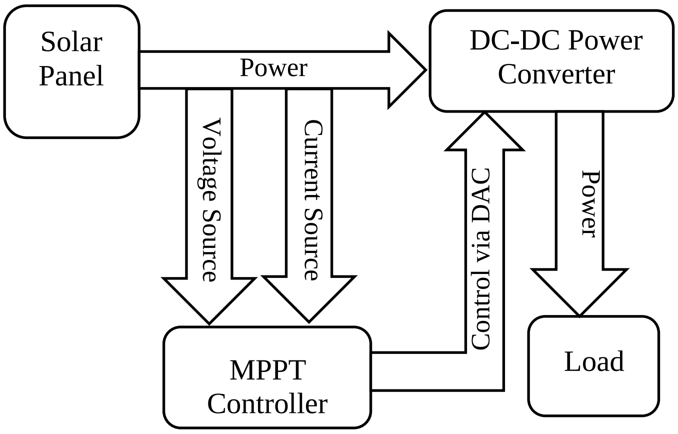

Figure 3-13 Block diagram of the MPPT system

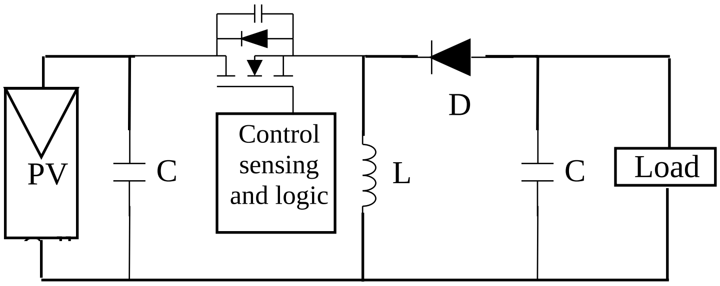

Figure 3-14 Block diagram of typical MPPT system

Several MPPT methods exist to maximizing output power. Those methods' characteristics of MPPT techniques are states in Table 3-11. Among all the MPPT methods, Perturb and Observe (P and O) commonly utilized since of its straightforward usage and lesser time to track the maximum power point additionally other financial reasons. Due to the complexity and detected parameter this research work has chosen the P and O MPPT procedure.

Table 3-11 Characteristics of different MPPT techniques

MPPT technique	Convergence Speed	Implementation complexity	Periodic Tuning	Sensed parameters
P & O	Varies	Low	No	Voltage
IC	Varies	Medium	No	Voltage, current
Fractional VOC	Medium	Low	Yes	Voltage
Fractional ISC	Medium	Medium	Yes	Current
Fuzzy Logic	Fast	High	Yes	Varies

3.7.3.1. Perturb and Observe MPPT Method

The P&O algorithms work by periodically perturbing (i.e. incrementing or decrementing) the array terminal voltage or current and comparing the PV output power with that of the past perturbation cycle. In the event that the PV array working voltage changes and power increments ($dP/dV > 0$), the control framework moves the PV array working point in that heading; something else the working point is moved within the inverse course. Within another perturbation cycle, the algorithm proceeds in the same way.

In certain circumstances, like changing climatic conditions and alter in irradiance the maximum power point shifts from its ordinary working point on the PV curve. In another cycle, it changes its direction and goes absent from the maximum power point and comes about in different nearby maxima at the same point. So, the maximum power point deviates from its original position. P and O MPPT techniques can follow the following algorithm. This algorithm is represented in a flow chart which is given in Figure 3-15.

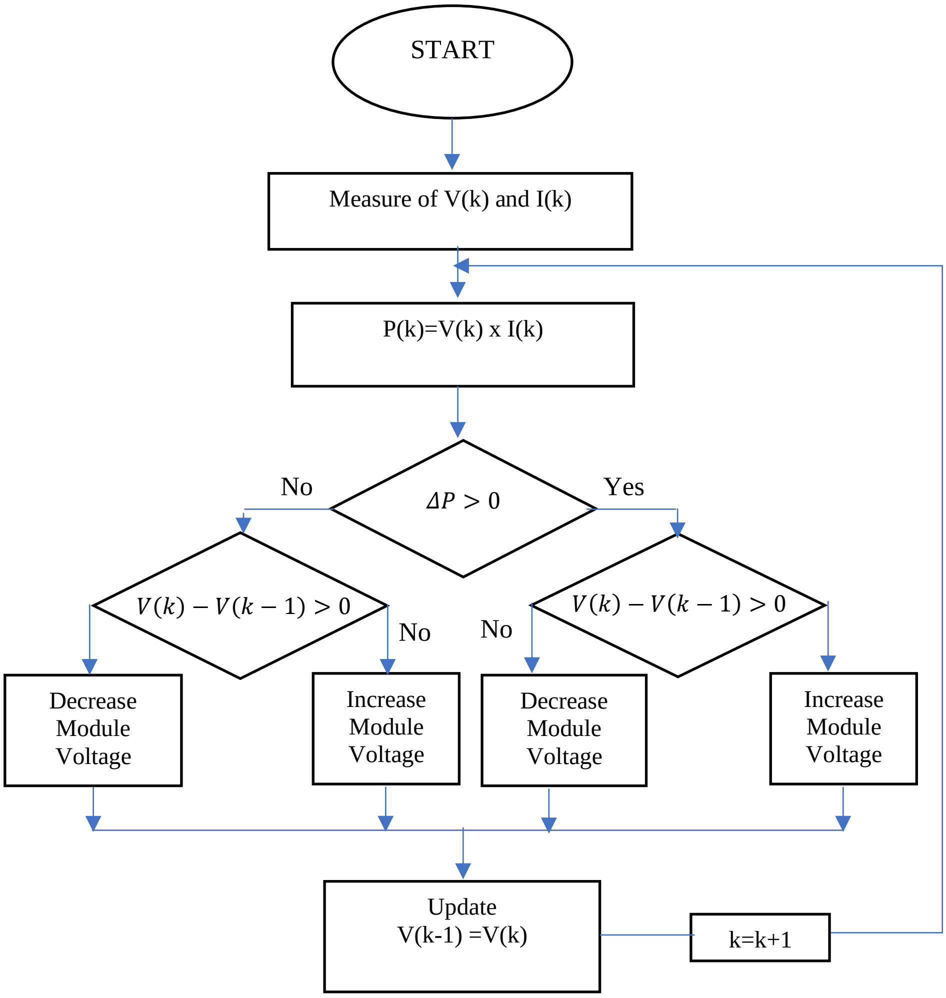

Figure 3-15 Flow chart of Perturb and Observe the MPPT algorithm

3.7.4. DC-DC Converter for Solar PV System

The DC-DC converter was utilized to supply a controlled DC output with the given DC input. These are broadly utilized as an interface between the photovoltaic panel and the load in photovoltaic producing frameworks. The load must be balanced to match the current and voltage of the sun-based board to provide maximum power.

DC-DC converters are depicted as power electronic switching circuits since they change over one level of voltage to another. These may apply to the transformation of different voltage levels. By and large, different basic types of converters are responsible as per their utilize. In this way, this research work has chosen a buck-boost converter to meet the wants of the power supply. The basic buck-boost converter block diagram is shown in Figure 3-16.

.

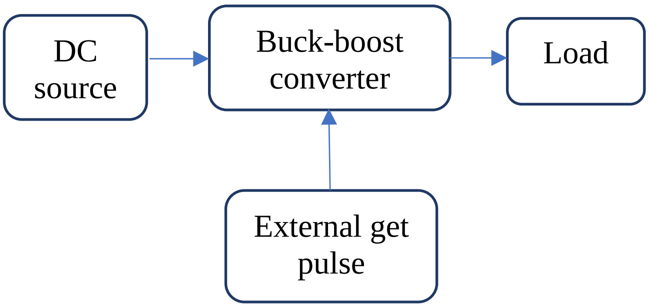

Figure 3-16 Block diagram model of the boost converter

3.7.4.1. Modeling of the Buck-Boost Converter

The DC-DC buck-boost converter circuit shown in Figure 3-17 consists of Inductor (L), Diode (D), Capacitor (C), a load resistor (R_L), the control switch(S). These components are connected in such a way with the input voltage source (V_{in}) to step up the voltage. The output voltage of the buck-boost converter can be either higher or lower than the input voltage. The duty cycle of the control switch controls the output voltage of the buck-boost converter. Hence by varying the ON time of the switch, the output voltage can be varied [34].

Analysis for the switch closed (DT**): -** When the switch is closed as shown in Figure 3-18, the voltage across the inductor is:

$$V_L = V_s = L\frac{di_L}{dt} \tag{3.44}$$

$$\frac{di_L}{dt} = \frac{V_s}{L}$$

The rate of change of inductor current is a constant, indicating a linearly increasing inductor current. The preceding equation can be expressed as:

$$\frac{\Delta i_L}{\Delta t} = \frac{\Delta i_L}{DT} = \frac{V_s}{L} \tag{3.45}$$

Solving for Δi_L when the switch is closed gives

$$(\Delta i_L)_{closed} = \frac{V_s DT}{L} \tag{3.46}$$

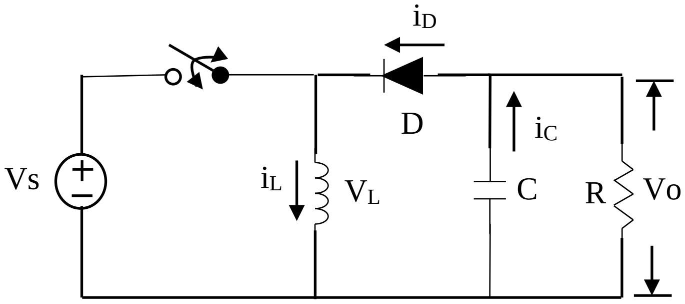

Figure 3-17 Circuit diagram of the DC-DC converter

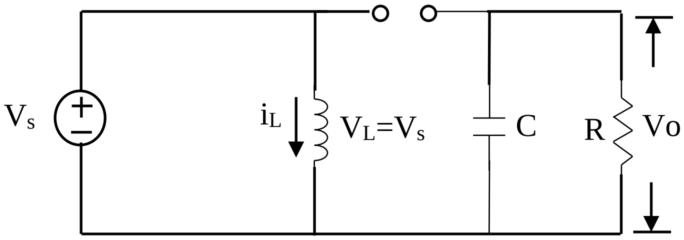

Figure 3-18 Equivalent circuit for switched closed

Analysis for the switch open ((1-D)T): - When the switch is open as shown in Figure 3-19, the current in the inductor cannot change instantaneously, resulting in a forward-biased diode and current into the resistor and capacitor. In this condition, the voltage across the inductor is expressed as follows:

$$V_L = V_o = L\frac{dI_L}{dt}$$
$$\frac{dI_L}{dt} = \frac{V_o}{L} \tag{3.47}$$

Again, the rate of change of inductor current is constant, and the change in current is

$$\frac{\Delta i_L}{\Delta t} = \frac{\Delta i_L}{(1-D)T} = \frac{V_o}{L} \tag{3.48}$$

$$(\Delta i_L)_{open} = \frac{V_o(1-D)T}{L} \tag{3.49}$$

For steady-state operation, the net change in inductor current must be zero over one period and it is expressed using Equation (3.46) and (3.49)

$$(\Delta i_L)_{closed} + (\Delta i_L)_{open} = 0$$

$$\frac{V_s DT}{L} + \frac{V_o(1-D)T}{L} = 0$$

Solving for ΔV_o using Equation (3.50)

$$V_o = -V_s\left(\frac{D}{1-D}\right) \qquad (3.50)$$

The required duty ratio for specified input and output voltages can be expressed as [34]

$$D = \frac{|V_o|}{V_s + |V_o|} \qquad (3.51)$$

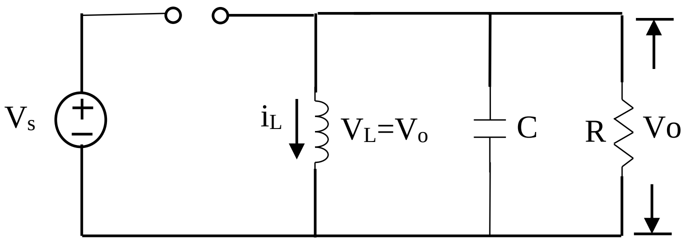

Figure 3-19 Equivalent circuit for switched open

The average inductor voltage is zero for periodic operation, resulting in solving for V_o yields the same result as Equation (3.50). Equation (3.50) shows that the yield voltage has an inverse polarity from the source voltage. The yield voltage size of the buck-boost converter can be less than that of the source or greater than the source, depending on the duty ratio of the switch. In case D>0.5, the yield voltage is bigger than the input; and on the off chance that D <0.5, the yield is smaller than the input. Subsequently, this circuit combines the capabilities of the buck and boost converters. In a perfect circuit, the yield control of the converter is rise to the input control which yields.

$$P_o = P_i$$

$$\text{i.e. } \frac{V_o^2}{R} = V_s I_s \qquad (3.52)$$

The efficiency of the system converter can be calculated as [L17]

$$\eta_{cov\_sys} = \frac{P_o}{P_o + P_D} \tag{3.53}$$

Where P_D total power loss of the converter, $P_D = V_o \times I_o \times \left(\frac{1-\eta_{conv}}{\eta_{conv}}\right)$

Selection of inductor: The average source current related to the average inductor current is given by:

$$I_s = I_L D$$

Resulting, $$\frac{V_o^2}{R} = V_s I_L D$$

Substituting for V_o using Equation (3.50) and solving for I_L,

$$I_L = \frac{V_o^2}{V_s RD} = \frac{P_o}{V_s D} = \frac{V_s D}{R(1-D)^2} \tag{3.54}$$

Maximum and minimum inductor currents that shown are determined using Equation (3.46) and (3.54) [34]

$$I_{max} = I_L + \frac{\Delta i_L}{2} = \frac{V_s D}{R(1-D)^2} + \frac{V_s DT}{2L} \tag{3.55}$$

$$I_{min} = I_L - \frac{\Delta i_L}{2} = \frac{V_s D}{R(1-D)^2} - \frac{V_s DT}{2L} \tag{3.56}$$

For continuous current, the inductor current must remain positive. To determine the boundary between continuous and discontinuous current, I_{min} is set to zero in Equation (3.56), resulting in Equations (3.57) and (3.58).

$$(Lf)_{min} = \frac{(1-D)^2 R}{2} \tag{3.57}$$

$$L_{min} = \frac{(1-D)^2 R}{2f} \qquad (3.58)$$

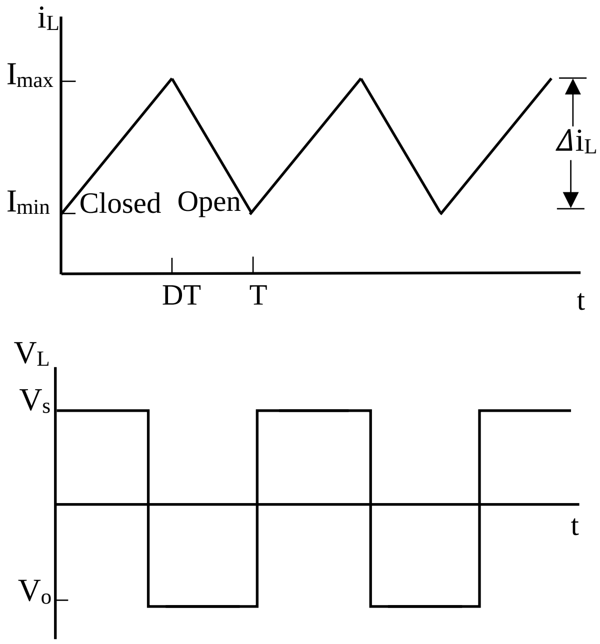

Figure 3-20 Buck-boost converter waveforms of inductor current and inductor voltage

Where f is the switching frequency and ΔI_L is the input current ripple. The current ripple factor (CRF) is the ratio between input current ripple and output current. For a good estimation of inductor value CRF should bound within 30% shown in Equation (3.48). The current rating of the inductor should be always higher than that of the maximum output current.

$$\frac{dI_L}{I_o} = 0.3 \qquad (3.59)$$

Selection of capacitor: The output voltage ripple for the buck-boost converter is computed from the capacitor current waveform of Figure 3-21.

$$|\Delta Q| = \left(\frac{V_o}{R}\right) DT = C\Delta V_o$$

Solving for ΔV_o

$$\Delta V_o = \frac{V_o DT}{RC} = \frac{V_o D}{RCf}$$

$$\frac{\Delta V_o}{V_o} = \frac{D}{RCf} = r \qquad (3.60)$$

Where ΔV_o is the output voltage ripple which is usually considered as 1% of the output voltage. The capacitor value can be obtained from Equation (3.60).

$$C = \frac{D}{rRf} \tag{3.61}$$

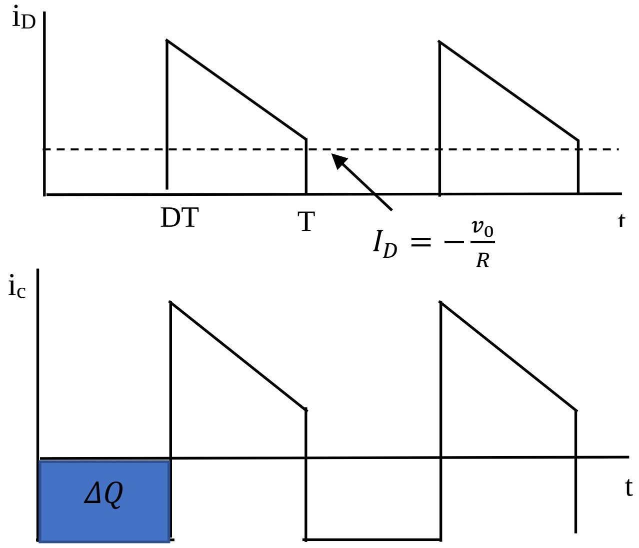

Figure 3-21 Buck-boost converter waveforms of diode current and capacitor current

The design values of inductor and capacitor: The DC-DC buck-boost converter for the developed system is V_{in} is 19.06v and V_{Load} is 12v, I_{in} 13.8A, and I_{out} 11.8A. Also, using these initial values and Equations (3.47), (3.57), (3. 58), (3. 60), and (3.61). The values of the components are calculated as follows L=7.04μH, C=1.208mF, the overall calculation of all months has been done in the appendix. By using Equation (3.53) the efficiency of the designed converter is 95.98% by selecting the DC-DC buck-boost converter with 96% [L18] of efficiency.

3.8. Temperature Regulation

Microcontroller: A microcontroller is an integrated circuit that's housed inside each component that it has to perform the fundamental operations which can perform a particular task routinely without requiring another boom [35]. The microcontroller could be a computer on a single integrated circuit that includes a CPU, RAM, some frame of ROM, and I/O ports shown in Figure 3-22. Microcontrollers with driving 8- and 16-bit processors are frequently favored for low fetched and ease of execution. Todays have a processing capacity of 32 and 64 bits [36].

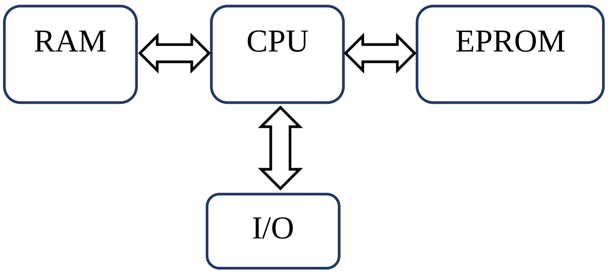

Figure 3-22 General block diagram of the microcontroller

Selection of microcontroller: Depending on the equipment required for communication interfacing (USB, SPI, UART, etc.) and uncommon forms (ADC, PWM, DSP, FPU). Also, the port associations that utilize for the input/output components such as sensor, LCD, accessibility of the hardware to be utilized, and energy utilization [L19], this research work has got to select the Arduino microcontroller to control the temperature of the refrigeration framework.

Selection of temperature sensor: Concurring to interaction with the device and temperature regulation handle, it needs the temperature sensors. There is a different type of temperature sensors that are accessible in the market [L20]. Depending on the accuracy, the power required, response time, and DHT22 temperature sensor is the finest choice. Since it has 0.05 to 1.5°C temperature precision, 0.12sec to 10sec response time, and accessible in low to moderate cost run [L21][L22]. Also, compatibility with the Arduino mega microcontroller and availability within the Ethiopian market.

3.9. Experimental Modeling

This experimental prototype is implemented to shows that the temperature regulation of the developed system. This prototype can develop as the block diagram indicated before shown in Figure 3-23. For experimental modeling, the following data will be considered

Independent variables:- this variable of the system is the temperature inside the system. As the input data, the microcontroller reads the data from the temperature sensor. For the case of senor, precise and accurate senora is needed, for that DHT22 is used.

Dependent Variable:- this variable is the Peltier module, fan, LCD, and LED. As an output temperature regulation give LED indicator light by turning on and off. The LCD also displays the current temperature and the status of the mini-refrigeration system.

Material required:- the equipment that uses in the prototype design is listed below.

- Pettier module TEC 12706
- BLDC fan
- Ice-box
- Arduino mega
- DHT22 sensor
- LCD
- Multi-LED
- Motor driver
- DC-DC buck-boost converter
- Heat sink
- Connecting wires
- 12v/10A power supply

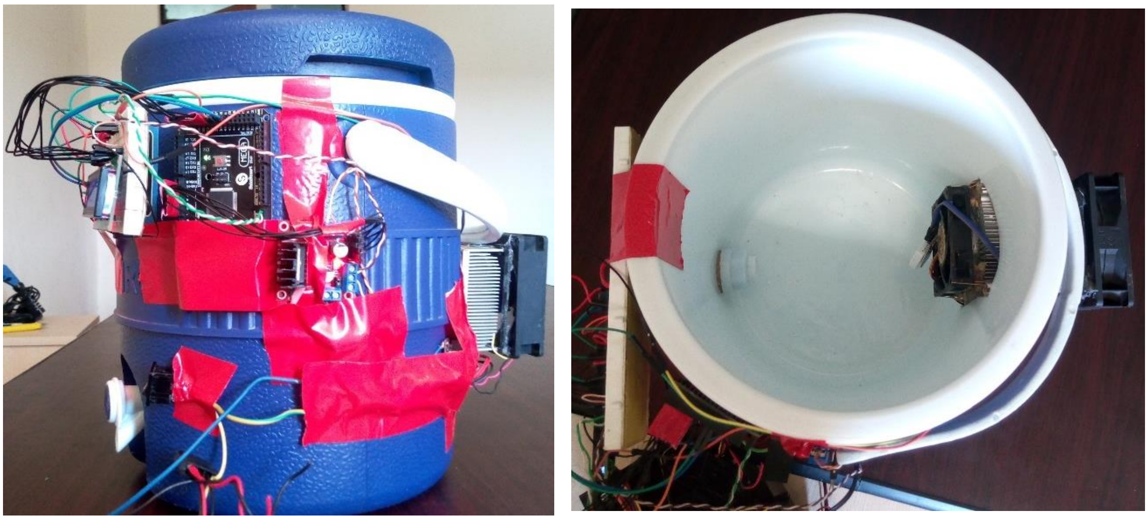

(a) (b)

Figure 3-23 Prototype modeling of the system (a) side view (b) inside view

CHAPTER 4

RESULT AND DISCUSSION

4.1. Chapter Overview

This chapter includes the result and analysis of the developed solar-powered refrigeration system. The simulation results of the developed system are compared with the different conditions of the Peltier module, the result, and analysis of the solar panel design of the developed model and simulation result and analysis of the temperature regulation system for this research work to fulfill the specific objectives of the research and answered RQ.5.

4.2. Result on TEC

In this section, this research work shows that the Peltier module performance result based on the selection environment and its ambient temperature. Those performance parameters are the cooling power that the power required to refrigerate the environment temperature, the input power that is required to meet the need of cooling power performance, and COP that the ratio of cooling power to input power. The simulation result shows the performance and analysis of the Peltier module and the comparison of the modules at the different condition that calls the maximum cooling power condition, the maximum COP condition, and the optimal (midpoint) condition. Besides, it answered the question that rise in RQ 2.

4.2.1. Simulation Result of Peltier Module

The performance parameters of the Peltier module that uses in the refrigeration system has the maximum cooling power of 51.865W, the maximum coefficient of performance is 0.692 and the maximum input power needs to meet the cooling power is 178.671W the simulation result is shown in Figure 4-1, Figure 4-2 and Figure 4-3 below respectively. This performance parameter depends on the environment temperature. So, all the parameter doesn't meet the maximum cooling power, maximum COP, and the minimum input power at the same times. Increasing input power above the maximum cooling power that is

51.865W, is causing a decrease in cooling power shown in Figure 4-1. Equation (3,16) states that increasing input power is increasing current and voltage. The current will decrease the cooling power with the square of the input current.

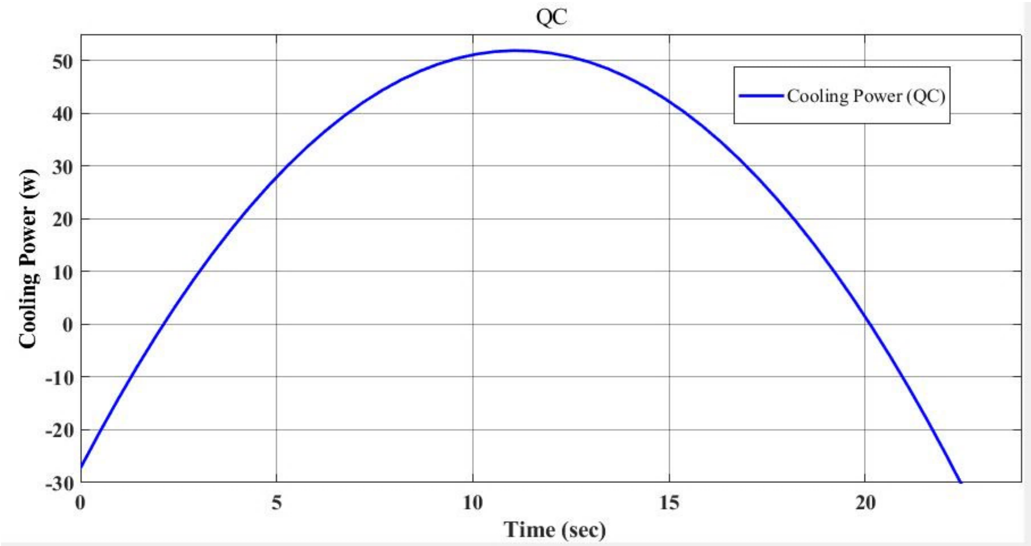

Figure 4-1 Result of cooling power (Q_C)

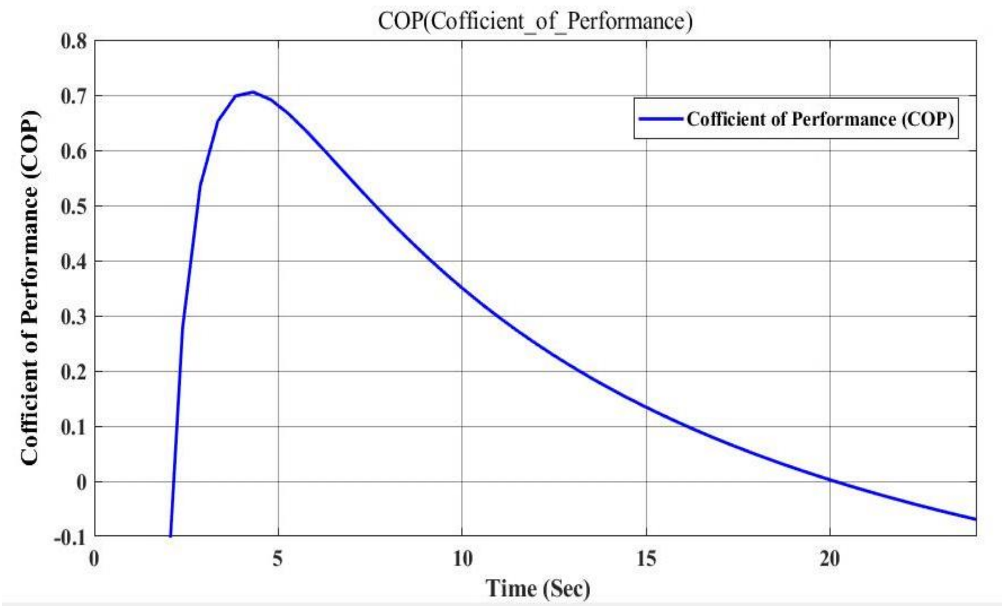

Figure 4-2 Result of the coefficient of performance (COP)

The COP of the Peltier module shows that further increase of input power is decreased the ratio of cooling power to input power that states in Equation (3,20). So, an increase of input power isn’t giving the desired result in the refrigeration system. The COP of the system is shown in Figure 4-2.

The input power of the Peltier module is shown in Figure 4-3. It illustrates that increase of power above the limit of Peltier intake is considered as wastage. Not only wastage but also it may damage the Peltier module. It has to be controlled before sent it to the module.

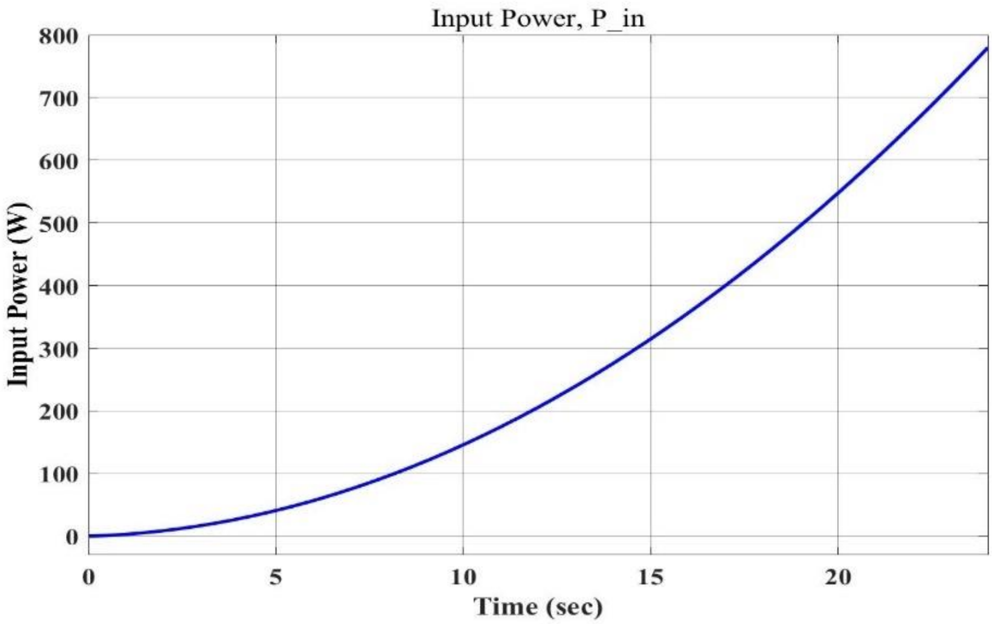

Figure 4-3 Result of input power (W)

4.2.2. Simulation Result of the Maximum Cooling Power of the Peltier Module

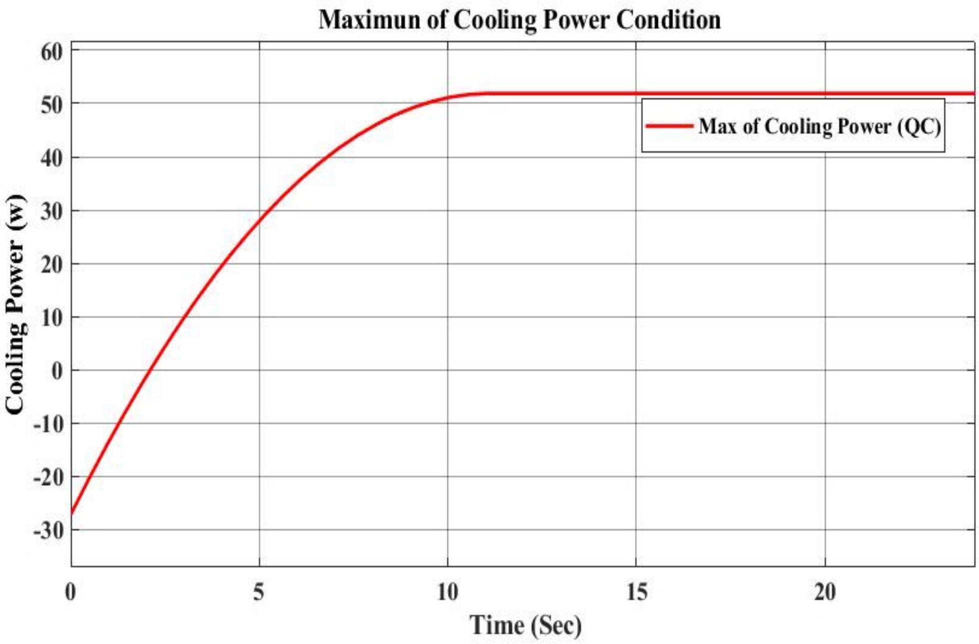

Figure 4-4 Cooling power (Q_C) at the maximum cooling power condition

In the maximum cooling power, the condition has used the Peltier module at the maximum cooling power of 51.865W shown in Figure 4-4. Compare to others in this condition the input power is high, the COP is low, and needs 2 Peltier modules to meet the desired refrigeration system.

This condition is uneconomical because of high-power is consumption. The advantage of this condition is giving the maximum cooling power, this gives a fast recovery of the temperature. But to get the maximum cooling power the solar panel size must be increased. This can be difficult to transport from place to place because the net weight will increase.

The coefficient of performance in this condition, that shown in Figure 4-5, is lowest than the other. It has a value of 0.289. because the intake input power is large to get the cooling power. The lowest COP causes the lowest energy efficiency that has 5.5% compared to others.

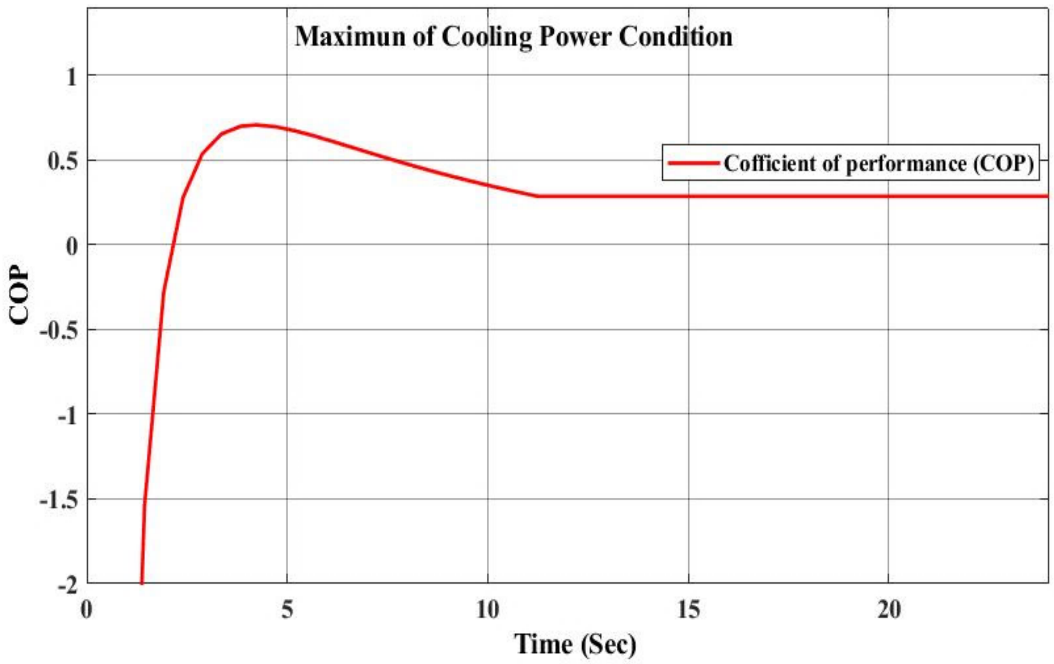

Figure 4-5 COP at the maximum cooling power condition

The maximum input power needs to meet the cooling power is 178.671W. it has an 11.126A input current, 16.059v input voltage shown in Figure 4-6 below. The Peltier module may be damaged by getting this current because the maximum current operating by this module is around 6A.

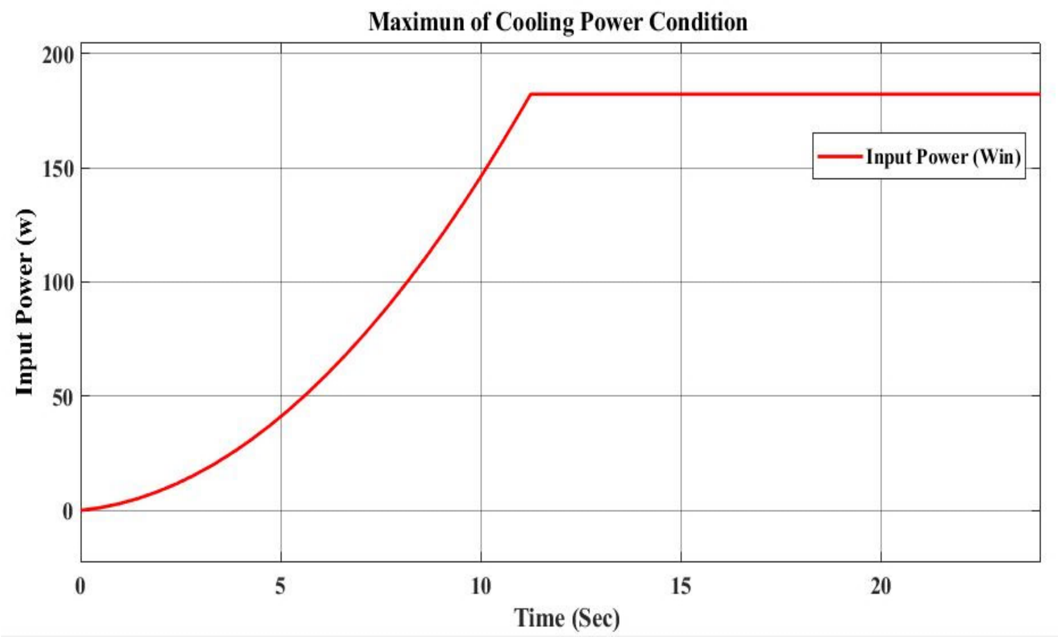

Figure 4-6 Input power (W_{in}) at the maximum cooling power condition

4.2.3. Simulation Result of the Maximum of COP of Peltier Module

The maximum coefficient of performance (COP) condition has the maximum coefficient of performance that is 0.692 shown in Figure 4-7. The advantage of this condition is it has high COP and low input power. The large COP leads the large energy efficiency of the system that has 13.2% compared to others.

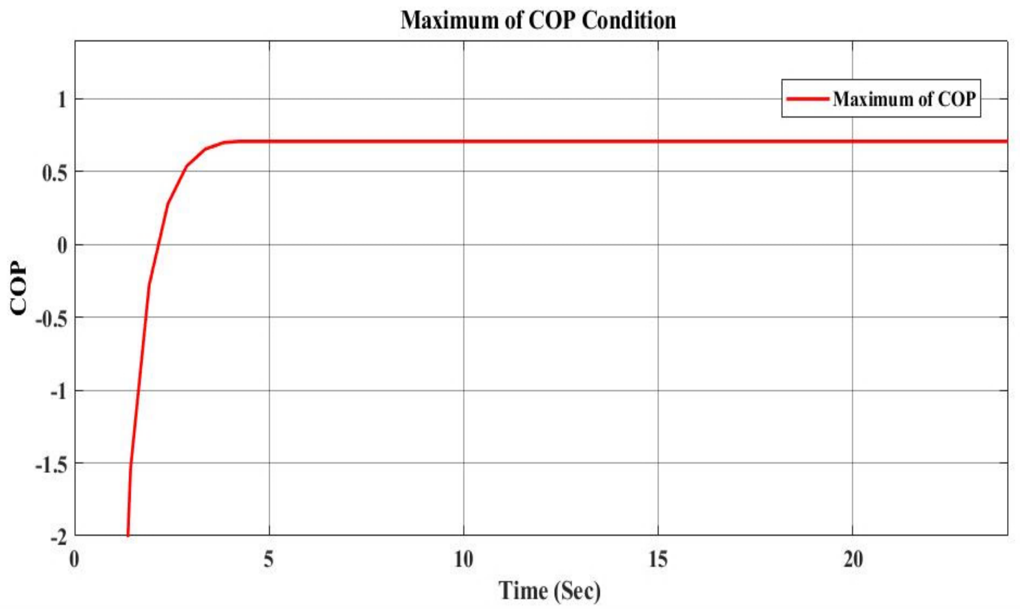

Figure 4-7 COP at the maximum COP condition

Maximum COP has the lowest cooling power compared to other performance conditions, it has 21.4W shown in Figure 4-8. The lowest cooling power uses a large number of Peltier modules. It needs 3 Peltier modules to meet the desired refrigeration system. This is considered as a disadvantage of this condition.

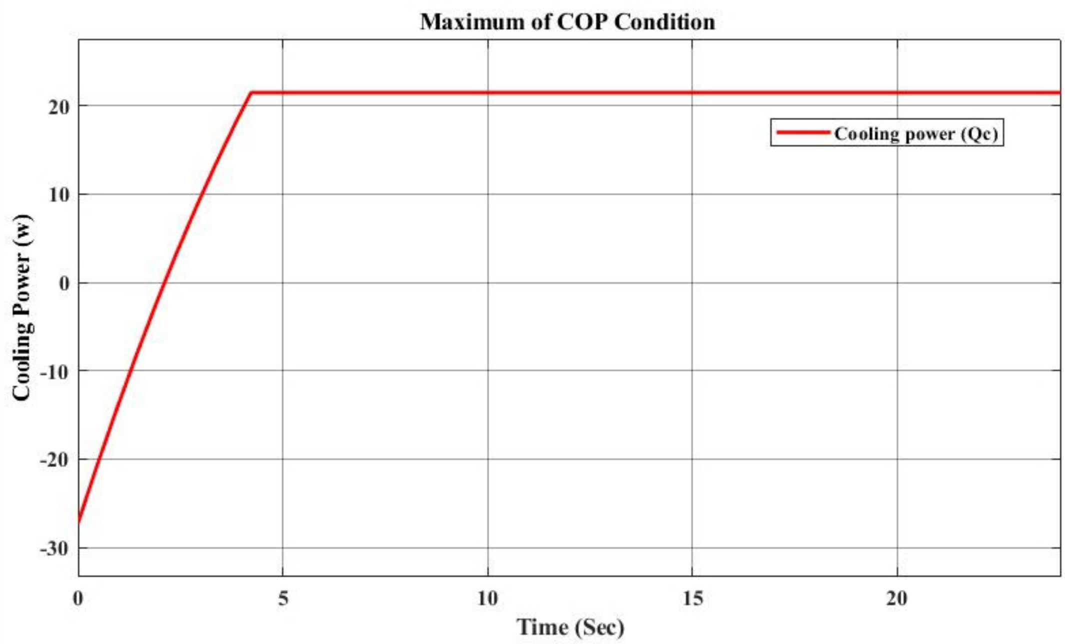

Figure 4-8 Cooling power (Q_C) at the maximum COP condition

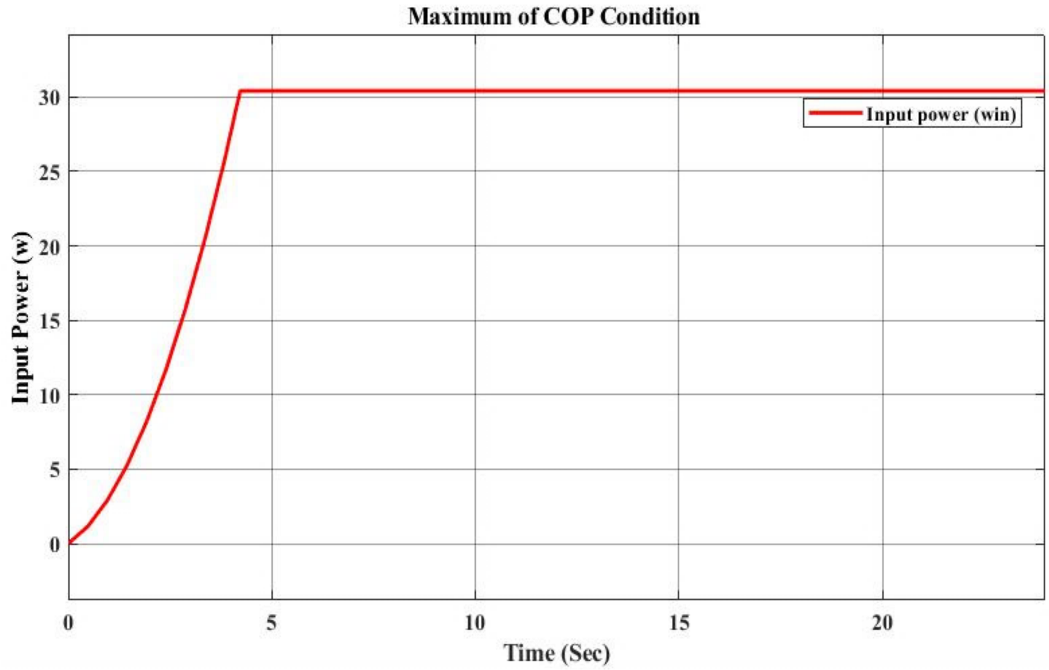

Figure 4-9 Input power (w_{in}) at the maximum COP condition

In this condition, the input power is low which is 30.516W, 4.224A input current, 7.224v input voltage. The smallest input power considers as an advantage because the solar panel also decreases in size. It can easily transport from place to place. This will help the health work carry and travel as long as they want. The net weight and complexity of the system also decrease.

4.2.4. Simulation Result at Optimal (the Midpoint) of the Peltier Module

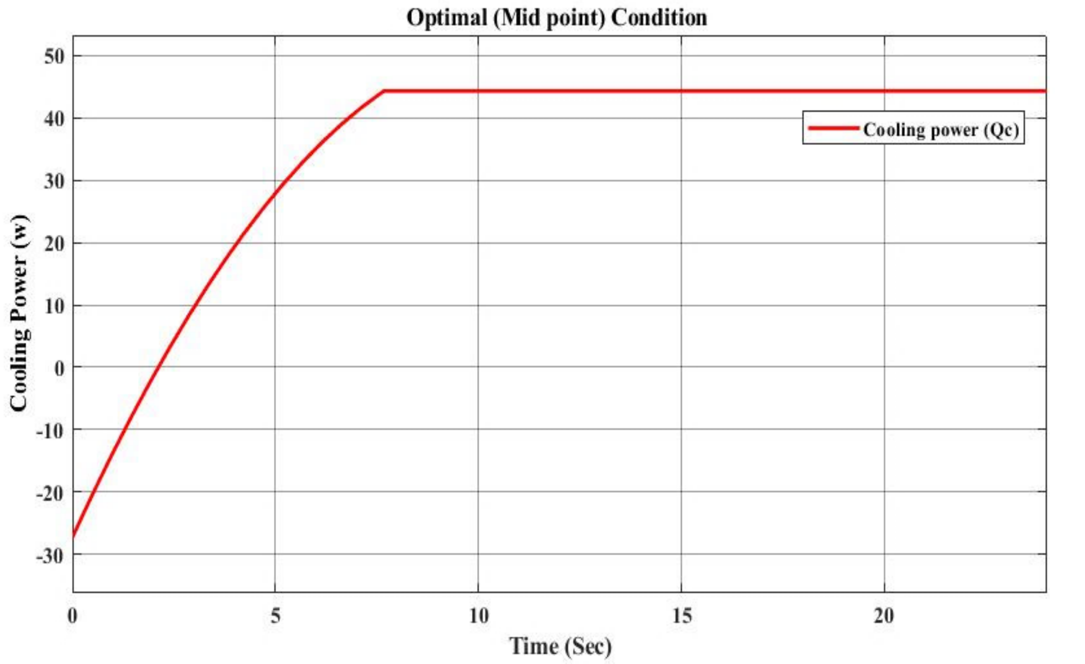

Figure 4-10 Cooling power (QC) at the optimal (midpoint) condition

The optimal (midpoint) condition uses the average current of the two maximum conditions. This condition has cooling power is 43.975W, and the simulation result is shown in Figure 4-10. In this condition has the optimal input power, the COP also optimal compared with others, and needs 2 Peltier modules to meet the desired refrigeration system.

The coefficient of performance is 0.482 as shown in Figure 4-11. The efficiency of the system is depending on the COP. So, this condition has better efficiency than maximum cooling power. this optimal condition efficiency has 9.2%. The input power that needs to meet the cooling power is 89.349W shown in Figure 4-12. It has a 7.675A input current, 11.642v input voltage. This condition is moderates based on input power and the number of modules. But the current still higher than the limit of the module datasheet.

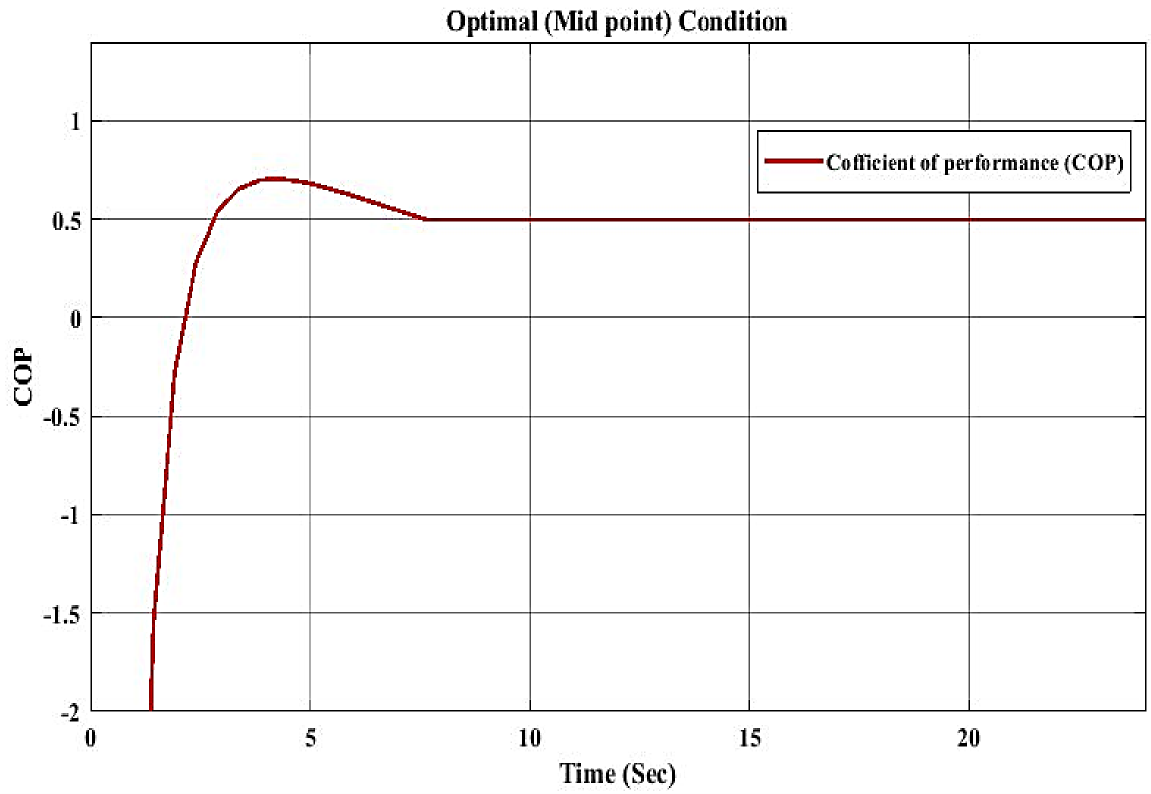

Figure 4-11 COP at the optimal (midpoint) condition

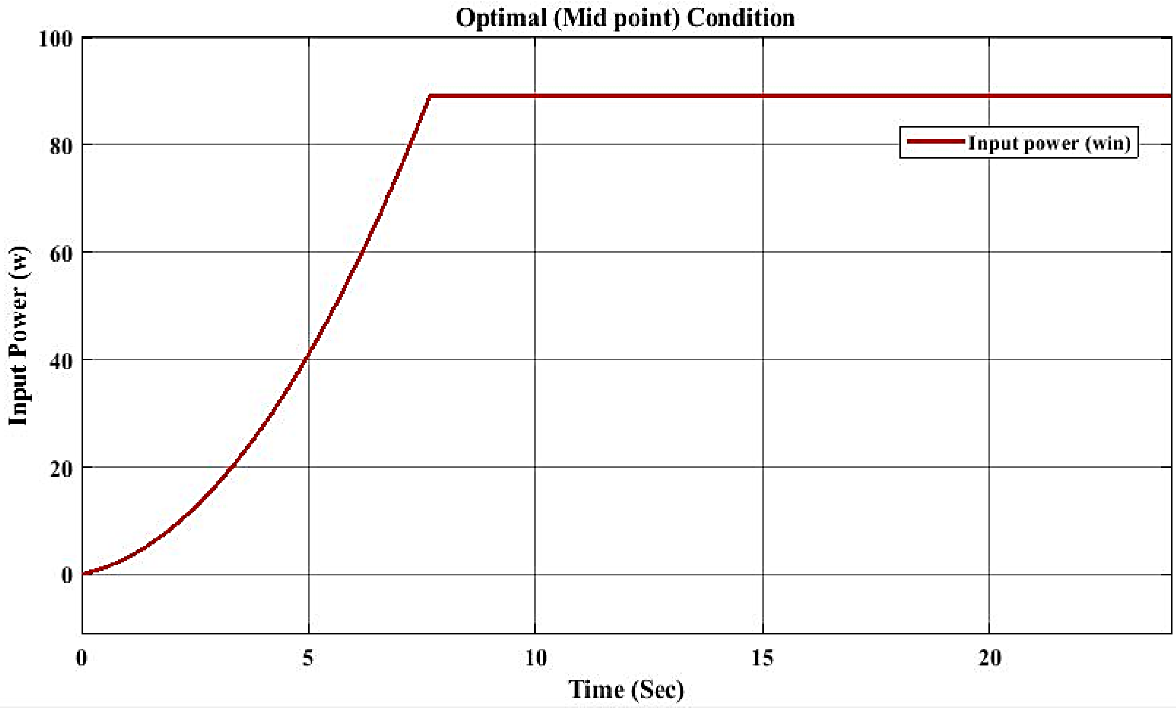

Figure 4-12 Input power (W_{in}) at the optimal (midpoint) condition

4.3. Result on Solar Panel

In this section, this research work shows that the performance result of solar panels based on the selection environment light irradiation and its environmental temperature. Show the result of the solar PV model with its short circuit current and open-circuit voltage values, shows the result of solar panel with the interaction of P and O MPPT, buck-boost converter and load, shows the result of solar panel performance variation of all months in a year, and its shows the result of charge controller performance.

4.3.1. Simulation Result of the Selection Solar Module

Based on the design and the selection of the solar module of the simulation analysis result. This result shows that the module has a short circuit current is 14A and an open circuit voltage is 25v shown in Figure 4-13 and has a maximum power of 287W at the voltage of 21.7v show in Figure 4-14.

The result gates by 5000 W-hr/m^2 solar irradiation that the lowest irradiation and 40.5^{0}C ambient temperature that the highest temperature. This result shows that it has the power to operate the Peltier module.

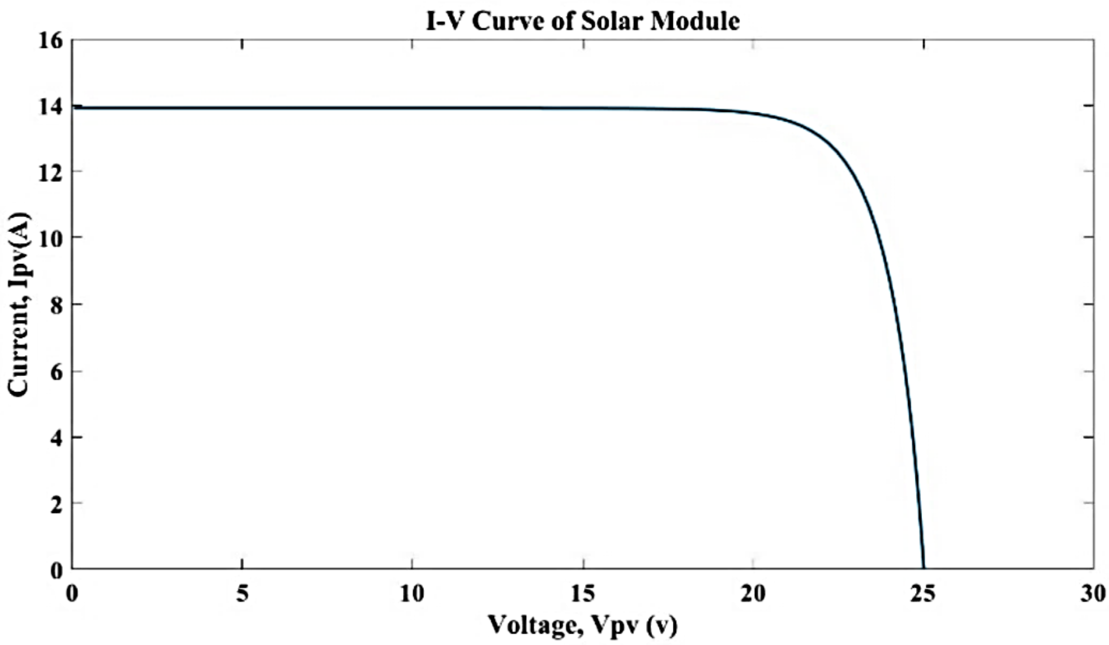

Figure 4-13 Result of the I-V graph of the PV module

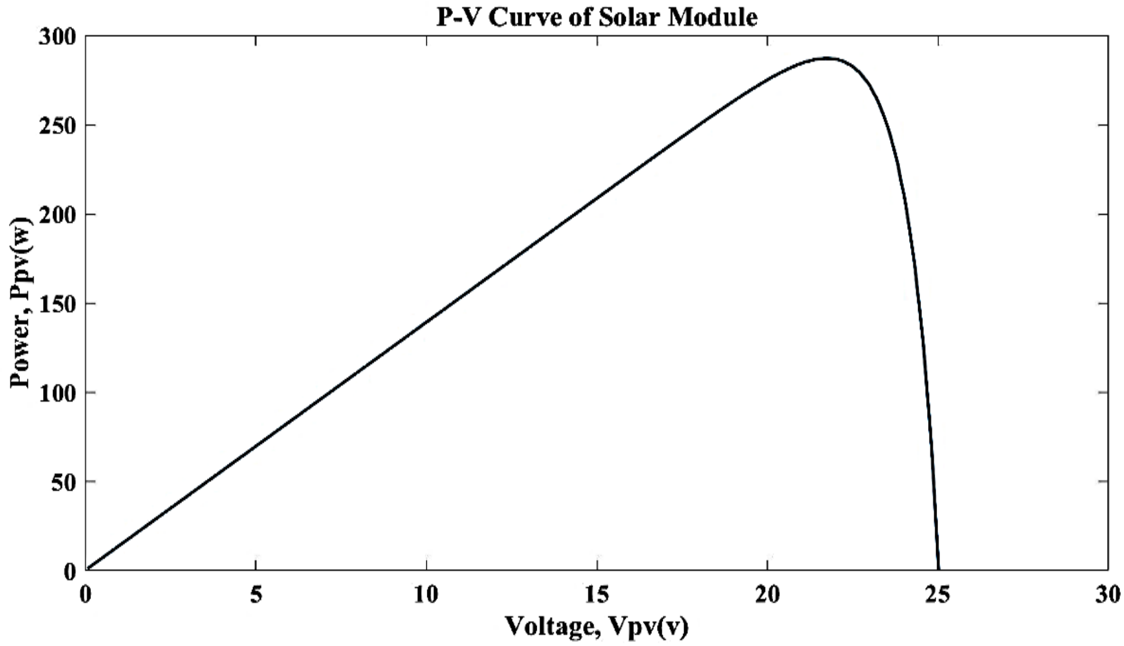

Figure 4-14 Result of the P-V graph of the PV module

4.3.2. Simulation Result of Input and Output Parameter of the System

The output voltage of the DC to DC converter is less than or greater than the input voltage. The output voltage of the magnitude depends on the duty cycle. In this simulation result, the developed system has a duty ratio of 0.248. This result shows the input voltage, which from the solar module, has to be stepping down the voltages. This operation is called a step-down mode.

There are many applications use of DC-DC buck-boost converter such as battery-powered systems, where the input voltage can vary widely, starting at full charge and gradually decreasing as the battery charge is used up. At full charge, where the battery voltage may be higher than the circuit being powered, a buck regulator would be ideal to keep the supply voltage steady. However, as the charge diminishes the input voltage falls below the level required by the circuit, and either the battery must be discarded or re-charged.

The input and the output voltage of the converter are shown in Figure 4-15. The duty ratio of the DC-DC converter is generating from the MPPT. The results show that the input voltage from the solar module is V_{in} is 19.06v and the output voltage at the load is V_{load} is 14.24v. The converter is step down the input voltage by 4.82v.

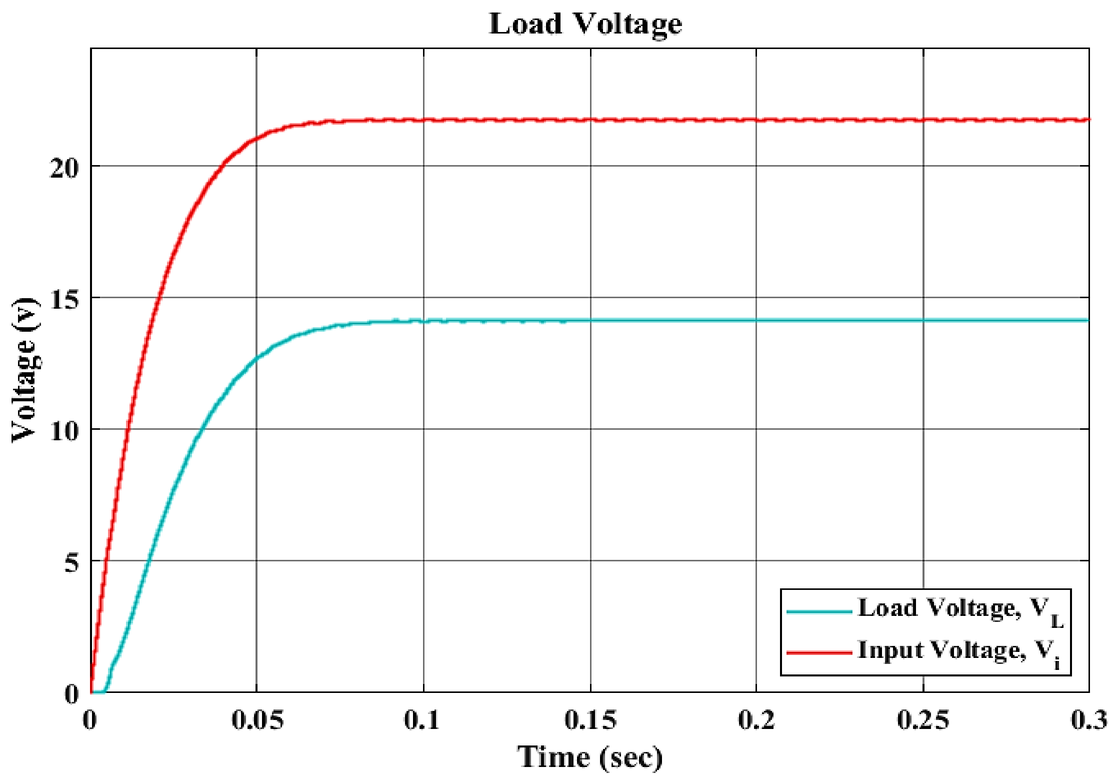

Figure 4-15 Result of input and load voltage

In the step-down mode, the input voltage is greater than the output voltage. It follows that the output current is greater than the input current. By using the law conversion energy, the input power is equal to the output power. The simulation result shown in Figure 4-16 has given the full verification of the above statements.

The input current from the solar module I_{in} is 13.8A and the output current at the load is l_{Load} is 14.2A. the DC-DC buck-boost converter can boost the current to meet the desired demands. Figure 4-17 shows the power vs time graph, depending on the load, the input power from the solar module P_{in} is 236.1W and the output power at the load is P_{Load} is 201.9W. the load power of the system is enough to power to operate the system.

The buck-boost converter can achieve the desired operational power supply. So it can improve the COP of the system which leads to gaining the maximum efficiency of the Peltier module. The overall efficiency is improving using this kind of DC-DC buck-boost converter or related.

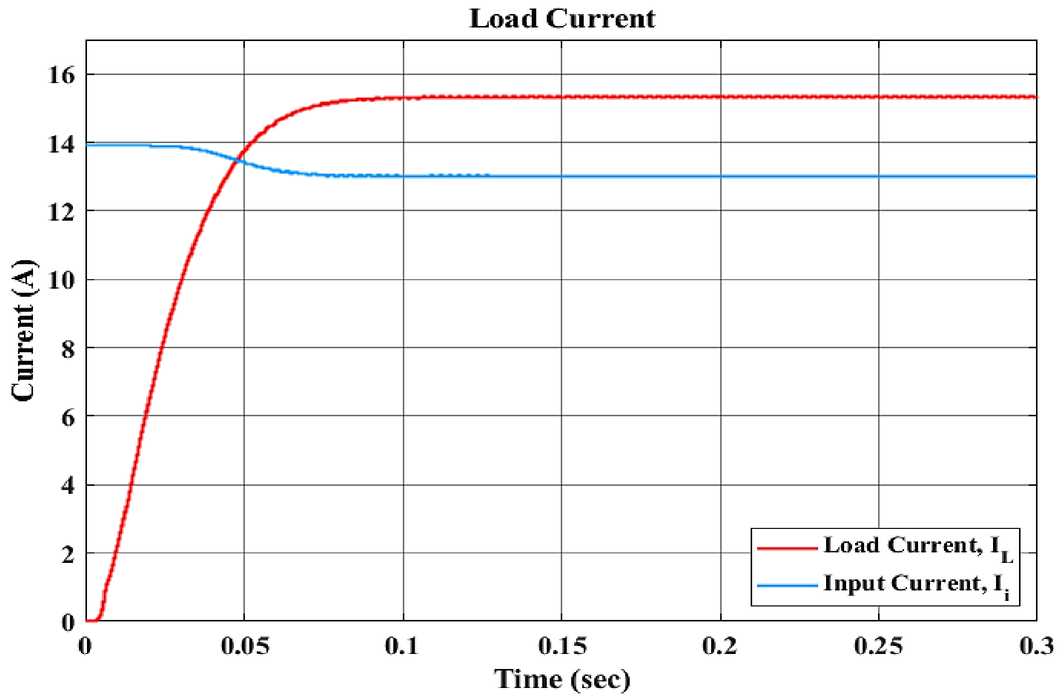

Figure 4-16 Result of input and load current

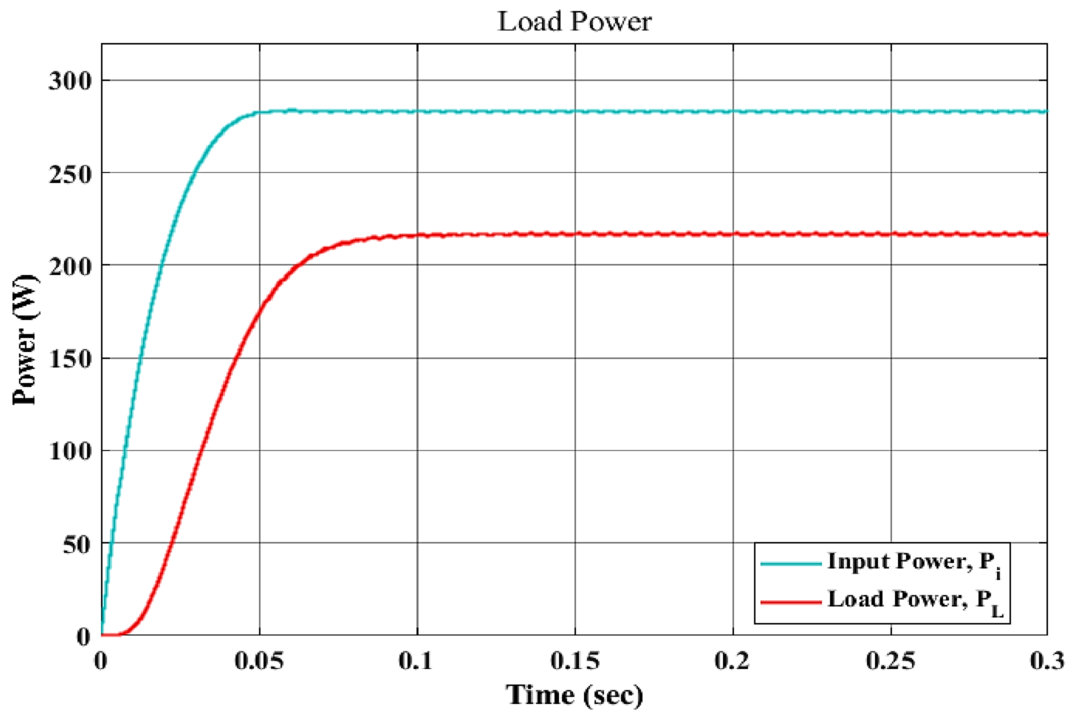

Figure 4-17 Result of input and load power

Equation (3.50) states that the duty ratio of the MPPT output determines the operation mode of the DC-DC converter. The simulation result, shown in Figure 4-18, clarifies the operation mode of the converter is stepping down of the input voltage. The duty ratio of this developed system is 0.248 and the control of the BJT switching is uses PWM techniques, this PWM gate pulse signal is shown in Figure 4-19.

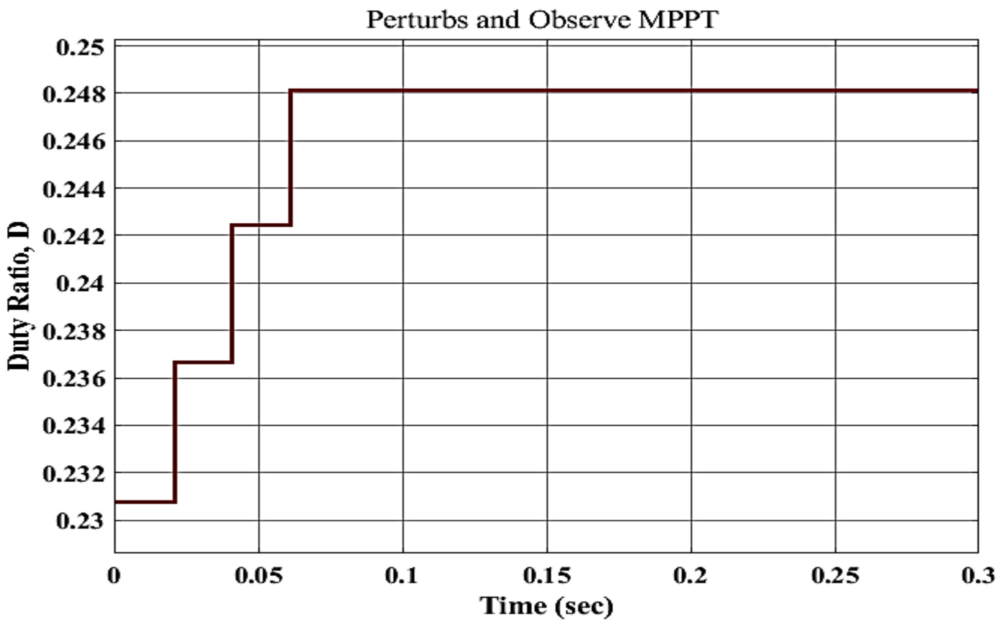

Figure 4-18 Result of P and O MPPT duty ratio

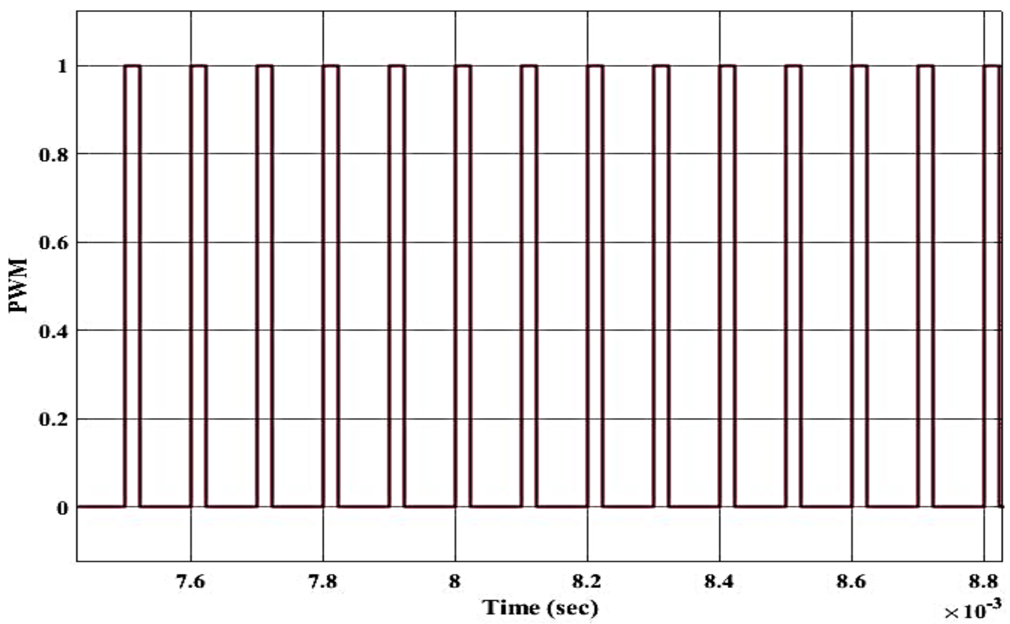

Figure 4-19 Result of the gate pulse

In the continuous conduction mode, the buck-boost converter conducts the switching ON and OFF periods. When the switch is ON the diode will be open-circuited since it does not allow currents in the reverse direction from input to output. This current in the ON period operation is zero. So, the inductor feeds the energy from the input and it stores the energy of magnetic energy. During this state, the inductor charge and the inductor current increases linearly as shown in Figure 4-20.

When the switch is OFF, L is charged and C is partially discharged. The inductor L now generates a back (Electro-Motive Force) e.m.f. and its value that depends on the rate of change of current as switches OFF and ON the amount of inductance the coil possesses; therefore, the back e.m.f can be any voltage over a wide range, depending on the design of the circuit. Notice particularly that the polarity of the voltage across L has now reversed, and so adds to the input voltage giving an output voltage that is at least equal to or greater than the input voltage. The diode is now forward biased and so the circuit current supplies the load current, and at the same time re-charges the capacitor that shown in Figure 4-21. Both operation and simulation results conclude that the design value of the inductor and capacitor is suitable for this developed system.

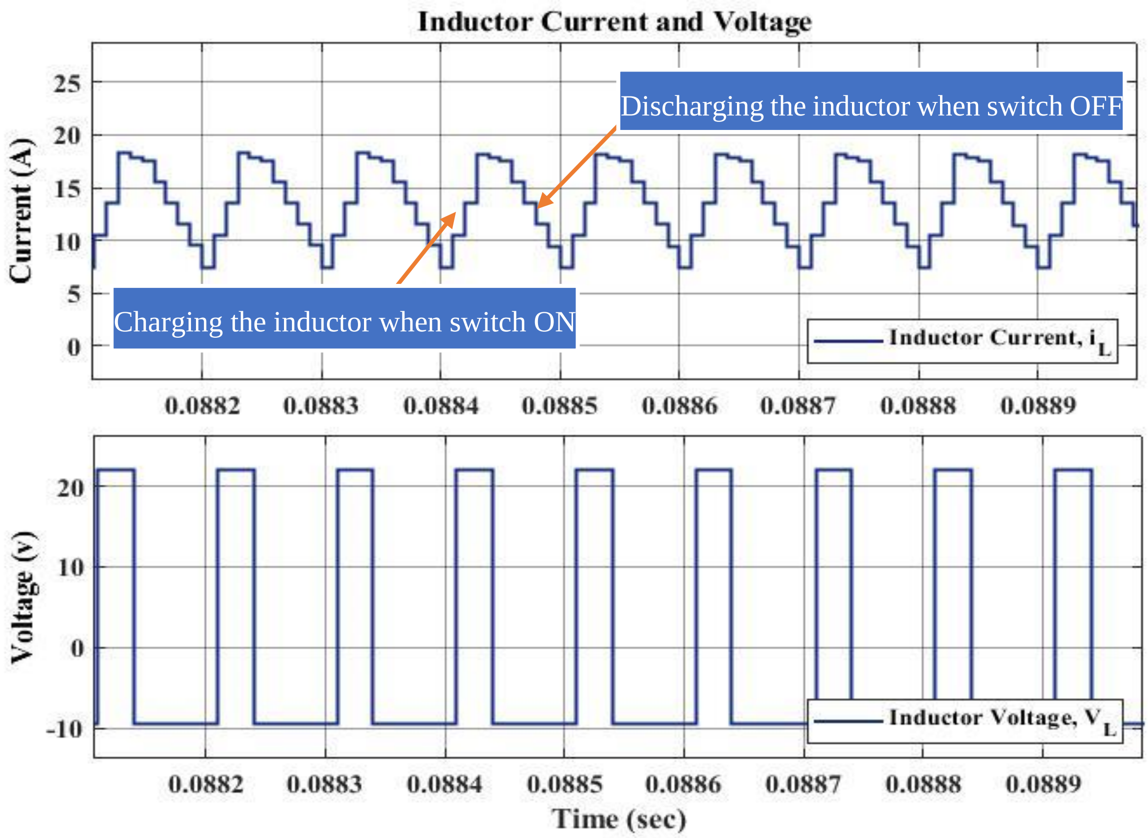

Figure 4-20 Inductor current and voltage

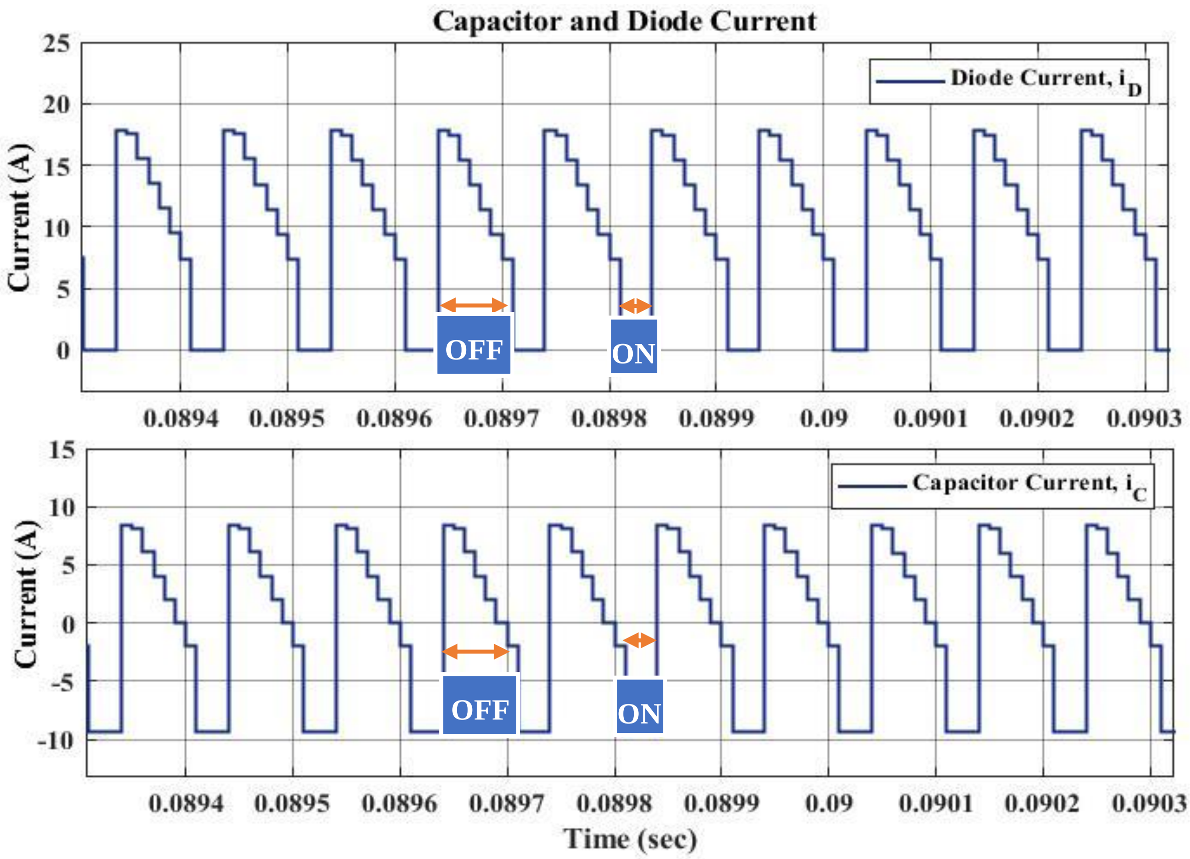

Figure 4-21 Diode current and capacitor current

4.3.3. Simulation Result of Annual Months

The following simulation result is indicating that the solar module tracking the irradiation change in the whole months. The irradiation is varying between 5 kW-hr/m^2 that the lowest irradiation and 7.75 kW-hr/m^2 that the highest irradiation and the temperature from the lowest 35^{o}C to the highest 40.38^{o}C

Figure 4-22 the load current is tracking the irradiation. The load current can vary between 13.8A to 15.1A depending on the variation of the irradiance respectively. The minimum current can operate the developed system because it was higher than the required current. So, the selected solar panel is suitable for this developed system.

Figure 4-23 the load voltage is tracking the irradiation. The load voltage can vary between 17v to 21.6v depending on the variation of the irradiance respectively. The minimum value of the voltage is higher than the required voltage.

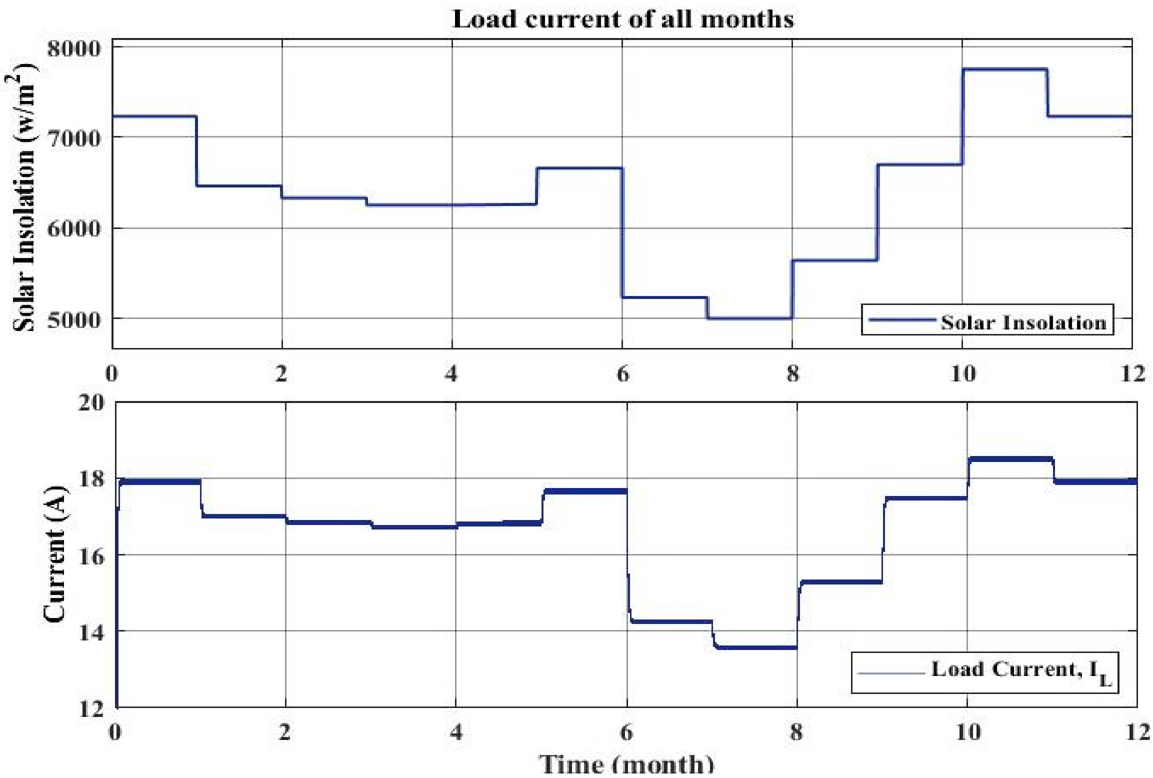

Figure 4-22 Load current

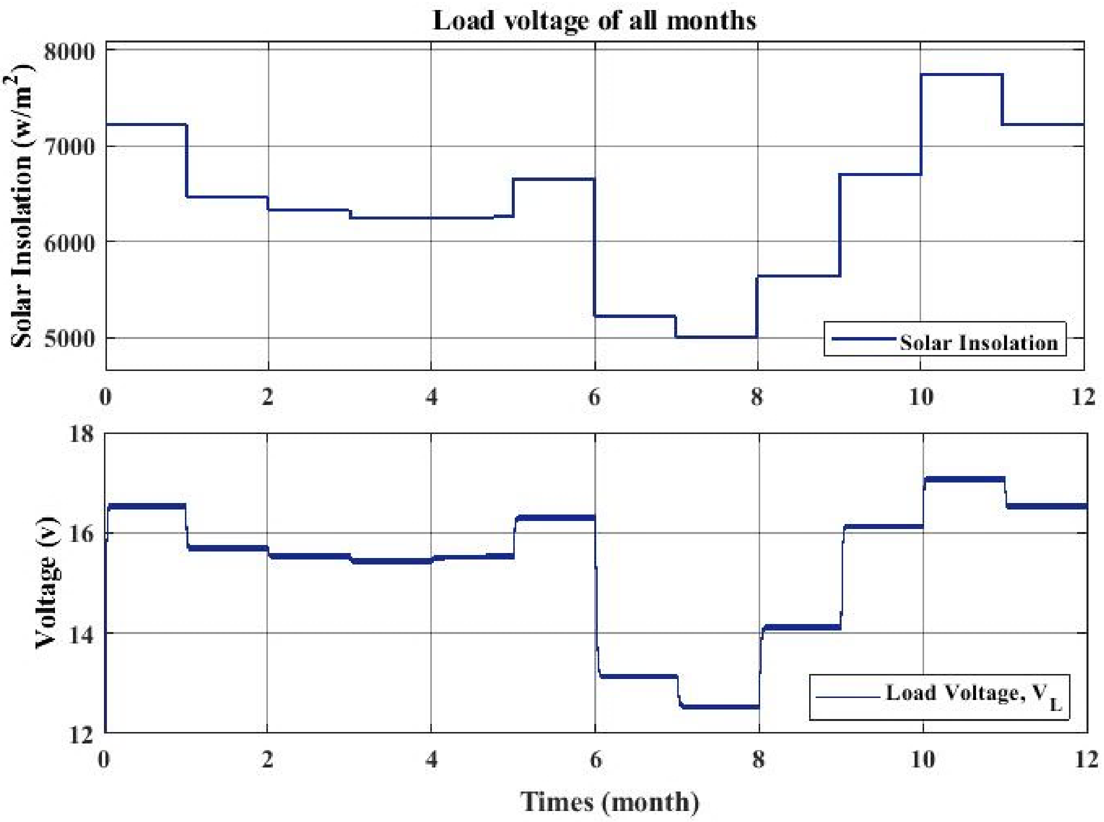

Figure 4-23 Load voltage

Figure 4-24 the load power is also tracking the irradiation like current and voltage. The load power will vary the result between 198W to 310W based on the variation of the irradiance respectively. This power indicates that it can fulfill the minimum requirement of the system. The developed system has an excess amount of power. So, it is possible to use this power for other purposes like charging the cell phone or laptop, electric lamp, and charges of the other fridge if the second one is not working.

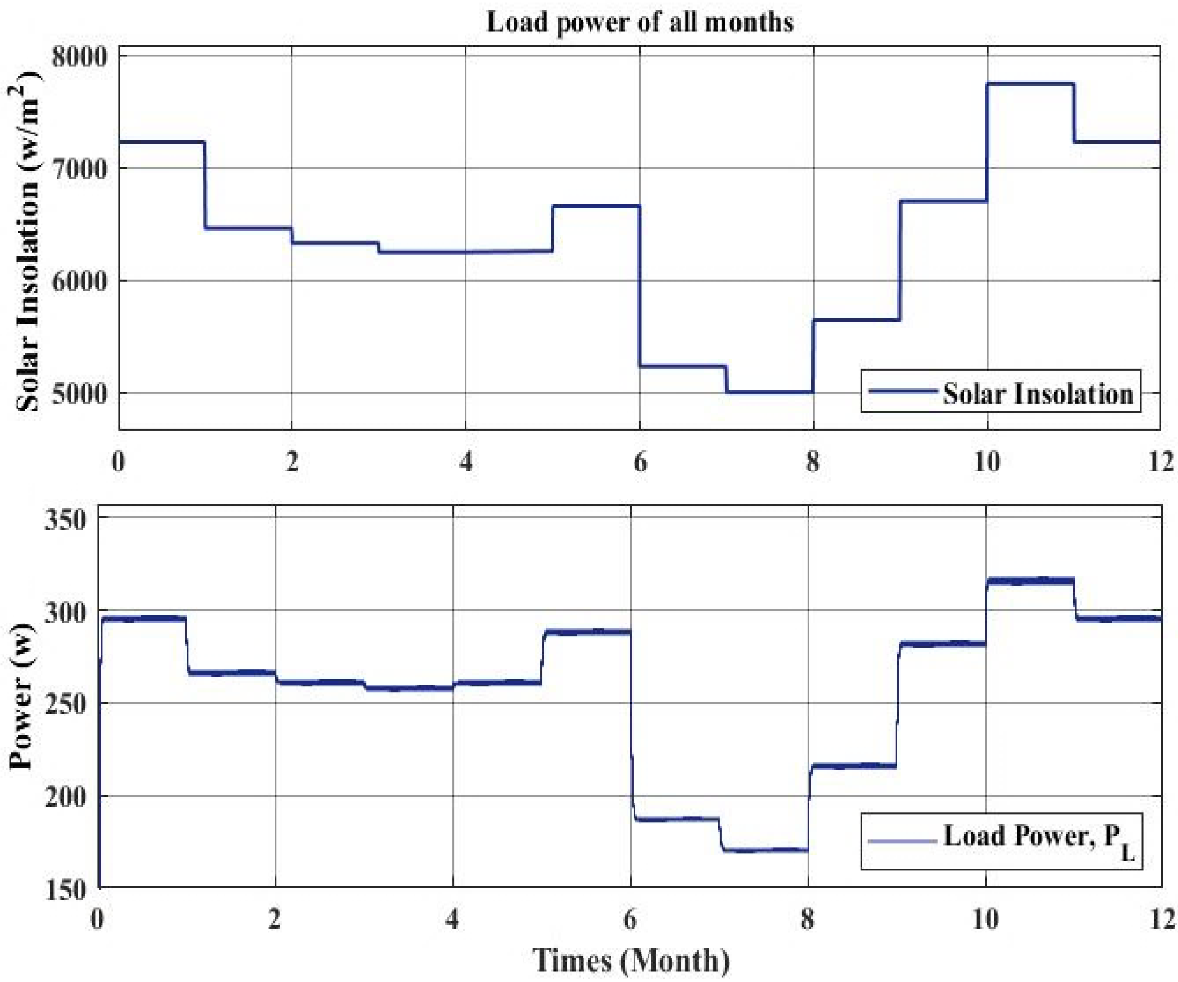

Figure 4-24 Load power

Figure 4-25 shows the P and O MPPT gives the duty ratio according to the solar module output. The duty ratio of the buck-boost converter is varying between 0.214 to 0.255. This variation indicates the DC-DC buck-boost converter can perform the buck operation throughout the whole year. The boost operation of the converter plays the role of safety operation. In case of some fault, it occurs and drops the input voltage, the step-up operation of the converter takes an action to overcome the fault. It takes an action also during the load user is increasing like the user wants to charge a cell phone, laptop, or use as electricity during the night time. So, the system is flexible to use rather than the refrigeration purpose.

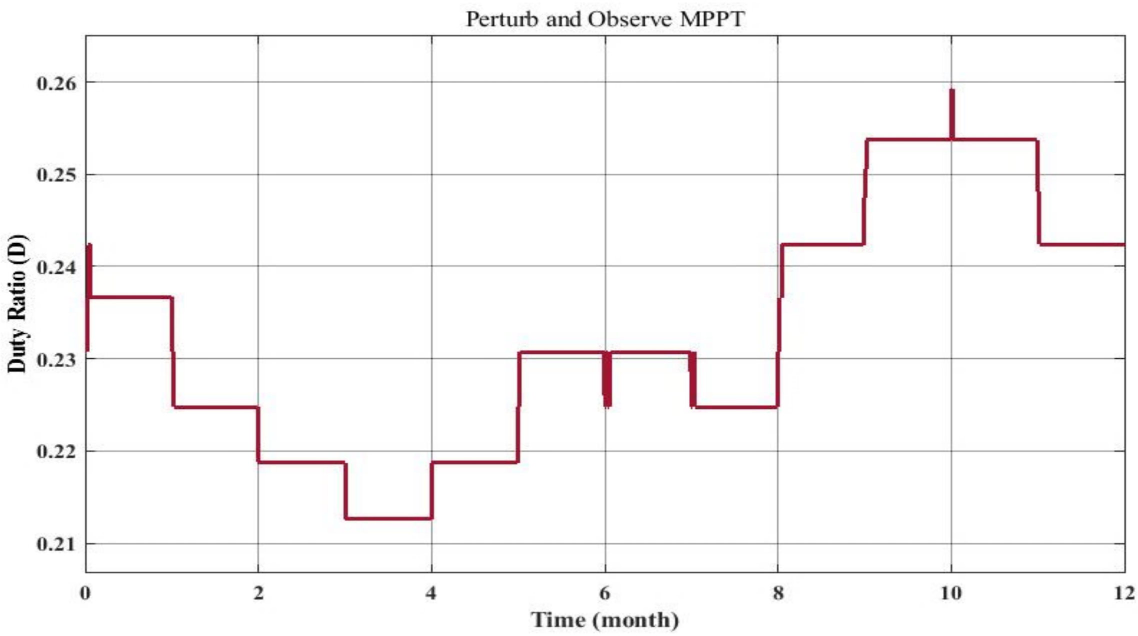

Figure 4-25 MPPT output

4.3.4. Simulation Result of the Battery Charge Controller

The battery of Li-ion manganese architecture forms is a three-dimensional spinel structure that improves ion flow on the electrode, which results in lower internal resistance and improved current handling. An advantage of spinel is high thermal stability and enhanced safety. Low internal cell resistance enables fast charging and high-current discharging.

The purpose of the battery in this system to deliver continuous power supply to the refrigeration system when the failure occurs and to get full-day (24hr.) operation refrigeration is needed. For 24 hr. operation the refrigeration system needs to increase the capacity of the batter to 30AH. This capacity of the battery can handle night time operation. In the result of the battery charge controller, the result shown the parameter of the batter based on current, voltage, and SOC. The selection Li-ion battery has 12v/ 10AH energy and gives the required power is 110W for the 3100 sec (up to 20% battery charge). The charging and discharging performance of the battery is shown in Figure 4-26.

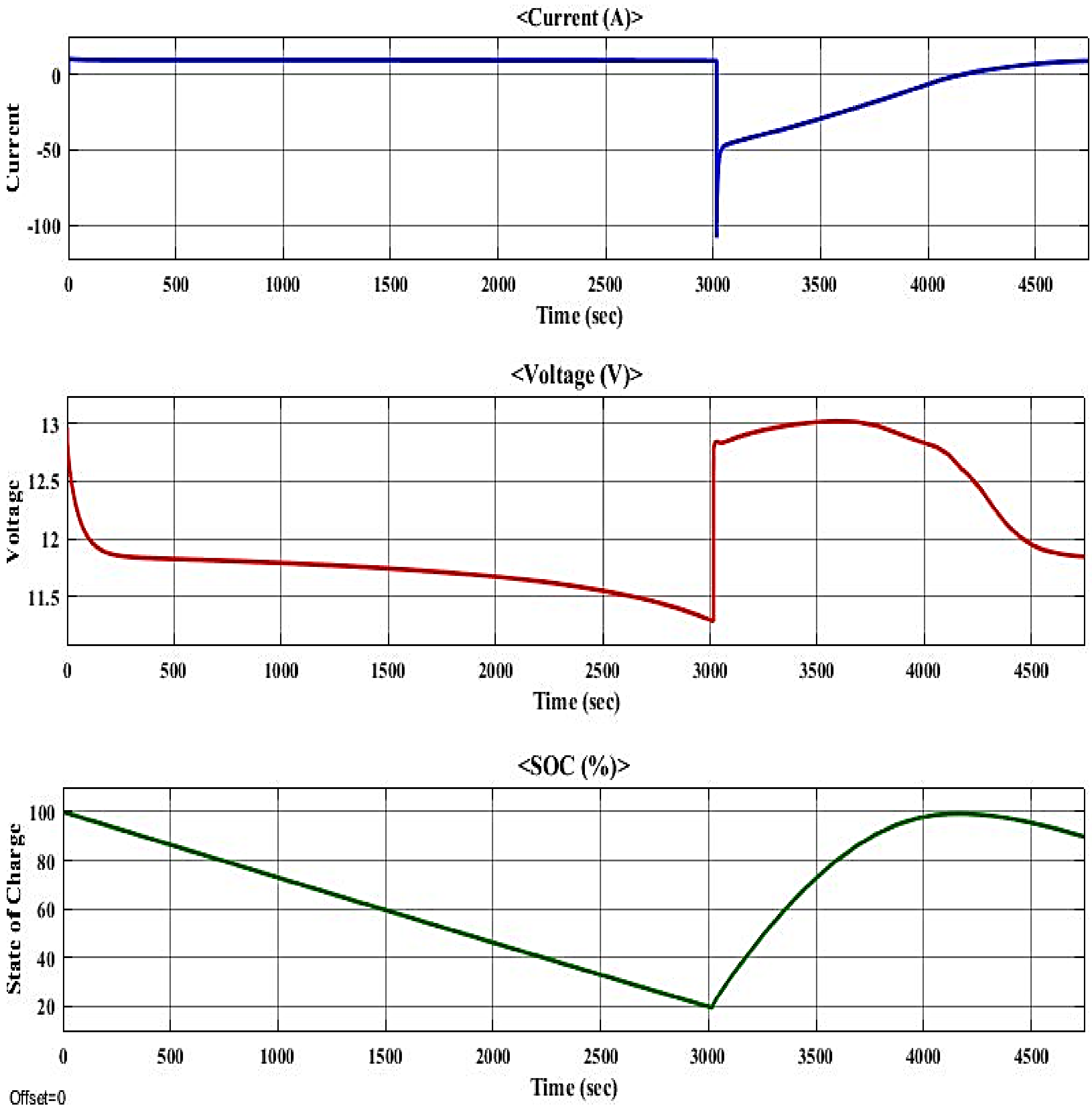

Figure 4-26 Result of current, voltage, and SOC of the battery

The interesting thing about this is the selected battery for one hour of working time to store a vaccine for 5 hours. To increase the working time of the battery has to increase the capacity. To fully operate the refrigeration system for 24 hours (one full day) the energy capacity of the battery has to increase to 30AH.

The battery used as a backup gives constant power to the load to increase the performance of the system. Based on the load resistance the load voltage, current and power are shown in Figure 4-27.

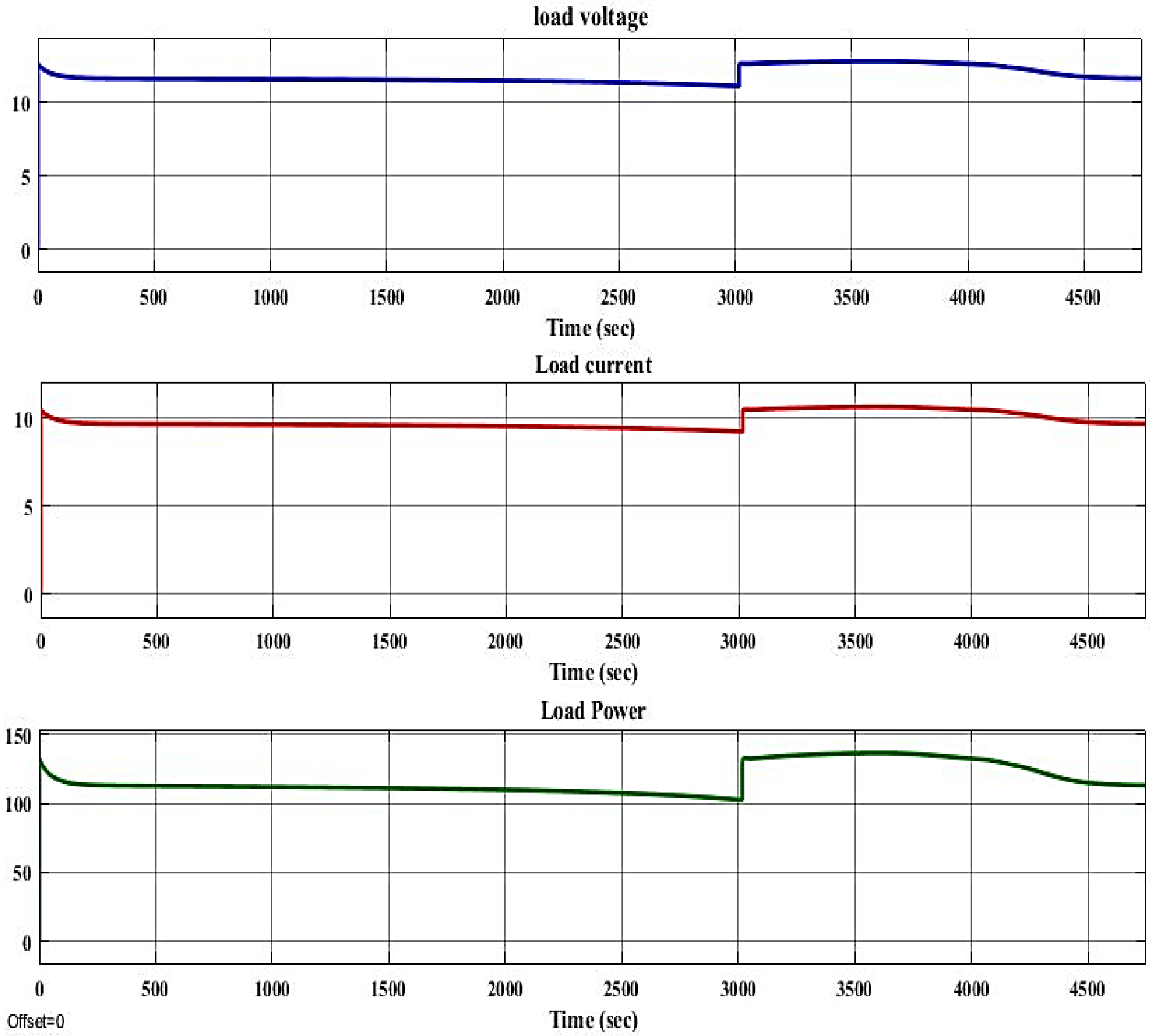

Figure 4-27 Result of load current, load voltage, and load power of the battery

4.4. Simulation Result of HOMER Software

In this section, the optimization and sensitivity analysis are simulated using HOMER software. The HOMER software is used in the proposed system doesn't have the designed solar panel and battery. So, this research uses the available solar panel and battery based on the specification. The developed model is 100% renewable and has excess electricity is 8.83% shown in Figure 4-28. The total net presented the cost of this developed model is $120.04, the cost of energy is $0.07295, and the operating and management cost is $4.89 this cost analysis also states in Figure 4-28. The net present cost is the sum of the costs of capita cost has $56.80, Operating management cost has $46.95, replacement cost has

$22.51and salvage cos has $6.21. Those costs are shown in Figure 4-29. Figure 4-30 shows the cash flow of the cost that states above

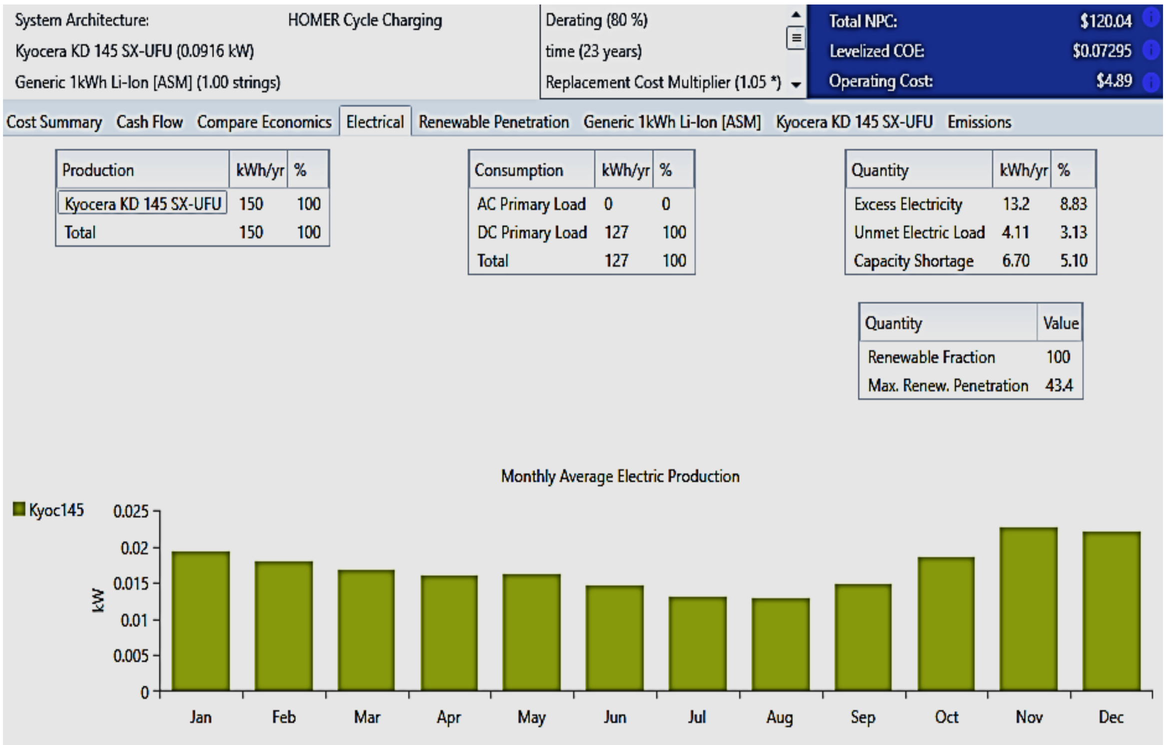

Figure 4-28 Monthly average electric production

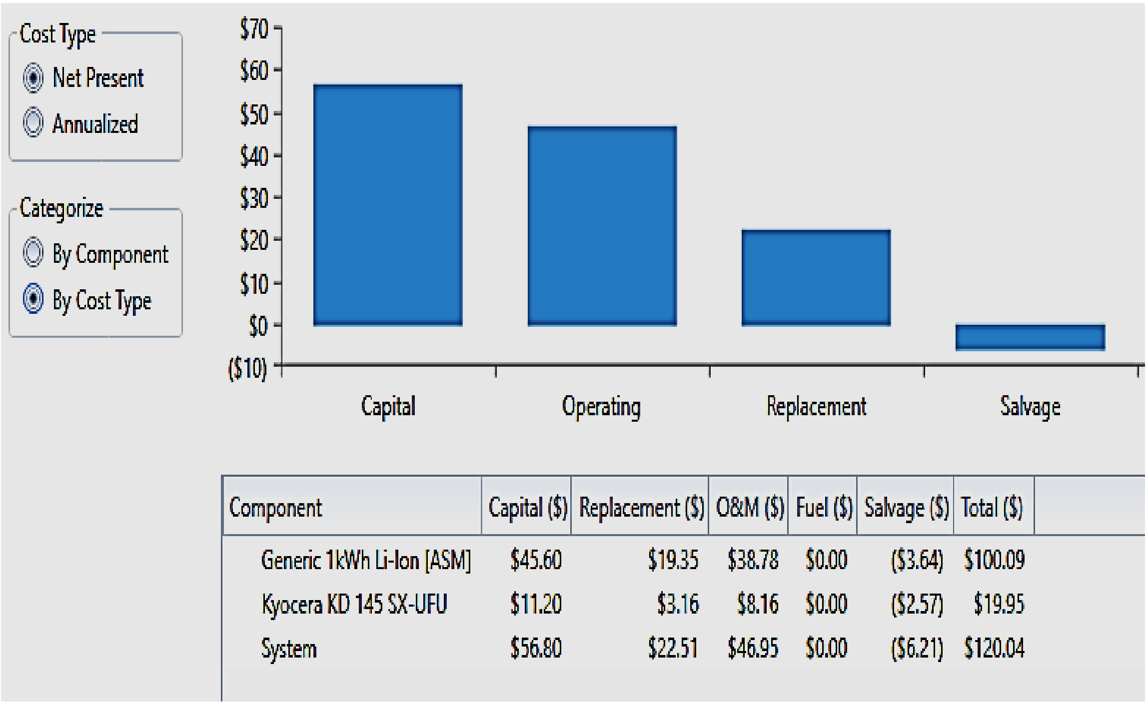

Figure 4-29 Net present costs listed by cost type

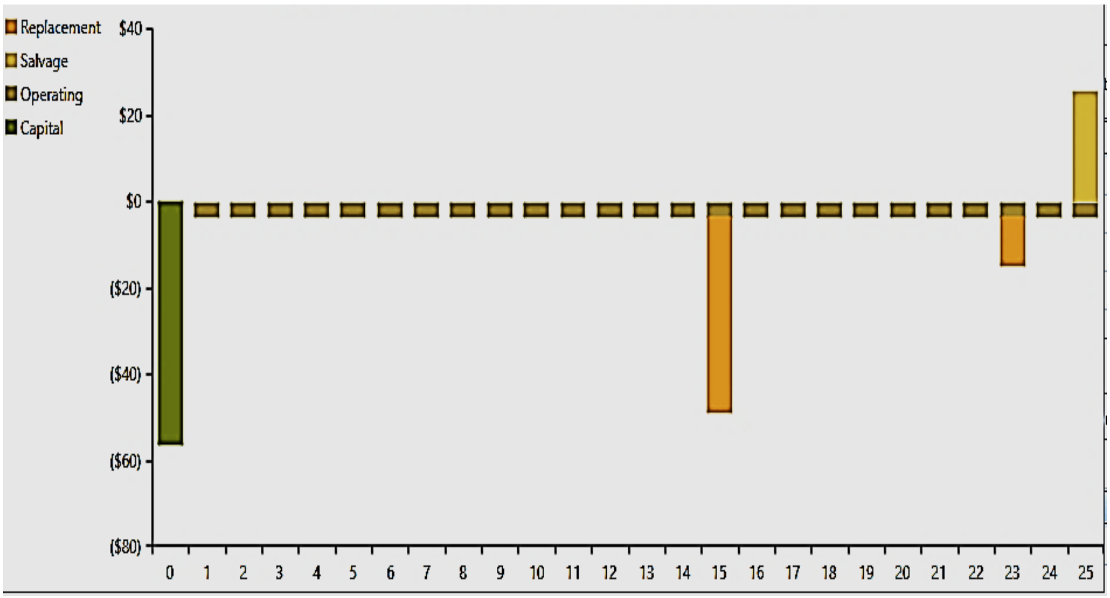

Figure 4-30 Nominal cash flow

The comparison of the current system cost and base case is shown in Figure 4-31. The sensitivity analysis that states in Table 4-1 simulation results are shown in Figure 4-32 that has a $130.60 total net presented cost and has $0.0797.

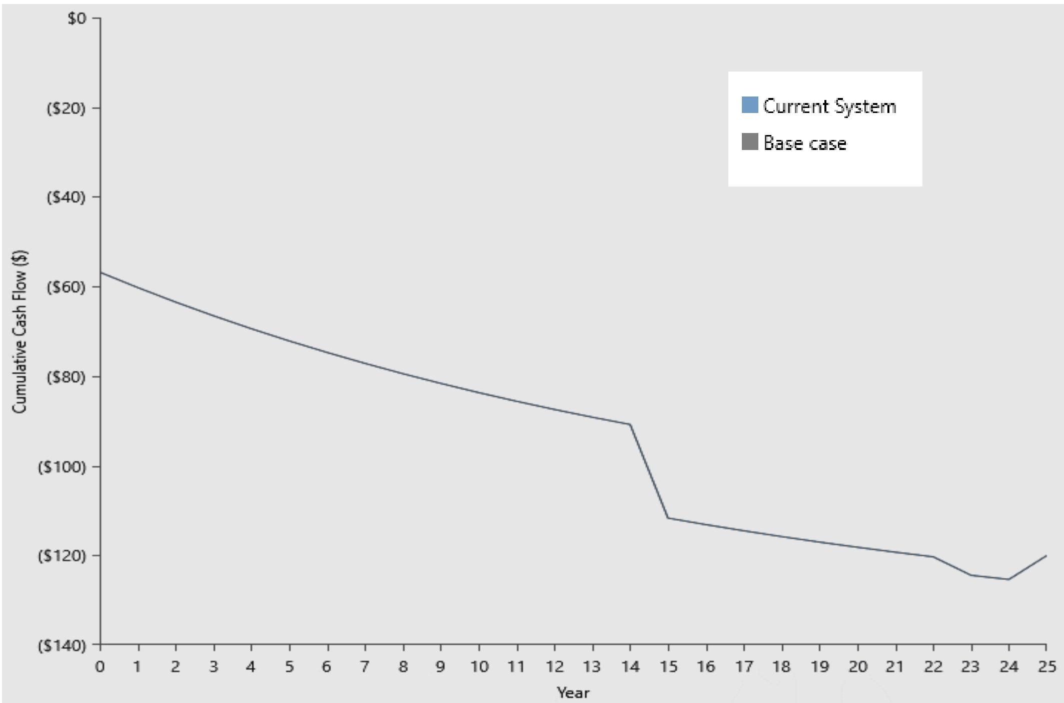

Figure 4-31 Cumulative cash flow

Table 4-1 Sensitivity analysis of solar system

Sensitivity parameters	PV
Replacement Cos multiplier	1.05
Solar Time	23yr.
Solar Scaled average	6kW/m^2
Temperature Scaled average	36^{o}C
Minimum state of charge	25%
Initial state charge	80%
minimum lifetime of the battery	4yr.
Derating	80%

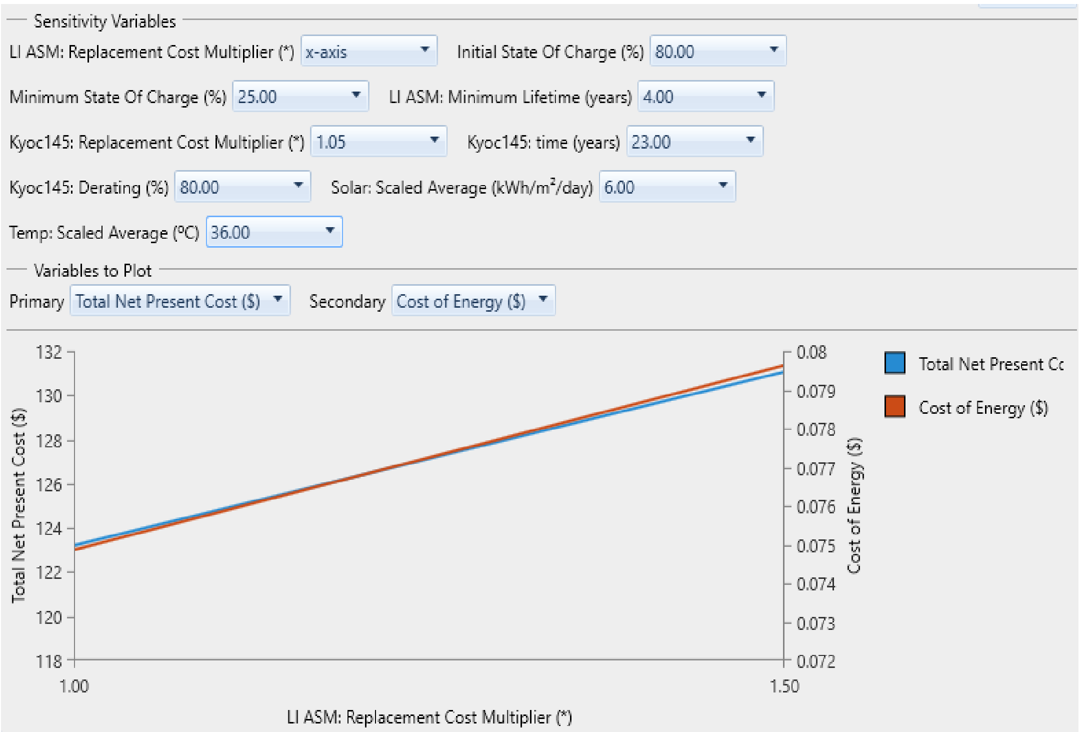

Figure 4-32 Sensitivity analysis graph

4.5. Experimental Result of Temperature Regulation

For experimental reasons the components used are those that are easily accessible and inexpensive. This however limits the quality and precision of the model which is not a primary concern at this time. So, the motor and the thermoelectric cooler which are the crucial components for temperature regulation were not able to achieve temperatures below

8 degrees Celsius. This is because the device characteristics are not designed for such low temperatures. And, using devices with such characteristics is expensive and unaffordable with the current budget. For the practical demonstration, the temperature range is instead between 14 degrees Celsius and 17 degrees Celsius. This does not affect the effectiveness of the system as the future devices with the specific characteristics required will be procured.

To regulate the input power the solar module uses a DC-DC converter and MPPT but to regulate the temperature uses a microcontroller to control the temperature inside the refrigeration system and a temperature sensor to detect the changing temperature inside the refrigeration. The microcontroller sends sigla to the driver to control the fan and receives the signal from the sensor. And the temperature sensor can detect 0.1°C of the temperature change in the refrigeration system. So, the temperature regulation process is more accurate and precise.

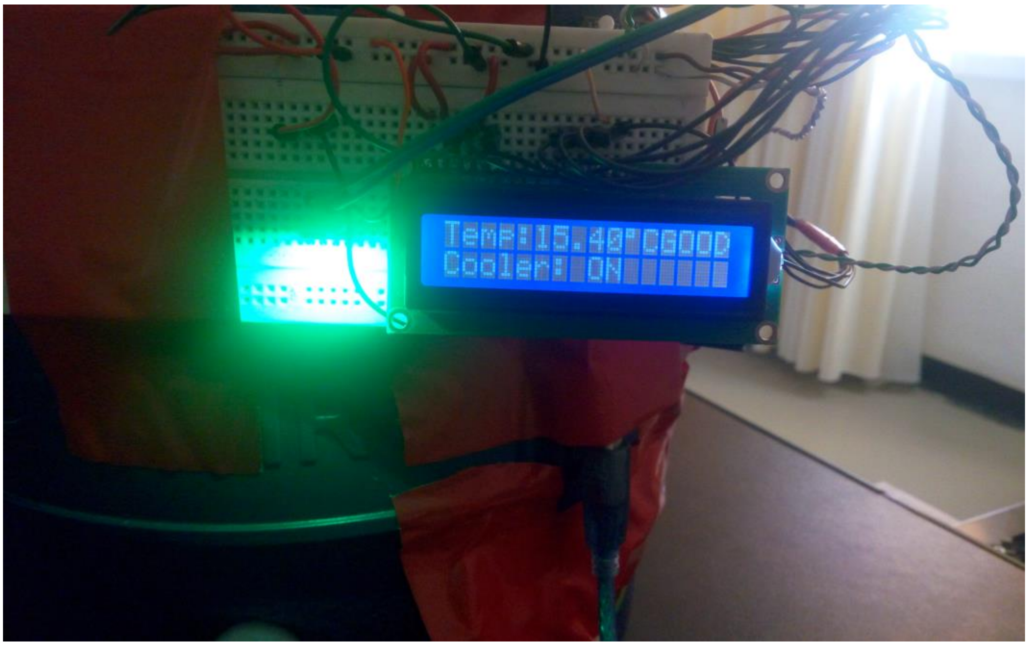

Figure 4-33 Result of temperature control when T is within the normal range

Figure 4-33 shows the temperature of the refrigeration system within range. The LCD show "GOOD". The fan and the Peltier module is turned on to further decrease the temperature to the lowest one. And LED turned on green to show that the temperature is in safe mode.

Figure 4-34 shows the simulation result of temperature regulation that inside temperature below the desired range (14°C to 17°C). In this range, the inside temperature is below 14°C so the display shows a "COLD" message to the user and the Peltier module and fan will off.

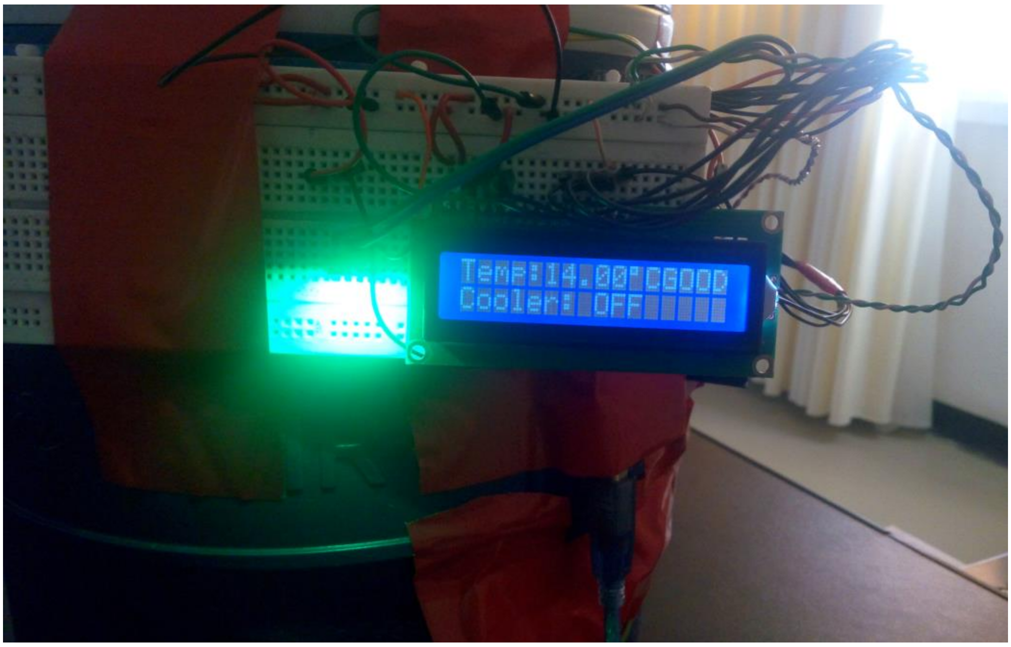

Figure 4-34 Result of temperature control below range

Figure 4-35 shows the simulation result of temperature regulation that inside temperature above the desired range (14^{o}C to 17^{o}C). This range temperature is above 17^{o}C thus the display shows a "HOT" message to the user, red LED light is turned on and the Peltier module and fan will on.

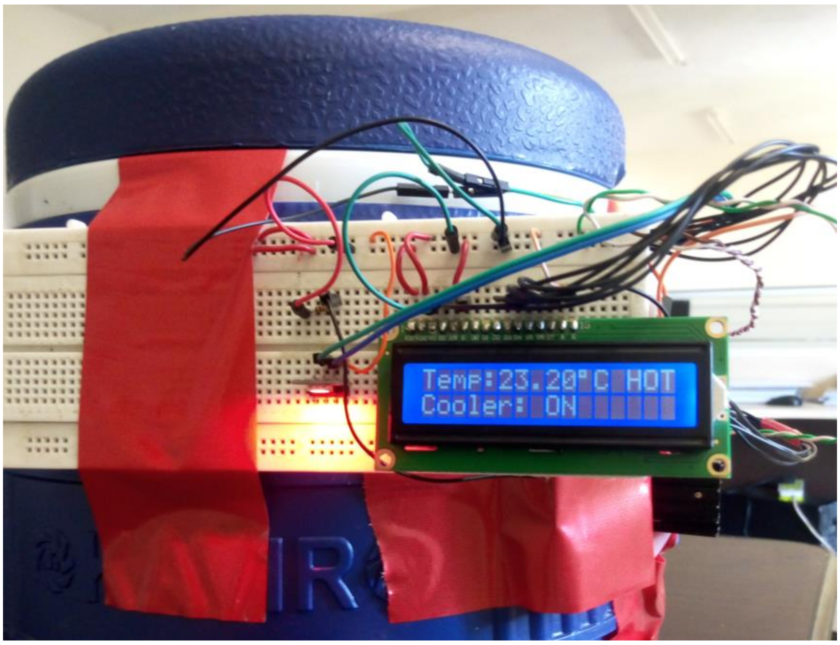

Figure 4-35 Result of temperature control above range

The experimental data appears in Figure 4-36. It shows that the row data of the temperature for 1.2 hours. As the conducting experiment shows that the temperature drops down from 25°C to 14°C in 21.5 min. and staying at the range for 8.75 min. the developed prototype can drop down 11°C within a short period. This is a good obtain of the system. It shows this system can feasible to manufacture for the market. Achieving fast cooling time is successful and answered RQ.4. But staying in the required temperature range is still has an issue. This is due to the thermal leakage of the refrigeration. The leakage will overcome by the use of a proper heat sink and cooling fan. During the time conducting this experiment it difficult to get the appropriate heat sink and a cooling fan because of the corona (COVID19) pandemic.

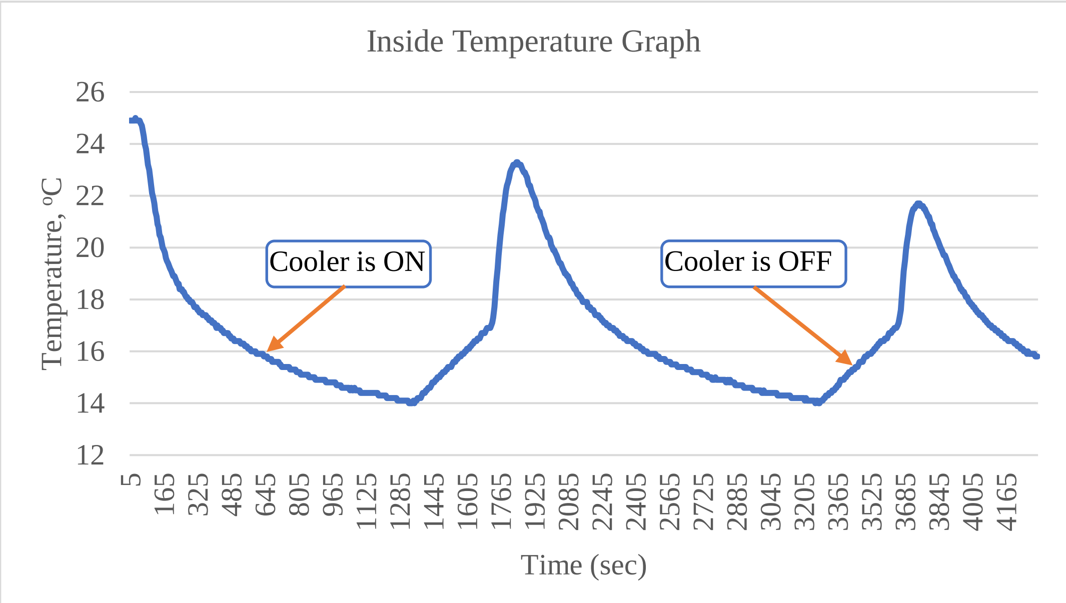

Figure 4-36 Inside temperature graph of the developed system

The summarize the temperature regulation system shown in Table 4-2 and the overall performance shown in Table 4-3.

Table 4-2 Summary of the result of the temperature controller

Temperature ranges	Cooler	LCD	Multi-LED
Temp > 17°C	ON	HOT	RED
17 °C < Temp <14 °C	ON	GOOD	GREEN
14 °C < Temp <17 °C	OFF	GOOD	GREEN
14 °C < Temp	OFF	COLD	RED

Table 4-3 Summary of performance parameter

Performance Parameters	Values
Current	5.25A
Voltage	12v
Cooling power	25.321W
Power	63W
COP	0.402
Lead-Acid battery	7.2AH
No. of Peltier module	2
Desired Temperature	15.0 ^{o}C
Ambient Temperature	25.1 ^{o}C
Time is taken to reach the lowest temperature	21.5 min
Time is taken to stay between the temperature range	8.75 min

4.6. Discussion of the Results

In this section, this research work discussed the simulation result of the developed system. Includes discussion of the TEC module based on performance parameter, discussion of solar modules based on the desired parameter of the system, and discussion on the temperature regulation system.

4.6.1. Discussion on the Result of TEC Module

This research work designed and simulated the Peltier module in the selected area and analyzed the performance parameter. The selected solar module has good performance depending on those parameters. The Peltier module would be refrigerated in the system environment in a different condition shown in Table 3-8. Those are maximum cooling power conditions, maximum COP conditions, and optimal conditions. Those conditions have an advantage and disadvantage. In the maximum cooling power condition shown in Figure 4-4, Figure 4-5, and Figure 4-6the Peltier module uses its maximum cooling power but it uses large power and large current compare with other conditions. This current may damage the Peltier module. Large power needs a large size of solar panel. And the efficiency of this condition is small compared with others.

In the maximum COP condition shown in Figure 4-7, Figure 4-8, and Figure 4-9Figure 4-7 the Peltier module reaches the maximum COP and efficiency of the module due to this condition it uses low power consumption compared with other condition but it uses too much number of Peltier module is needed in the developed system. This condition has large efficiency and it applies to medical application. In the optimal condition shown in Figure 4-10, Figure 4-11, and Figure 4-12 cases the design uses low power compare with the maximum power condition and a small number of Peltier modules compare with maximum COP.

Based on those comparisons of the condition and Table 3-8 this research work was chosen as the maximum power COP condition to meet the system specification and answered RQ.2. Figure 4-37 and Figure 4-38 demonstrate the Peltier module performance parameters (Cooling power, power input, COP, current, and voltage) graphical comparison of each condition (maximum cooling power, maximum COP, and midpoint). The graph shows that the maximum COP condition has better performance parameters than the others.

Note: The total energy efficiency system that photovoltaic driven thermoelectric cooling devices can be increased with the enhancement of photovoltaic system efficiency and with the use of thermoelectric materials with better performance and quality.

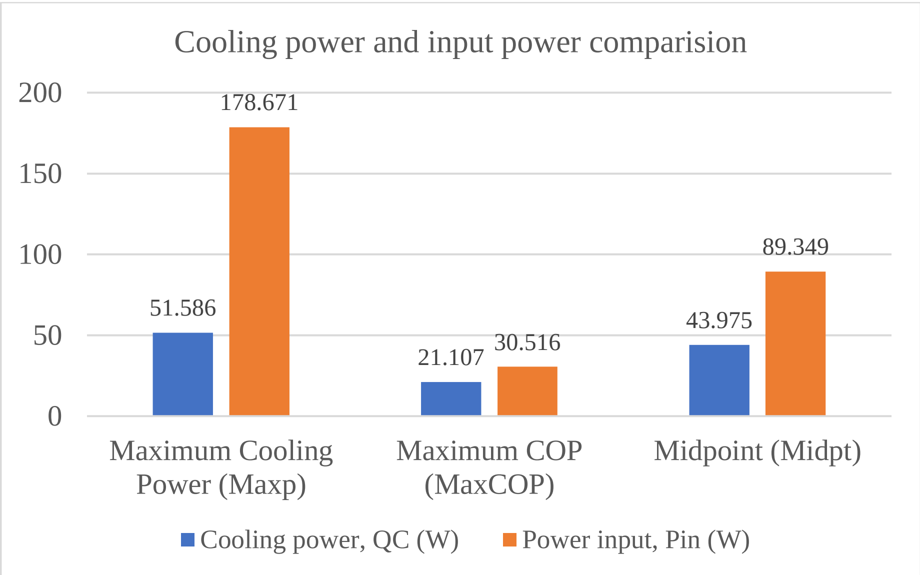

Figure 4-37 Graphical representation of the performance comparison of the Peltier module

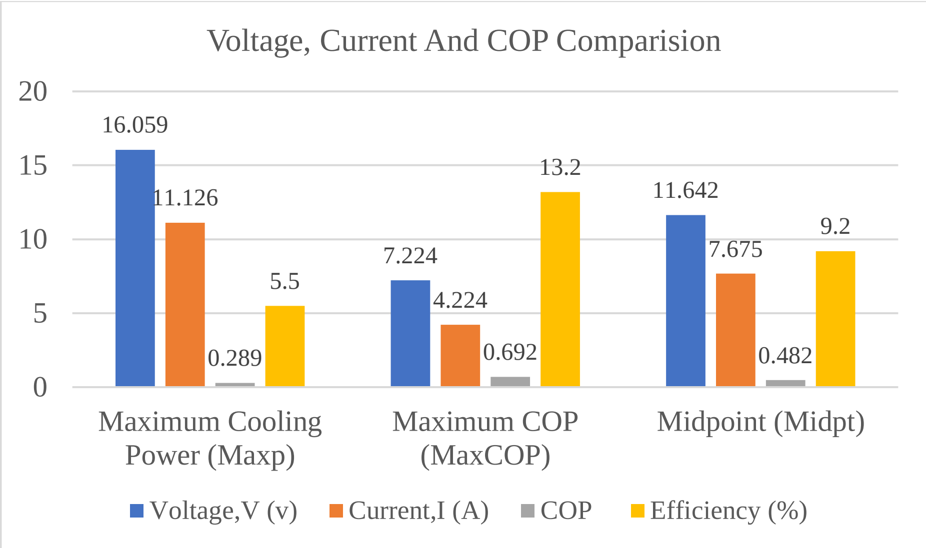

Figure 4-38 Graphical representation of the performance comparison of the Peltier module

4.6.2. Discussion on the Result of Solar Panel

Based on the maximum COP condition, the designed solar module is simulated by considering of worst-case condition. This condition is the lowest solar irradiation and the highest ambient temperature. The selected and designed solar panel has a good performance and answered the RQ.3. Based on the literature reviewed and some standards stand-alone solar module is not sufficient for regulated power input so it must use a converter and MPPT. This research work uses DC-DC buck-boost converter and P and O MPPT techniques to deliver regulated power to the load. Depending on the load resistance, the buck-boost converter is stepdown the solar module voltage to the desired voltage and current shown in Figure 4-15and Figure 4-16 with the help of the Duty ratio generated by MPPT.

Solar irradiation is not the same in the selected environment it's varying depending on the seasons in a year. The MPPT gives the duty ratio by tracking the irradiation change shown in Figure 3-3 and adjust the converter bases on gate pulse to regulate the input powers shown in Figure 4-24. The selected solar module that states in Equation (3.33) is the best choice based on the above Peltier module conditions. In the case of emergencies, the system uses secondary battery storage as a backup of power. The selected battery stated in Equation (3.36) and the performance shown in Figure 4-26 is the best choice according to the developed system.

Based on the variety of solar radiation the buck-boost converter can step down the voltage as shown in Figure 4-39. Within the case of current, it's step-up within the range of low solar insolation accessibility that's June to September months shown in Figure 4-40. The power at the load is ventured down like a voltage. This stepped down power is shown in Figure 4-41.

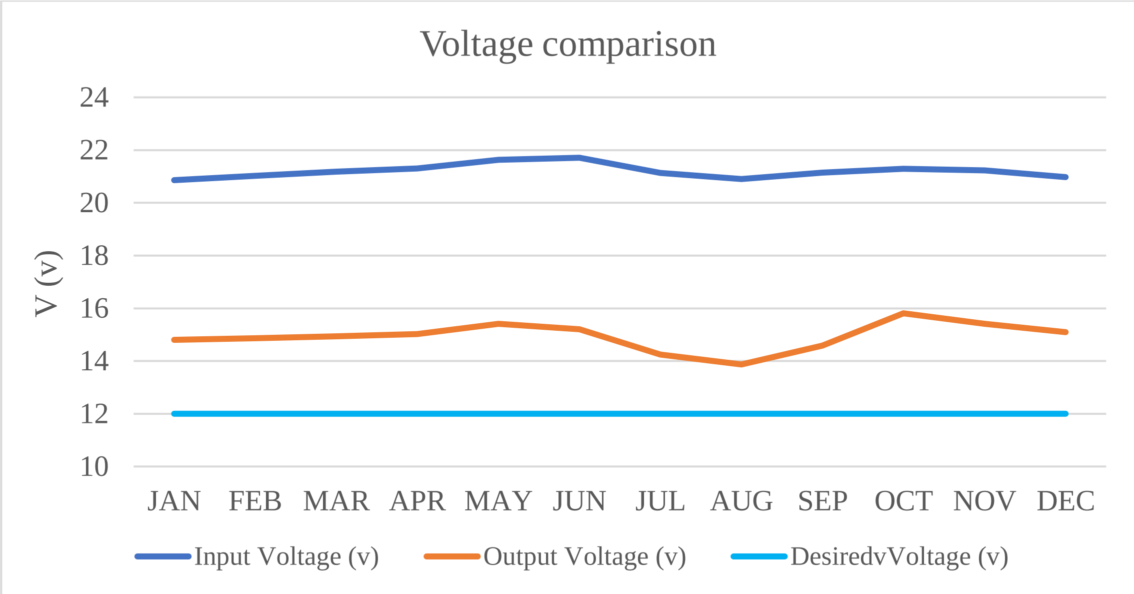

Figure 4-39 Voltage comparison

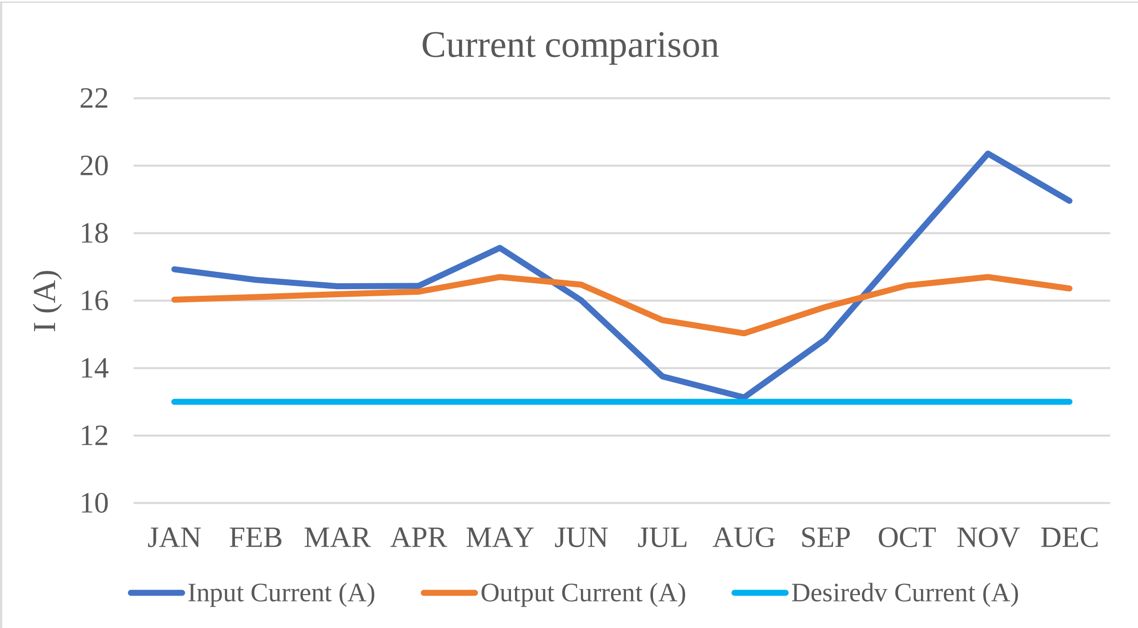

Figure 4-40 Current comparison

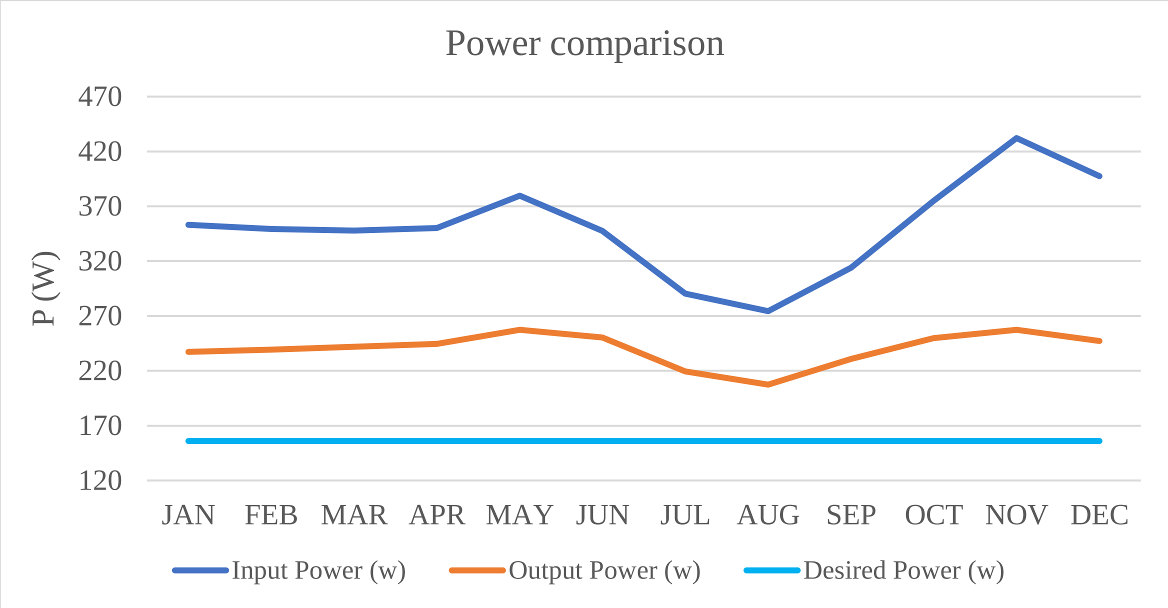

Figure 4-41 Power comparison

4.6.3. Discussion on the Result of HOMER Software

The cost analysis and optimization are shown in Figure 4-28 and Figure 4-29 indicates that the developed system is fully renewable and cost-effective. It can develop at a small amount of cost. The sensitivity analysis shows that the overall cost variation is changing in a small amount. So, this system applies to the selected environment and other regions. Table 4-4 shows that the greenhouse gas emission simulation result of the developed system. It indicates that the system doesn't have a greenhouse effect at all. All greenhouse effect has zero values in the whole month.

Table 4-4 Greenhouse gas emission

Quantity	Value	Units
Carbon Dioxide	0	kg/yr
Carbon Monoxide	0	kg/yr
Unburned Hydrocarbons	0	kg/yr
Particulate Matter	0	kg/yr
Sulfur Dioxide	0	kg/yr
Nitrogen Oxides	0	kg/yr

4.6.4. Comparison of the Performance of the Developed System

The overview of the performance comparison of the developed system with the experimental result to the simulation result shown in Table 4-5 and the developed system to literature reviewed shown in Table 4-6.

Table 4-5 Comparison of the experimental result with simulation result

Paper	Temperature range	No. of modules	COP	Time required
Developed prototype	25.1^{o}C-14.0 ^{o}C	2	0.41	21.5min
Developed simulation	40.38^{o}C-5.0 ^{o}C	3	0.692	60min

Table 4-6 Comparison of the developed system with literature reviews

Paper	Temperature range	No. of modules	COP	Time required
Developed prototype	25.1^{o}C-14.0 ^{o}C	2	0.41	21.5min
Developed simulation	40.38^{o}C-5.0 ^{o}C	3	0.692	60min
M. Barawkar et.al	35^{o}C -5^{o}C	Multi-stage	-	150min
K. Rokde et.al	35^{o}C -15^{o}C	3	-	570min
Abhijit Raju et.al	27^{o}C -12^{o}C	10	0.17	50min
Jatin Patel et.al	Up to 10^{o}C	3 Multi-stage	1.21	-

To summarize the discussion section, to get is enough power to operate 7L of a portable mini- ridge, this research choosing the maximum COP designed based on Table 3-8 attain's the maximum efficiency of the Peltier cooling effect among other performance conditions. The demonstrated developed system is cost-effective for developing countries.

CHAPTER 5

CONCLUSION AND RECOMMENDATION

5.1. Conclusion

Ethiopia is one of the countries in Africa that face vaccine transportation problem in the medical health care sectors. Especially the Logiya town in the Afar region is suffering from this kind of problem. To overcome this problem this kind of research work is needed. The application of this mini-refrigeration is very wide and it can be used in various places for a variety of operations. Likewise, The one reason for this research is being satisfied with the space interior the cooler is adequate sufficient to cool the suitable amount of stuff, such as medicines, vaccines, and injections needed at the primary health care centers in the rural area where power supply is scarce.

Based on the cooling load estimation the result of this work indicates that the developed system has an efficient and effective cooling effect for the selected environment and an accurate and precise temperature regulation system. This developed system is fully eco-friendly it doesn't have a greenhouse effect and fully renewable source. Not only renewable and eco-friendly but also cost-effective, the system could develop at a small amount of cost. So, the developing country like Ethiopia can develop this kind of system for their medical service advancement.

Improving the efficiency of the Peltier module depends on the improvement of the COP. To improve COP the system uses the efficient power supply and power converters like DC-DC buck-boost converters and decreases the temperature difference between the cold and the warm side by using well thermal designed. This research achieving 0.692 of COP, it's higher than the comparatives. 95.99% of the efficiency of DC-DC buck-boost converters. And the total Peltier efficiency obtain is 13.2%. By considering some factors, practically the refrigeration system achieves the goal of decreasing cooling time. That is reaching a 12^{o}C difference of temperature in 21.5 minutes of fast cooling time. But it stays in the range for 8.75 minutes due to the thermal leakage of the refrigeration. This leakage is overcome by the use of an appropriate heat sink and cooling fan as well as increasing the Peltier module number.

This refrigeration system can be implemented with a small amount of power consumption. that uses a 12V/ 45W solar panel and a DC-DC buck-boost converter to achieve the design requirements achieve efficiency. It can work for 15hr with the help of a battery. To store the vaccine for 24 hours the only thing is increasing the battery size to 30AH capacity. This mini-refrigeration system meets the WHO vaccine handling toolkit requirements and lightweight to travel anyplace especially for pastoralist areas in Ethiopia.

5.2. Recommendation

There are several different types of cooling devices available to remove the heat from industrial enclosures as well as medical enclosures, but as the technology advances, thermoelectric cooling is emerging as a truly viable method that can be advantageous in the handling of certain small to medium applications. this research work strongly recommended that a solar-powered Peltier based mini refrigeration system is suitable for the Logiya. Not only in Logiya but also in other rural areas in Ethiopia.

As the efficiency and effectiveness of thermoelectric cooling steadily increase, the benefits that it provides including self-contained, solid-state construction that eliminates the need for refrigerants or connections to chilled water supplies, superior flexibility, and reduced maintenance costs through higher reliability will increase as well**.** It can be used in an ambulance for storing medical equipment, it can also be used in the remote area for storing medicines, blood plasma, antibodies, and blood samples. Ethiopia is one of the developing countries in Africa depending on that it has only 40% of power supply therefore this kind of research is important for the use of alternative power systems and advanced technology of medical service. It saves the cost of the millions of the vaccine, saves a lot of children from disease, and infant mortality.

5.3. Future Work

Solar power nowadays is playing a major role in meeting the energy requirement of our country. It is being developed at a very fast rate and its applications in many areas are being explored. The fridge is intended at exploring the same and provides. An efficient and economical solution to the areas where there is no electricity and cooling is required.

Though this mini-refrigeration system is working satisfactorily to its full capacity, still many changes and improvements can be done in this fridge to make it more user friendly and classy. These measures and changes, if implemented can play an important role in future models to be developed. Some of these measures and changes are:

1. The number of Peltier units can be increased to the fastest decrease in the temperature inside the fridge.
2. The same fridge can be used for heating purposes if we also insulate the other side i.e. the heating side of the fridge within the box.
3. To regulate temperature uses a PID controller rather than an on/off controller.

Acknowledgement for ASTU

This research thesis is funded by Adama Science and Technology University under the grant number **ASTU/SM-R/074/19**, Adama, Ethiopia.

REFERENCES

[1] P. G. Sonkhede and P. A. K. Pathrikar, "Portable Thermoelectric Refrigeration System for Medical Application," *International Journal of Innovative Research in Computer and Communication Engineering (IJIRCCE),* vol. 4, no. 3, pp. 3190-3195, 2016.

[2] Dr.V.V.Karthikeyan, L.Kalaivani, L.Naveena, and B.Nivetha, "Solar Refrigerator For Vaccines In Rural Areas," *IOSR Journal of Engineering (IOSRJEN),* vol. 4, no. 3, pp. 38-42, 2014.

[3] Heidi J Larson, Louis Z Cooper, Juhani Eskola, Samuel L Katz, Scott Ratzan, "Addressing the vaccine confidence gap," *Lancet,* vol. 378, p. 526–535, 2011.

[4] Abdul Majid1, Nashrul Fazli bin Mohd Nasir1, and Izzuddin Zaman2, "Cooling Performance of Thermoelectric Cooling (TEC) and Applications: A review," *MATEC Web of Conferences,* vol. 3, no. 12, p. 225, 2018.

[5] Committee, WHO immunization practices advisory, "IMMUNIZATION SUPPLY CHAIN AND LOGISTICS," WHO, GENEVA, SWITZERLAND, 2014.

[6] IIP, "The Vaccine Cold Chain Module 2," WHO, Geneva, Switzerland, 2015.

[7] S. Carlos, "History of the development of thermoelectric materials for electric power generation and criteria of their quality," *International Standard Serial Number (ISSN),* vol. 17, no. 5, pp. 1516-1439, 2014.

[8] A. Polozinea, S. Sirotinskayab, and L. Schaeffer, "History of Development of Thermoelectric Materials for Electric Power Generation and Criteria of their Quality," *ISSN,* vol. 12, no. 5, pp. 1516-1439, 2014.

[9] netzsch, "Thermoelectric Materials," 8 2013. [Online]. Available: www.netzsch.com/n47875. [Accessed 4 3 2020].

[10] L. T. Systems, "Electronic Enclosure Cooling: Thermoelectric vs. Compressor Based Air Conditioners," Laird Thermal Systems Application Note, 2016.

[11] Gamarachchi and B. Pasindu, "THERMOELECTRIC SYSTEM MODELING AND DESIGN," *Researchgate,* vol. 2, no. 12, pp. 2-4, 2017.

[12] T. M. Pravinchandra, "Peltier Cooling Module," *researchgate,* vol. 3, no. 12, pp. 6-11, 2016.

[13] A. G. G. Vega, "Designing a Solar PV System to Power a Single Phase Distribution System," 5 2019. [Online]. Available: https://scholarworks.uark.edu/eleguht. [Accessed 3 2 2020].

[14] AL-JUBOORI and S. SAADOON, Energy Science and Technology, vol. 6, Al-Kitab University: Studium Press LLC, 2016, pp. 141 - 163.

[15] M. A. Muqeet, A. Fatima, Md.Ismail.B and Md.Abdullah, "Concept Design and Parameter Estimation of a Solar Photovoltaic UPS and Supplementation System," *International Journal of Advanced Research in Electrical, Electronics and Instrumentation Engineering,* vol. 4, no. 12, pp. 9691-9696, 2015.

[16] Y. Chu, Review and Comparison of Different Solar Energy Technologies, Global Energy Network Institute (GENI), 2011.

[17] V. Karthikeyan, S. Rajasekar, V. Das, P. Karuppanan, and A. K. Singh, "Grid-Connected and Off-Grid Solar Photovoltaic System," in *Smart Energy Grid Design for Island Countries*, Springer, Cham, Springer, 2017, pp. 125-157.

[18] C. R. (Ph.D.), "Solar Electric System Design, Operation and Installation," Washington State University Extension Energy Program, Olympia, 2009.

[19] S. A. Lopa, S. Hossain, M. K. Hasan, and T. K. Chakraborty, "Design and Simulation of DC-DC Converters," *International Research Journal of Engineering and Technology (IRJET),* vol. 2, no. 1, pp. 63-70, 2016.

[20] Jatin Patel, Matik Patel, Jigar Patel, Himanshu Modi, "Improvement In The COP Of Thermoelectric Cooler," *INTERNATIONAL JOURNAL OF SCIENTIFIC & TECHNOLOGY RESEARCH,* vol. 5, no. 5, pp. 2277-8616, 2016.

[21] M. Barawkar1, A. Kulkarni, N. Tayade and P. Chistalkar, "Smart Refrigeration System Based On Embedded System," *International Journal of Innovative Research in Computer and Communication Engineering,* vol. 07, no. 02, 2019.

[22] J. P. Supriya, B. P. Pooja, B. S. Nikita, and P. S.Borate, "Solar Powered Eco-friendly Mini Fridge," *International Journal of Electrical, Electronics and Computer Systems (IJEECS),* vol. 5, no. 2, p. 89, 2017.

[23] K. Rokde, M. Patel, T. Kalamdar, R. Gulhane, and R. Hiware, "Peltier Based Eco-Friendly Smart Refrigerator for Rural Areas," *International Journal of Advanced Research in Computer Science and Software Engineering,* vol. 7, no. 5, 2017.

[24] Dr.V.V.Karthikeyan, L.Kalaivani, L.Naveena, and B.Nivetha, "Solar Refrigerator For Vaccines In Rural Areas," *IOSR Journal of Engineering (IOSRJEN),* vol. 04, no. 03, p. 38, 2014.

[25] Abhijith Raju, Ajeesh J, Akash S, Akhil T J, Vishnu Bose, and Jinshah BS, "Development of Portable Solar Thermoelectric Refrigerator," *International Journal of Scientific & Engineering Research,* vol. 7, no. 4, pp. 2229-5518, 2016.

[26] Abhishek Sharma, Dr. Alka Bani Agrawal, and Dr. Nitin Shrivastava, "Solar Energy based Refrigeration System using Peltier Device," *International Journal of Theoretical & Applied Sciences*, vol. 10, no. 1, pp. 110-116, 2018.

[27] Advisory Committee on Immunization Practices (ACIP), "Vaccine Storage and Handling Toolkit," The Centers for Disease Control and Prevention (CDC), Georgia, USA, 2019.

[28] D. o. V. a. Biologicals, "Guideline for establishing or improving primary and intermediate vaccine stores," World Health Organization, Geneva 27, Switzerland, 2002.

[29] ASHRAE, REFRIGERATION, ASHRAE, 1791 Tullie Circle, N.E., Atlanta, GA 30329: ASHRAE®, 2014.

[30] H. Lee, THERMOELECTRICS DESIGN AND MATERIALS, Western Michigan University, USA: John Wiley & Sons Ltd, 2017.

[31] G. Luthra, "Comparison of Characteristics of Various Motor Drives Currently used in Electric Vehicle Propulsion System," *International Journal of Mechanical and Production Engineering*, vol. 5, no. 6, 2017.

[32] A. J. Varghese, R. Roy, and P. S. Thirunavukkarasu, "Optimized Speed Control for BLDC Motor," *International Journal of Innovative Research in Science, Engineering and Technology*, vol. 3, no. 1, 2014.

[33] S. R. Jape and A. Thosar, "Comparison of Electric Motors for Electric Vehicle Application," *International Journal of Research in Engineering and Technology*, vol. 6, no. 9, p. 2017.

[34] D. W. Hart, Power Electronics, 1221 Avenue of the Americas, New York, NY 10020: McGraw-Hill, a business unit of The McGraw-Hill Companies, Inc, 2011.

[35] Altaf Hussain, Muhammad Hammad, and Kamran Hafeez, "Programming a MicrocontrollerProgramming a Microcontroller," *International Journal of Computer Applications*, vol. 155, no. 1, p. 0975 – 8887, 2016.

[36] Yılmaz GÜVEN, 2Ercan COŞGUN, 3Sıtkı KOCAOĞLU, Harun GEZİCİ,5Eray YILMAZLAR, "Understanding the Concept of Microcontroller Based Systems To Choose The Best Hardware For Applications," *International Journal of Engineering And Science*, vol. 6, no. 9, pp. 38-44, 2017.

[37] D. E. Franklin, "Solar Photovoltaic (PV) System Components," The University of Arizona College of AgriCUlTUre And life sCienCes, Tucson, Arizona, 2018.

[38] S. P. Jamble, P. P. Bachal, N. S. Barge and B. S. P., "Solar Powered Eco-friendly Mini Fridge," *International Journal of Electrical, Electronics and Computer Systems (IJEECS),* vol. 5, no. 2, pp. 2347-2820, 2017.

[39] Mali, M. Awasthi, and K. V, "Design and Development of Thermoelectric Refrigerator," *International Journal of Mechanical Engineering and Robotics Research (IJMERR),* vol. 1, no. 3, pp. 389-390, 2012.

[40] Genus Fekadu, Gadise Merga, and Mohammed Gebre, "Assessment of Medicines Cold Chain Storage Conformity with the National Requirements in Governmental Health Care Facilities of Nekemte Town, Western Ethiopia," *Journal of Bioanalysis & Biomedicine,* vol. 10, no. 6, pp. 118-122, 2018.

REFERENCE LINKS

[L1] meerstetter, "www.meerstetter.ch," meerstetter, [Online]. Available: https://www.meerstetter.ch/customer-center/compendium/70-peltier-elements#COP. [Accessed 13 10 2020].

[L2] www.meerstetter.ch, "www.meerstetter.ch," www.meerstetter.ch, [Online]. Available: https://www.meerstetter.ch/customer-center/compendium/71-peltier-element-efficiency. [Accessed 13 10 2020].

[L3] HNN, "www.healthynewbornnetwork.org," The Healthy Newborn Network (HNN), [Online]. Available: https://www.healthynewbornnetwork.org/country/ethiopia/. [Accessed 22 5 2020].

[L4] netzsch, "Thermoelectric Materials," 8 2013. [Online]. Available: www.netzsch.com/n47875. [Accessed 4 3 2020].

[L5] wikipidia, "www.wikipidia.com," wikipedia, 14 2 2020. [Online]. Available: https://en.wikipedia.org/wiki/Thermoelectric_materials#Applications. [Accessed 4 3 2020].

[L6] S. Das, "www.electronicsandyou.com," Electronics and You, 1 2 2020. [Online]. Available: http://www.electronicsandyou.com/pv-cell-working-principle-how-solar-photovoltaic-cells-work.html. [Accessed 3 3 2020].

[L7] https://www.energysage.com/solar/101/types-solar-panels/

[L8] BatteryUniversity, "www.batteryuniversity.com," Cadex Electronics Inc., 06 08 2019. [Online]. Available: https://batteryuniversity.com/learn/article/secondary_batteries. [Accessed 18 4 2020].

[L9] ethiovisit, "www.ethiovisit.com," EthioVisit, [Online]. Available: https://www.ethiovisit.com/afar/66/.

[L10] NASA, "power.larc.nasa.gov," NASA, [Online]. Available: https://power.larc.nasa.gov/data-access-viewer/?fbclid=IwAR2owPBKGFkCYP7ZASos9zhCzvPP2LN3m0g5XcTtHRckaoCAkS7h7UVvEhk. [Accessed 6 6 2020].

[L11] https://www.europeanthermodynamics.com/news/

[L12] https://www.google.com/imgres?imgurl=x-raw-image%3A%2F%2F%2Fefe5f0358ef217f57805a062cc7e0d1780c02d5a55d7883fad6ba0984010a26a&imgrefurl=http%3A%2F%2Fhomepages.wmich.edu%2F~leehs

%2FME539%2FChapter%25203.pdf&tbnid=9RfyjjXw5e_WhM&vet=12ahUKEwjBoZ-ZlsrsAhUOTBoKHXxlAYYQMyhJegQIARBX..i&docid=lxELVIAqpee4iM&w=490&h=339&q=Cutaway%20of%20a%20typical%20thermoelectric%20module&client=firefox-b-d&ved=2ahUKEwjBoZ-ZlsrsAhUOTBoKHXxlAYYQMyhJegQIARBX

[L13] https://electric-skateboard.builders/t/how-does-the-torque-curve-change-with-voltage/25760

[L14] T. E. Company, "https://www.tme.eu/," TEM Electronics Company, [Online]. Available: https://www.tme.eu/en/details/pe60201b3-a99/dc12v-fans/sunon/pe60201b3-000u-a99/. [Accessed 20 6 2020].

[L15] Cooltechleisure, "www.cooltechleisure.co.uk," Cooltechleisure, [Online]. Available: https://cooltechleisure.co.uk/faqs-thermoelectric-solutions/.

[L16] https://www.researchgate.net/figure/The-two-diode-circuit-model-for-PV-module_fig1_305828795

[L17] T. Instrument, "www.ti.com," 1 3 2020. [Online]. Available: https://www.ti.com/lit/an/slva390a/slva390a.pdf?ts=1602453126250&ref_url=https%253A%252F%252Fwww.google.com%252F. [Accessed 6 8 2020].

[L18] ALIBABA, "ALIBABA," guandong, [Online]. Available: https://www.alibaba.com/product-detail/DC-8-36V-12V-24V-TO_62290260760.html?spm=a2700.galleryofferlist.normal_offer.d_title.6fd84592qMRiAa. [Accessed 10 10 2020].

[L19] Amazon, "https://www.amazon.com/," Amazon, [Online]. Available: https://www.amazon.com/Arduino-A000066-ARDUINO-UNO-R3/dp/B008GRTSV6. [Accessed 20 6 2020].

[L20] J. Gums, "https://www.digikey.com/," Digi-Key Electronics, 26 01 2018. [Online]. Available:https://www.digikey.com/en/blog/types-of-temperature sensors#:~:text=There%20are%20four%20types%20of,based%20integrated%20circuits%20(IC).. [Accessed 20 6 2020].

[L21] Omega, "https://www.omega.co.uk/," omega, [Online]. Available: omega.co.uk/temperature/z/thermocouple-rtd.html. [Accessed 20 6 2020].

[L22] Indiamart, "https://www.indiamart.com/," Indiamart, [Online]. Available: https://www.indiamart.com/proddetail/lm35dz-module-21832806688.html. [Accessed 20 6 2020].

APPENDIX

Appendix A: MATLAB Block Diagram

1. Overall MATLAB block diagram

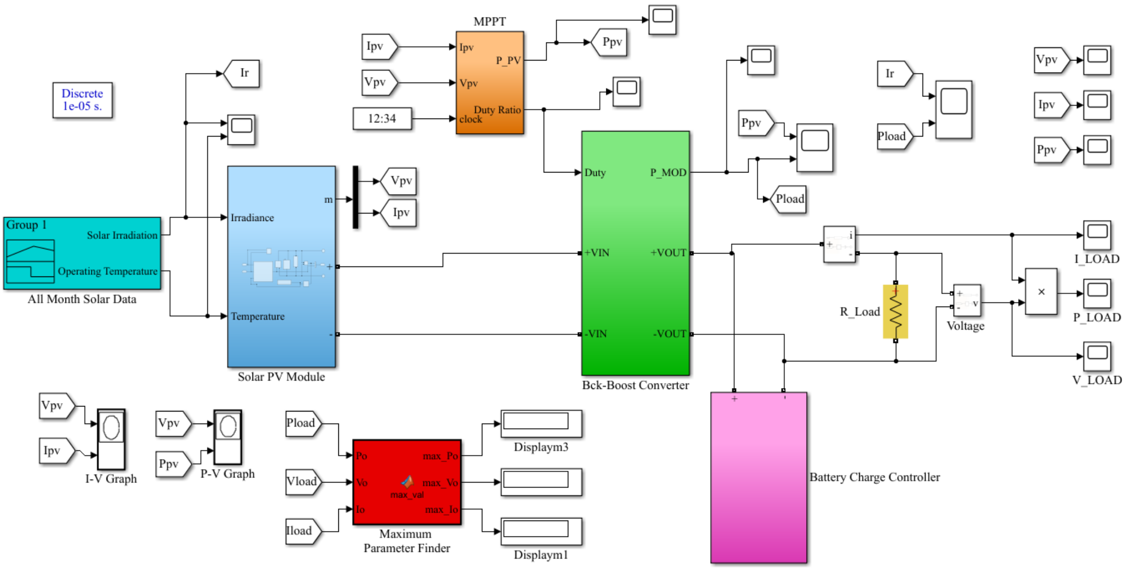

2. Solar PV block diagram

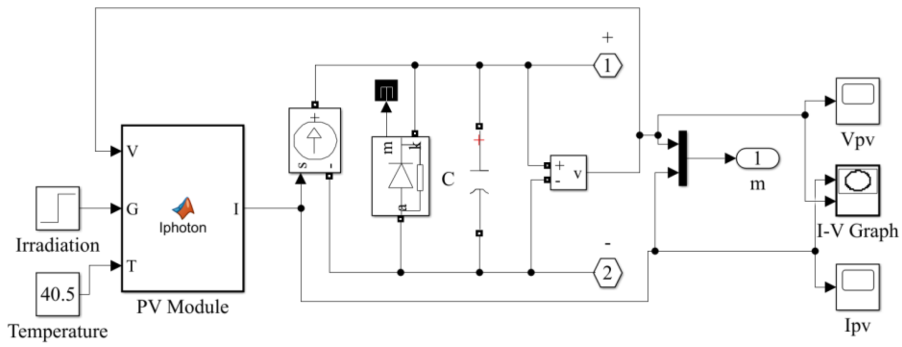

3. MPPT P an O block diagram

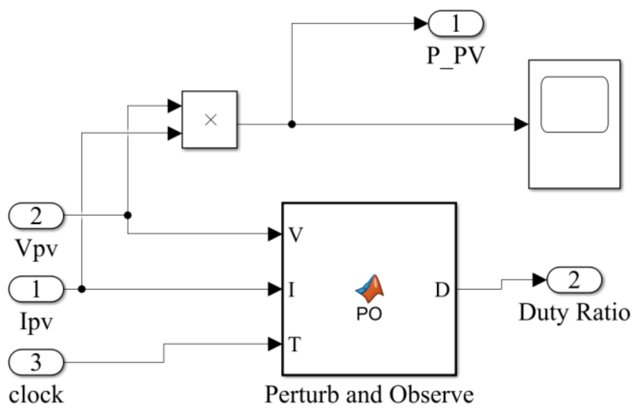

4. DC-DC Buck-Boost converter block diagram

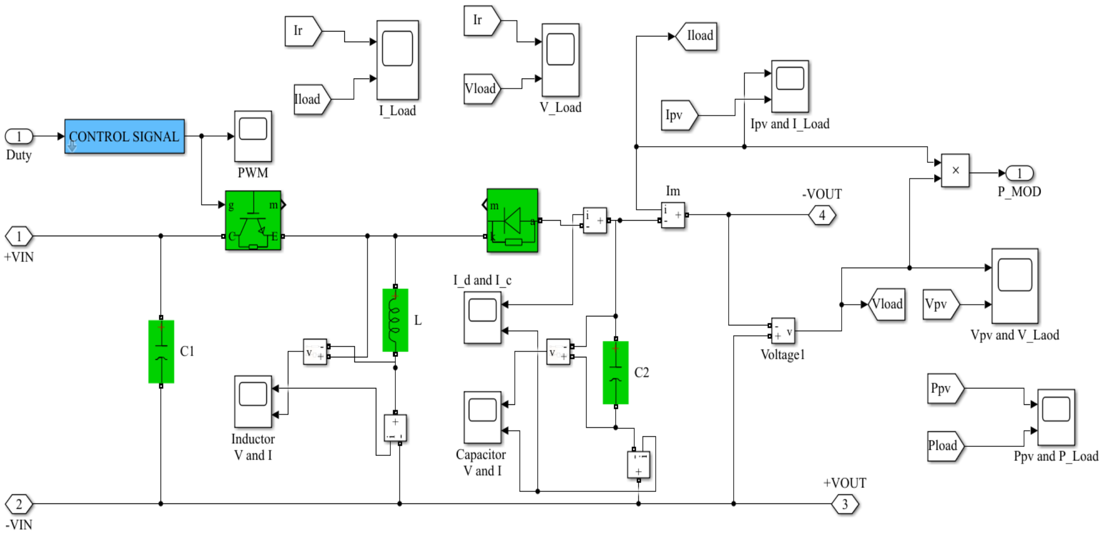

5. Battery charge controller

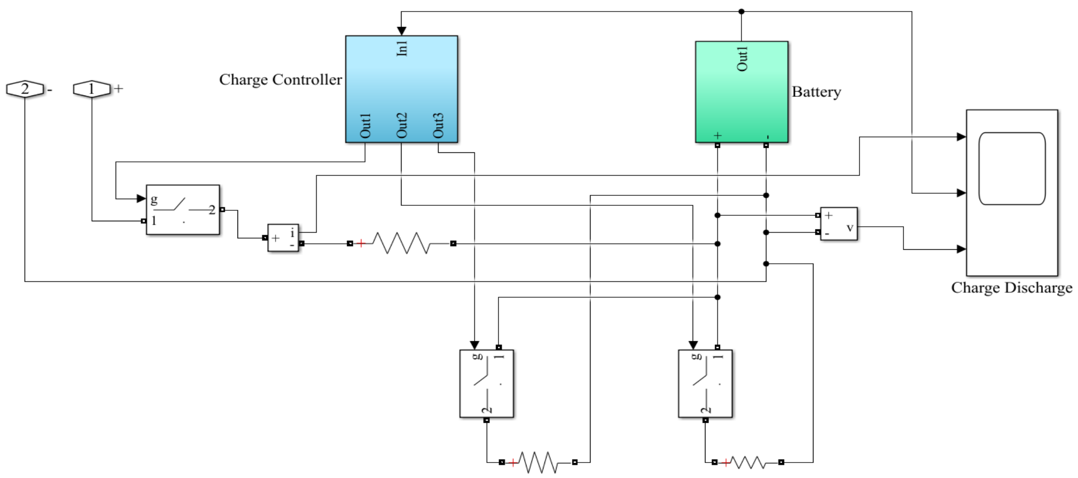

6. Battery block diagram and Charge controller block diagram

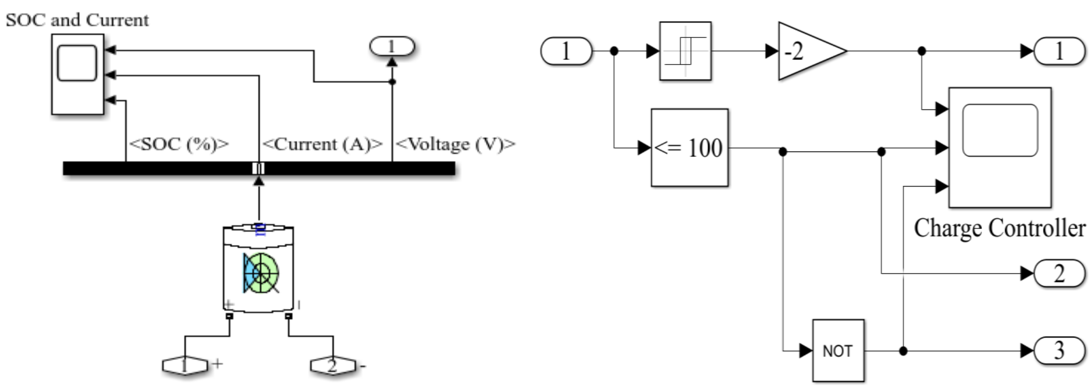

7. Peltier module diagram

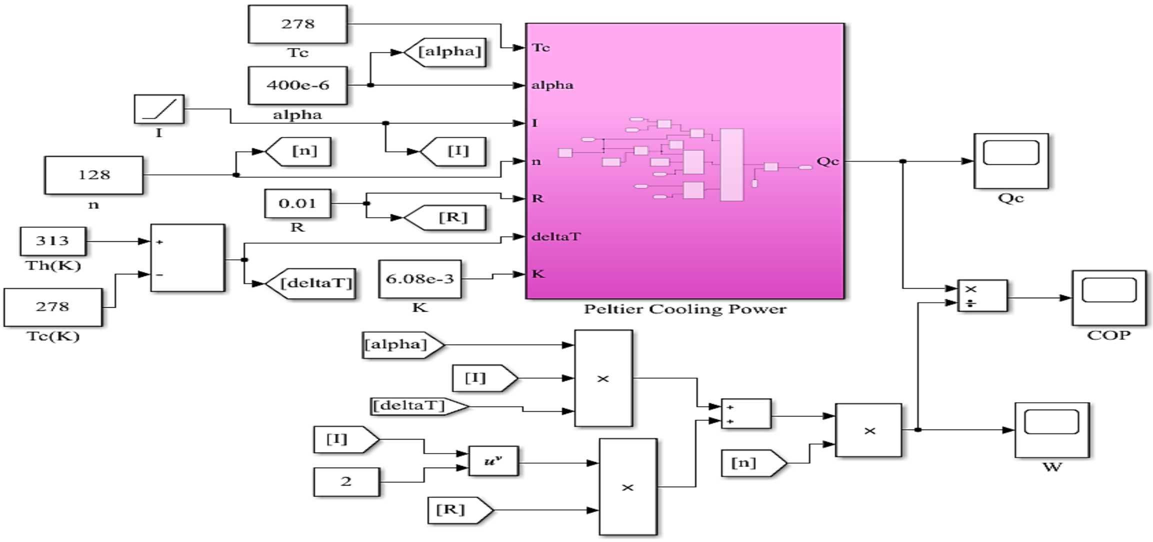

8. Peltier cooling power diagram

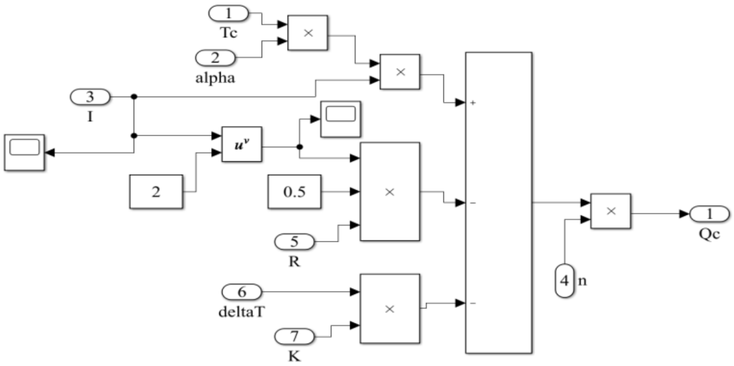

Appendix B: HOMER Block Diagram

1. Schematic diagram of the system

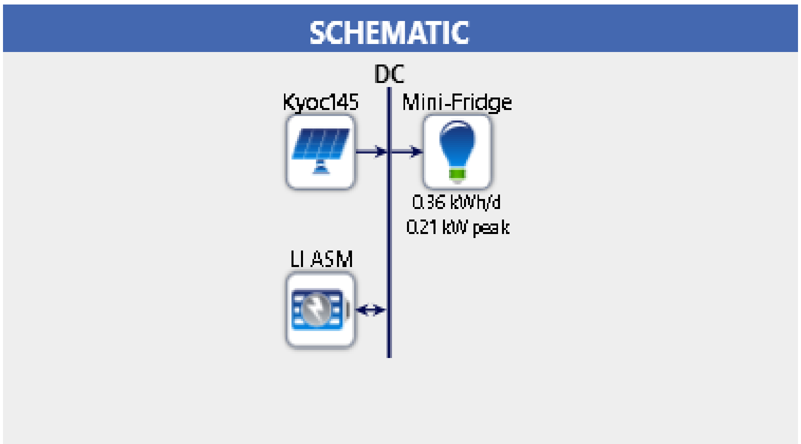

2. The selection environment location

Appendix C: MATLAB Simulation Code and Arduino Code

1. Solar panel simulation MATLAB code

```
function I = Iphoton(V, G, T)
k = 1.3806488e-23;
q = 1.6021766e-19;
n = 1.3;          % 1.3 for poly crystalline solar cell (1<n<2)
ki = 1.33e-3;     % 0.065A/C
Eg = 1.12;        % Si-1.12, GaAs-1.42
Ns = 6;
Np=2;
Tr = 273.15+25;    % 25C  0C=273.15K
Voc = 21.24/Ns;
Isc = 2.75/Np;
Tk = 273.15+T;
Vc = V/Ns;
Vt = (n*k*Tr) / q;
Vta = (n*k*Tk) / q;
b = (Eg*q) /(n*k);
Iss = Isc * (1 + (ki * (Tk - Tr)));
Iph = G * Iss;
Ir = Isc / (exp(Voc / Vt) -1);
Is = Ir * (Tk/Tr)^(3/n) * exp(b * (1/Tr - 1/Tk));
dVdI = -2.0/Ns;
Xv = Ir / Vt * exp(Voc / Vt);
Rs = - dVdI - 1/Xv;
```

```
I = zeros(size(Vc));
for j=1:5;
   I = I - (Iph - I - Is .* ( exp((Vc + I .* Rs) ./ Vta) -1))...
      ./ (-1 - Is * (Rs ./ Vta) .* exp((Vc + I .* Rs) ./ Vta));
end
I=I*Np;
End
```

2. MPPT (P and O) and Maximum Parameter Finder MATLAB Function

<table>
<tr><th>P and O MATLAB Function</th><th>Maximum Parameter Finder</th></tr>
<tr><td><pre>
function D = PandO(V, I)
% Dp:
Dint = 0.6;
Dmax = 0.8;
Dmin = 0.2;
deltaD = 1/100;
 persistent Vpre Ppre Dpre;
 dataType = 'double';
 if isempty(Dpre)
Dpre = Dint;
Vpre=0;
Ppre=0;
end
 P= V*I;
dV= V - Vpre;
dP= P - Ppre;
 % if dP ~= 0
   if dP < 0
      if dV < 0
         D = Dpre - deltaD;
      else
      if dV > 0
         D = Dpre + deltaD;
      else
         D=Dpre;
      end
      end
   else
      if dV < 0
         D = Dpre + deltaD;
      else
      if dV > 0
         D = Dpre - deltaD;
      else
         D=Dpre;
      end
</pre></td><td><pre>
function [max_Po, max_Vo,max_Io] =
max_val(Po,Vo,Io)

persistent Ppre Vpre Ipre

if isempty(Ppre)
   Ppre=0;
   Vpre=0;
   Ipre=0;
end

if (Ppre >Po)
   max_Po = Ppre;
   max_Vo = Vpre;
   max_Io = Ipre;

else
   max_Po = Po;
   max_Vo = Vo;
   max_Io = Io;

end
   Ppre = max_Po;
   Vpre = max_Vo;
   Ipre = max_Io;
</pre></td></tr>
</table>

end end % else D=Dpre; % end if D >= Dmax || D<= Dmin D=Dpre; end Dpre=D; Vpre=V; Ppre=P;	

3. Arduino temperature regulation code

```
/*
  @Author: Dawit Dubela
  @Date: 05/09/2020
  @Version: 0.5
*/
#include "DHT.h"
#include <LiquidCrystal.h>
/*****Input-Output PINs setup*****/
//DHT22 setup
#define DHTPIN 36
#define DHTTYPE DHT22
DHT dht(DHTPIN, DHTTYPE);
//LCD setup
const int rs = 22, en = 24, d4 = 26, d5 = 28, d6 = 30, d7 = 32;
LiquidCrystal lcd(rs, en, d4, d5, d6, d7);
//Outer fan                  #Inner fan              #multi-LED
const int ENA = 2;           const int IN3 = 5;      const int LED_R = 40
const int IN1 = 3;           const int IN4 = 6;      const int LED_G = 42;
const int IN2 = 4;           const int ENB = 7;

/*****Input-Output PINs setup*****/

/****Variables Declaration****/
const float min_temp = 10, max_temp = 16;
//float temp;
bool cool;
/****Variables Declaration****/

void setup() {
  dht.begin();
  lcd.begin(16, 2);
  lcd.clear();

  Serial.begin(9600);
```

```
  pinMode(ENA, OUTPUT);
  pinMode(IN1, OUTPUT);
  pinMode(IN2, OUTPUT);
  pinMode(IN3, OUTPUT);
  pinMode(IN4, OUTPUT);
  pinMode(ENB, OUTPUT);
  pinMode(LED_R, OUTPUT);
  pinMode(LED_G, OUTPUT);
  digitalWrite(IN1, 1);
  digitalWrite(IN2, 0);
  digitalWrite(IN3, 1);
  digitalWrite(IN4, 0);
  digitalWrite(ENA, LOW);
  analogWrite(ENB, 0);
}

void led_ctrl(){
  float temp = dht.readTemperature();
  if (temp > max_temp || temp < min_temp){
    digitalWrite(LED_G, LOW);
    digitalWrite(LED_R, HIGH);
  }
  else {
    digitalWrite(LED_R, LOW);
    digitalWrite(LED_G, HIGH);
  }
}

void lcd_ctrl(){
  float temp = dht.readTemperature();
  if (temp < min_temp){
    lcd.clear();
    lcd.setCursor(0, 0);
    lcd.print("Temp:");
    lcd.print(temp);
    lcd.print("\337C");
    lcd.print(" LOW");
    lcd.setCursor(0, 1);
    lcd.print("Turn-off Cooler!");
  }

  else if(temp >= min_temp && temp <= max_temp){
    lcd.clear();
    lcd.setCursor(0, 0);
    lcd.print("Temp:");
    lcd.print(temp);
    lcd.print("\337C");
    lcd.print("GOOD");
```

```
    lcd.setCursor(0, 1);
    lcd.print("Cooler: ");

    //Check whether the fan is ON or OFF
    if(cool == true){
      lcd.print("ON");
    }

    else{
      lcd.print("OFF");
    }
  }

  else{
    lcd.clear();
    lcd.setCursor(0, 0);
    lcd.print("Temp:");
    lcd.print(temp);
    lcd.print("\337C");
    lcd.print(" HOT");
    lcd.setCursor(0, 1);
    lcd.print("Cooler: ");

    lcd.print("ON");
  }
}

void loop() {
  float temp = dht.readTemperature();
  Serial.print("Temp: ");
  Serial.println(temp);
  if (temp >= max_temp){
    digitalWrite(ENA, HIGH);
    analogWrite(ENB, 200);
    cool = true;
  }

  else if(temp <= min_temp){
    digitalWrite(ENA, LOW);
    analogWrite(ENB, 0);
    cool = false;
  }

  led_ctrl();
  lcd_ctrl();
  delay(2000);
}
```

Appendix D: Solar Module and Accessories

1. **Selected Solar module of** Ocean solar FZ453

Peak power	45W	Open Circuit Voltage	21.24V
Production Tolerance	±3%	Short Circuit Current	2.75A
Maximum Power Voltage	DC12V/5V USB	solar Cell Type	mono cell
Maximum Power Current	2.75A	Folding Size	350*270*20mm
Solar Cell Efficiency	18%-20%	Unfolding Size	1070*340mm
Weight	1.5kg	Folding Times	Over 5000

2. **HOMER selected solar panel** KD145SX-UFU

P_{max}	145w
V_{mp}	17.0v
I_{mp}	8.11A
V_{oc}	22.4v
I_{sc}	8.78A
$P_{tolerance}$	+10/-0 %

3. **Selected BLDC Fan** of PE60201B3-000U-A99 SUNON

Manufacturer	SUNON
Type of fan	DC
Kind of fan	axial
Supply voltage	12V DC
Fan dimensions	60x60x20mm
Power consumption	1.24W
Current rating	0.103A
Fan efficiency	33.13m^3/h
Noise level	30dBA
Rotational rate/speed	3600 (±15%) rpm
Weight	52g
Fan motor	brushless DC motor
Operating voltage	6-13.8V

4. **Selected microcontroller**

Type	Sensor Development Boards and Kits
Chipset	for Arduino Uno R3 Development Board
Place of Origin	China
Model Number	Arduino Uno R3 Development Board
Brand	for Arduino Uno R3 Development Board
Product Name	UNO R3 Compatible with Arduino IDE

5. **Selected temperature sensor** LM35DZ temperature sensor

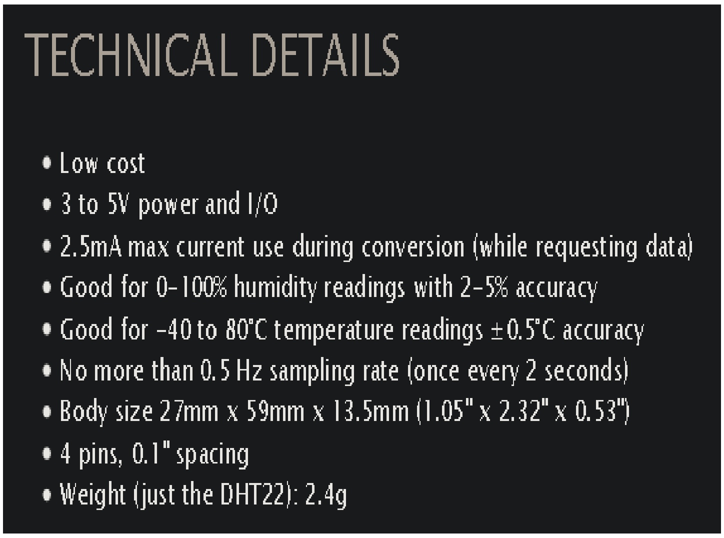

6. **A selected** Sukam MPPT Solar Charger Controller Unit, 12 V/17A

Is Discontinued	No
Product Dimensions	150 x 126 x 54 cm; 200 Grams
Date First Available	8 August 2016
Manufacturer	Su-Kam Power Systems Ltd.
ASIN	B01JYWEXDY
Item part number	Solar Charger Controller unit
Manufacturer	Su-Kam Power Systems Ltd.
Item Dimensions	150 x 126 x 54 Centimeters
Item Weight	200 g
Included Components	1 Solar Charger Controller unit
Best Sellers Rank	#43,438 in Garden & Outdoors

7. Li-ion Battery

Product Specification	
Battery Capacity	10Ah
Model Number	EZ1210A
Usage/Application	Storage battery solar battery etc
Battery Life	2 Year
Warranty	1 Year
Battery Voltage	12V
Voltage	12V
Capacity	10Ah
Battery Type	Lithium-Ion
Size	Cylindrical
Battery Shape	Customized
Cycle Life	500 Cycles

8. TEC (Termoelectrical cooler)

Model: TEC1-12706
Voltage: 12V
Umax (V): 15V
Max Current (A): 4-4.6A
Cooling Power: Qcmax 50-60W
Resistance: 2.1-2.4Ω
△Tmax(Qc=0): up to 67°C
Operates Temperature: -55°C to 83°C
Power Cord: 29cm
Dimensions : 40mm x 40mm x 3.75mm (L*W*T)

Appendix F: The Overall Calculation of Inductor and Capacitor Values

Month	Ir	T	P max	V mppt	D	I max	delta I_o	delta V_o	L	C
Jan	6.46	32.43	358.7	21.1	0.263	29.89	8.968	0.12	9.75259E-06	0.0012085
Feb	6.33	34.04	354.5	21.23	0.261	29.54	8.863	0.12	9.79604E-06	0.0012037
Mar	6.25	35.56	353.1	21.5	0.258	29.43	8.828	0.12	9.8855E-06	0.0011940
Apr	6.25	36.59	355.4	21.52	0.258	29.62	8.885	0.12	9.89208E-06	0.0011933
May	6.66	38.87	385.6	21.86	0.254	32.13	9.64	0.12	1.00032E-05	0.0011813
Jun	6.07	40.38	352.6	21.96	0.253	29.38	8.815	0.12	1.00355E-05	0.0011779
Jul	5.23	36.69	294.1	21.33	0.26	24.51	7.353	0.12	9.82929E-06	0.0012001
Aug	5	35.12	277	21.6	0.257	23.08	6.925	0.12	9.91837E-06	0.0011905
Sep	5.65	36.16	318.3	21.47	0.259	26.53	7.958	0.12	9.87561E-06	0.0011951
Oct	6.7	35.81	380.9	21.57	0.257	31.74	9.523	0.12	9.90852E-06	0.0011915
Nov	7.75	34.06	440.1	21.5	0.258	36.68	11.003	0.12	9.8855E-06	0.0011940
Dec	7.23	32.4	404.4	21.23	0.261	33.7	10.11	0.12	9.79604E-06	0.0012037
ANN	6.3	35.67	356.4	21.5	0.2582	29.7	8.91	0.12	9.8855E-06	0.00119403
Design	5	40.5	287	21.7	0.2561	23.92	7.175	0.12	9.9511E-06	0.001186944